# Redox behaviour of model systems for spent nuclear fuel surfaces

Cakir, Pelin

**DOI**
10.4233/uuid:d51d8117-7b1f-4aca-a488-c3bc57f39167

**Publication date**
2018

**Document Version**
Final published version

**Citation (APA)**
Cakir, P. (2018). *Redox behaviour of model systems for spent nuclear fuel surfaces*. [Dissertation (TU Delft), Delft University of Technology]. https://doi.org/10.4233/uuid:d51d8117-7b1f-4aca-a488-c3bc57f39167

**Important note**
To cite this publication, please use the final published version (if applicable).
Please check the document version above.

# Redox Behaviour of Model Systems for Spent Nuclear Fuel Surfaces

# Redox Behaviour of Model Systems for Spent Nuclear Fuel Surfaces

## Dissertation

for the purpose of obtaining the degree of doctor
at Delft University of Technology
by the authority of the Rector Magnificus, prof.dr.ir. T.H.J.J. van der Hagen,
Chair of the Board for Doctorates
to be defended publicly on
Tuesday 23 October 2018 at 10:00 o'clock

by

**Pelin Çakir**

Master of Science in Nuclear Sciences, Ege University, Turkey
Born in Islahiye, Turkey

This dissertation has been approved by the promoter and the copromoter.

Composition of the doctoral committee:

| | |
|---|---|
| Rector Magnificus | chairperson |
| Prof. dr. R. J. M. Konings | Delft University of Technology, promoter |
| Dr. T. Gouder | European Commission, JRC-Karlsruhe, copromoter |
| | |
| Independent members: | |
| Prof. dr. P. Dorenbos | Delft University of Technology |
| Prof. dr. H. T. Wolterbeek | Delft University of Technology |
| Prof. dr. habil. T. Schäfer | Friedrich-Schiller-University Jena |
| Prof. dr. ir. J. L. Kloosterman | Delft University of Technology |
| | |
| Other members: | |
| Dr. R. Eloirdi | European Commission, JRC-Karlsruhe |
| Dr. A. L. Smith | Delft University of Technology |

The doctoral research has been carried out within a cooperation of the Joint Research Centre (JRC)-Karlsruhe of the European Commission (formerly known as the Institute for Transuranium Elements (ITU)) and the Department of Radiation Science and Technology, Faculty of Applied Sciences, Delft University of Technology, The Netherlands.



*Keywords:* Thin Films; Actinide Oxides; Redox; Photoelectron Spectroscopy

*Printed by:* ProefschriftMaken || www.proefschriftmaken.nl



ISBN 978-94-6380-048-8

An electronic version of this dissertation is available at
http://repository.tudelft.nl/.

*to my most precious parents and brother*

*Benim canim annem, babam ve kardeşime*

*und*

*für Sebastian*

# SUMMARY

Safety assessments are the main pillars of the analysis of the impact of storage of the spent nuclear fuel. There are many scenarios to describe what might happen during the storage and disposal time of the nuclear waste. Even though the main composition of the spent nuclear is $UO_2$, the matrix contains transuranium elements and fission products, which have different chemical behaviour and lead to an altered physical state after the irradiation. Thus, the complex nature of the spent nuclear fuels requires understanding of several mechanisms through investigation of individual parameters and their effect on one and another. This is achieved by single effect studies, starting from simple systems to gradually more complex systems. In this thesis, thin films have been used as model systems to simulate the spent fuel in a systematic manner. The main focus was given to the actinide (mixed) oxides (Th, U, Np, Pu, and Ce as surrogate for Pu and as fission product).

Throughout this thesis, the suitability of the use of thin films instead of bulk material has been demonstrated, and the investigation of redox properties of model systems for spent fuels using different methods is described.

Surface models for spent nuclear fuels have been produced by using the sputter deposition technique under Ultra-High Vacuum (UHV) conditions. This technique allows using multiple source materials as well as changing the ratios between the sources. In addition, changing the environment during the deposition, such as adding oxygen into the UHV chamber, results in producing variety of stoichiometric films for the purpose of the studies. Thanks to those abilities of the sputter deposition technique, we were able to produce films starting from the simplest systems to more complex ones. All the samples prepared were measured by using the X-Ray photoelectron (XPS) and Ultraviolet photoelectron spectroscopies (UPS) providing the chemical composition of the surfaces.

In the first part the results from investigations of thorium oxide films are described. Thorium is particularly interesting as it has only one stable oxidation state. Oxidation of thorium has been followed using two different methods. At first, the thorium metal films were deposited and exposed to atomic and molecular oxygen. While atomic oxygen was able to penetrate to deeper layers of the metal, molecular oxygen only oxidized the upper surface layers. XPS and UPS measurements provided information on the O/Th ratio of the films and the depth of oxidation process taking place. In the second part, the thorium oxide films were deposited using different amount of partial oxygen pressure and the O/Th ratio of the films was calculated from XPS and UPS results. The next step was to study the effect of thorium on uranium dioxide film when they are deposited as mixed oxides. Thorium has shown higher affinity to oxygen than uranium from low to high partial pressure during deposition. (U-Th) mixed oxides with different ratios were deposited onto gold substrates, allowing electrochemical studies by cyclic voltammetry. It has been found that thorium does affect the oxidation of uranium leading to lower solubility.

Cerium was chosen for the next step in the study as it has both trivalent and tetravalent redox states. The redox influence between uranium and cerium was investigated by XPS in mixed (U-Ce) oxide and their single oxides of the two elements after they were submitted to strong reductive and oxidative agents. The comparison has shown that cerium is more prone to reduction when it is mixed with uranium, while uranium easily oxidises in the mixture. It has also been found that formation U(V) in single uranium oxides requires oxidising post treatments of the films, but when uranium is co-deposited with cerium, U(V) forms directly due to charge transfer occurring between uranium and cerium.

Finally, mixed oxide of uranium-thorium, uranium-plutonium and neptunium dioxide surface alteration was investigated. The aim was to follow the corrosion of the thin film surfaces by water under radiation enhanced conditions. However, since water in its liquid form is not stable in the ultra-high vacuum conditions ice has been used. XPS and UPS analyses showed that the ice-covered film surfaces reduced after the exposure to ultraviolet (UV) light. Exposure to only ice or only UV light did not lead to reduction of the surface. Therefore the surface reduction was explained as photocatalytic reaction which was triggered by excitation of electrons from valence band to conduction band creating a redox mechanism to promote reduction on the surface and oxidation of the ice.

In this thesis actinide mixed oxide thin films were studied for first time. The results show that they are good representative of the bulk materials, and can be studied as model systems for spent nuclear fuels to understand the redox behaviour of the surface. Two important observations were made that need to be taken into account when modelling real spent fuel are: (i) Metal ions substitution in the uranium dioxide matrix can restrain or enhance the dissolution behaviour depending on the redox states of the ions, (ii) Photoactivated reaction can lead to oxidation of water and surface reduction of the $UO_2$ matrix, restraining the dissolution.

# SAMENVATTING

Veiligheidsanalyses zijn de belangrijkste pijler voor de analyse van de gevolgen van opslag van gebruikte splijtstof. Er bestaan vele scenario's die beschrijven wat kan gebeuren gedurende de tijdelijke en definitieve opslag van radioactief afval. Hoewel de matrix van gebruikte splijtstof $UO_2$ is, bevat hij tevens transuranium-elementen en splijtingsprodukten, die een ander chemisch gedrag hebben, en tot een veranderde fysieke toestand na de bestraling leiden. De complexiteit van gebruikte splijtstof vraagt dus om inzicht in verschillende mechanismen door middel van onderzoek van individuele parameters en hun effect op elkaar. Dit kan worden gerealiseerd door middel van zogenaamde "single effect"studies, van simpele systemen naar geleidelijk meer complex. In dit proefschrift zijn dunne lagen gebruikt als model om gebruikte splijtstof op een systematische wijze te simuleren. De aandacht was vooral gericht op de mengoxiden van de actiniden (Th, U, Np, Pu en Ce at surrogaat voor Pu en als splijtingsproduct).

Dwars door het proefschrift is de toepasbaarheid van dunne lagen in plaats van bulk materiaal aangetoond, en de studie van de redox eigenschappen van model systemen voor gebruikte splijtstof met verschillende methoden wordt beschreven.

Oppervlakte modellen voor gebruikte splijtstof zijn gefabriceerd met behulp van de sputterdepositie techniek onder ultrahoog vacuüm (UHV) omstandigheden. Deze techniek maakt het mogelijk meerdere bronmaterialen te gebruiken en tevens de verhouding tussen de bronnen te veranderen. Daarnaast kan een breed spectrum van verbindingen met verschillende stoichiometrische samenstelling worden verkregen door het veranderen van de omstandigheden in de UHV kamer, bijvoorbeeld door toevoegen van zuurstof. Door deze mogelijkheden van de sputterdepositie techniek zijn dunne lagen geproduceerd, van de eenvoudigste systemen tot complexere. Alle monsters zijn analyseerd met Röntgenfotoelectron- en Ultravioletfotoelectronspectroscopie om informatie over de chemische samenstelling van het oppervlak te verkrijgen.

In het eerste deel worden de resultaten van het onderzoek aan thoriumoxide dunne lagen beschreven. Thorium is van interesse omdat het slechts een oxidatietoestand heeft. De oxidatie van thorium is op twee manieren onderzocht. Eerst zijn dunne lagen van thorium metaal gemaakt die vervolgens zijn blootgesteld aan atomair en moleculair zuurstof. Terwijl atomair zuurstof in staat was door te dringen tot de diepste lagen van het metaal, was moleculair zuurstof in staat enkel de oppervlakte laag te oxideren. XPS en UPS metingen leverden informatie over de O/Th verhouding in de films en de diepte van het oxidatieproces. In het tweede deel zijn thoriumoxide lagen gemaakt bij verschillende partiele zuurstofspanningen en de O/Th verhouding is afgeleid uit de XPS en UPS metingen. Vervolgens is het effect van thorium op uraniumoxide lagen onderzocht wanneer ze als mengoxide worden gevormd. Thorium heeft een grotere affiniteit voor zuurstof in vergelijk met uranium bij alle zuurstofspanningen. (U-Th) mengoxiden met verschillende samenstellingen zijn op goud substraten afgezet, waardoor electrochemische studies mogelijk waren met behulp van cyclovoltametrie. Hierbij werd waargenomen

dat thorium de oxidatie van uranium, en dat de oplosbaarheid van uranium afneemt.

Voor de volgende stap van de studie is gekozen voor Cerium omdat het zowel een driewaardige en vierwaardige oxidatietoestand kan hebben. Het redox effect tussen uranium en cerium is onderzocht met behulp van XPS in zowel (U-Ce) mengoxide als de enkele oxiden van de twee elementen nadat ze blootgesteld zijn aan sterk oxiderende en reducerende condities. Het vergelijk heeft aangetoond dat Cerium makkelijker gereduceerd wordt wanneer het met uranium is gemengd, terwijl uranium makkelijk wordt geoxideerd in het mengsel. Het is waargenomen dat U(V) in de enkele oxiden gevormd kan worden met behulp van oxiderende nabehandeling van de lagen, maar wanneer uranium met cerium samen wordt afgezet wordt U(V) direct gevormd door ladingsoverdracht tussen uranium en cerium.

Tot slot is de oppervlakteverandering van mengoxiden van uranium-thorium-uranium-plutonium- en neptuniumdioxide onderzocht. Het doel was het in beeld brengen van de corrosie van de dunne lagen door water tijdens bestraling. Omdat vloeibaar water niet stabiel is onder ultrahoog vacuüm omstandigheden is ijs gebruikt. XPS and UPS analyse hebben aangetoond dat de met ijs bedekte dunne lagen gereduceerd waren wanneer zij aan UV licht blootgesteld werden. Blootstelling aan alleen ijs of alleen UV licht leidde niet tot reductie. Op basis hiervan kan de oppervlaktereductie worden verklaard door een fotocatalytische reactie die wordt geïnitieerd door excitatie van elektronen van de valentieband naar de geleidingsband, waarmee een redox mechanisme wordt gecreëerd dat leidt tot reductie van het oppervlak en oxidatie van ijs.

In dit proefschrift zijn dunne lagen van mengoxiden van de actiniden voor het eerst onderzocht De resultaten tonen aan dat ze bulkmateriaal op goede wijze kunnen representeren en kunnen worden onderzocht als modelsysteem voor gebruikte splijtstof om het redoxgedrag van het oppervlak te begrijpen. Twee belangrijke waarnemingen moeten worden betracht bij het modelleren van gebruikte splijtstof onder echte omstandigheden: (i) vervanging van metaalionen in de matrix van uraniumdioxide kan het oplossen afremmen of versnellen, afhankelijk van de redoxtoestand van de ionen. (ii) Lichtondersteunde reactie van water kan leiden tot reductie van het oppervlak van de $UO_2$ matrix, waardoor het oplossen wordt afgeremd.

# CONTENTS

# 1

# INTRODUCTION

*The most exciting phrase to hear in science, the one that heralds new discoveries, is not 'Eureka!' but 'That's funny...'*

Isaac Asimov

## 1.1. MOTIVATION TO THIS WORK

THE challenge of having the power generated by nuclear power plants does not end once the electricity reaches to the society. The remaining source of the nuclear fuel (referred as Spent Nuclear Fuel, SNF), contains high level radioactivity which is active up to thousands of years. There are already quite a lot of discussions running over the fate of the nuclear waste for the safety of the environment. The general strategy is to bury the high level nuclear waste in a deep stable geological formation. This is considered the safest way and thought to provide the protection of mankind and of the environment from radioactivity. Safety assessments of the SNF are mainly based on the failure scenario of the container which surrounds the SNF under deep geological repository and of the potential contact of the SNF with groundwater.

The stability of containers is expected a thousand years, however the failure of a container should be assumed for the safety assessments and this scenario must be evaluated with a great deal of attention. So, the assumptions such as "it is not expected soon" is not an acceptable statement. Therefore, the worst case scenarios are constantly under investigation and each year more data are reported into literature. The ideal analysis would be the observation of the fuel over thousands of years, but this is not a realistic approach. Since the time scale is beyond any ideal experimental approach, model studies are in high demand to shed light on the fate of SNF during the disposal period.

To assess the consequences of possible waste fuel corrosion and dispersion to the biosphere requires investigation of many parameters. This consists of the physical form,

chemical composition of the waste, the groundwater and the container material characteristic investigations. To be able to fully comprehend each parameter's role in the safety assessments, single effect studies are conducted. It is important to point out that upon exposure to groundwater, corrosion will start from the upper surface of the waste, and then gradually move into the lower layers. Thus, surface characterization investigations are fundamental and crucial for evolution of the nuclear safety assessments.

## 1.2. SPENT NUCLEAR FUEL AND CORROSION

Uranium dioxide, $UO_2$, is the most popular fuel for the water-cooled reactors. Uranium consists of two isotopes; $^{235}U$ fissile (0.72 atomic %) and $^{238}U$ fertile (99.27 atomic %). For most light-water reactors (LWR) uranium fuel is enriched to 3 to 5 % $^{235}U$. Some LWRs also use Mixed Oxide Fuels, commonly referred as MOX fuels, consisting of about 5 % plutonium. Typical fuel is quite close to stoichiometry, $UO_{2.001}$ [1]. The composition and the microstructure of the fuel changes during the irradiation depending on the time of irradiation and at which power it is operated. After the irradiation SNF becomes a very complex matrix consisting of different microstructures and elemental fractions compared to the initial material. This differences in composition and microstructure have been studied extensively over the years [2–4]. Many fission products and actinides formed during the in-reactor irradiation time are categorised and summarised below according to their chemical role in $UO_2$ host matrix[2, 5].

- Fission-product gases, such as Xe and Kr, which occur as finely dispersed bubbles in the fuel grains.
- Metallic fission products, such as Mo, Tc, Ru, Rh, and Pd, which occur as immiscible, micron- to nanometre-sized metallic precipitates ($\varepsilon$-particles)
- Fission products that occur as oxide precipitates of Rb, Cs, Ba, and Zr.
- Fission products that form solid solutions with the $UO_2$ fuel, such as Sr, Zr, Nb, and the rare-earth elements.
- Transuranium elements that substitute for U in the $UO_2$.

After irradiation, $UO_2$ is still the major component, about 95% of the total matrix. The rest of the matrix is the combination of (as stated above) fission products, and transuranium elements which are embedded into $UO_2$. Considering this, SNF can be seen as doped $UO_2$. Dissolution of the embedded elements is linked to $UO_2$ corrosion. The dissolution rate of $UO_2$ increases by many orders of magnitude as a function of oxidation to hyperstoichiometry ($UO_{2+x}$) [6]. If $UO_2$ becomes hyper-stoichiometric in contact of oxidants, the embedded elements dissolve along with it. Since the groundwater is expected to be anoxic, the presences of the oxidants should not be as extensive as surface water. However, when considering the radioactivity of the spent fuel is increased by a factor of a million ($10^{17}$ Becquerel / metric tonne of fuel) after burn-up in a reactor, this level of radioactivity is more than enough for radiolysis of groundwater, creating oxidants ($HO^{\cdot}$, $HO_2^{\cdot}$ and $H_2O_2$) and reductants ($e_{aq}^{-}$, $H^{\cdot}$, $H_2$)[7]. Under nomal pH conditions the oxidants will dominate the redox chemistry on the surface of the fuel, leading to an oxidative dissolution [6, 8].

The electronic structure of tetravalent uranium in $UO_2$ is [Rn]$5f^2$. The narrow 5f band lies between filled valence band and empty conduction band. When it is oxidized, a hole in the 5f band is created. Because of that, holes can migrate with a low activation energy leading to higher conductivity, causing dissolution as $UO_2{}^{+2}$ dissolved species [9]. Oxidative dissolution of $UO_2$ is a two-step reaction. $UO_2$ is in the U(IV) oxidation state which is poorly soluble under anoxic conditions. However, the oxidants coming from water radiolysis will oxidize U(IV) to U(VI) which has higher dissolution rate. Consequently, as second step U(VI) dissolves. The mentioned chemical process is shown below.

U(IV) + Ox –> U(VI) + Red

U(VI) –> $UO_2{}^{2+}$ (aq)

However, also reductants are present, as a result of the radiolysis of water. Thus, the competition between oxidants and reductants will be deciding the rate of the corrosion. $H_2$, as a reductant, especially has been subjected to studies many times. It has been showed that might hinder the oxidative dissolution[10–12]. In addition, the influence of the metallic fission product in matrix has been also observed to produce $H_2$ which is inhibiting the corrosion[13, 14].

However alongside its different chemical phases produced during in-reactor time, the mixed oxide as U-Pu can be used as initial fuel. Plutonium is also a redox sensitive element with two stable oxidation states, Pu(III) and Pu(IV). Plutonium dioxide as well as other minor actinide dioxides have chemical similarities to $UO_2$ such as crystal structure and due to this they incorporate into $UO_2$ matrix. Therefore, those need to be involved in the equation when corrosion/dissolution under deep geological formations are examined in laboratory conditions. Considering the many parameters which might increase or decrease the corrosion, model systems are required.

## 1.3. SPENT NUCLEAR FUEL MODEL SYSTEMS AND SURFACE SCIENCE INVESTIGATIONS

To overcome the complexity, single effect studies are used that aim at understanding the effect of one parameter at a time. Single effect studies are based on model systems to mimic the complex material starting from simple to gradually increasing complex systems. Surface of the materials plays an important role to elucidate the corrosion behaviors and products, as first contact occurs on the surface which leads to oxidation and arouses the reactions in underlying layers. In this work thin films are adopted to be used as model systems to investigate surface properties which govern the corrosion of SNF. Using actinide oxides in thin film form produced by sputter deposition technique has been developed for its purpose to use as model surfaces to SNF[15], and up to this date there have been many successful studies which will be mentioned below.

The development of the Photoelectron Spectroscopy has been very important for actinide research and much of the attention has been given to the actinide oxides to understand the role of 5f electrons in the bonding. Photoelectron spectroscopy techniques (X-ray Photoelectron and Ultra-Violet Photoelectron Spectroscopy, XPS and UPS, respectively) are surface sensitive, mainly dealing with speciation of the upper layers such as determining the electronic structures, for both quantitative and qualitative analysis.

They are the major investigation tools used in this thesis. XPS and UPS measurements can show the evolution of chemical bonding of actinides as a function of oxygen concentration under UHV condition in controlled environments[16, 17]. The light actinide oxides may form several oxidation state, e.g. U, such as $UO_2$, $U_4O_9$, $U_3O_8$, $UO_3$, while starting from Pu the actinides in the series become more stable as sesquioxides ($An_2O_3$) [18]. Below, some of the key literatures about XPS and UPS findings of actinide oxides electronic structure investigations are reviewed generally for better comprehending of the upcoming chapters.

One of the most interesting element in the actinide series is thorium, Th. Thorium alongside uranium is naturally abundant radioactive element. It lacks 5f electrons in the valence band and forms only one stable oxide, $ThO_2$. This behaviour of thorium led scientists to compare its bonding and reactivity with other actinide oxides [19–23]. The thorium exposure to oxygen has shown valence 6d7s electrons transfer to 2p electrons of the oxygen ions [24] where it only forms dioxide but none of the other oxide forms. Uranium, due to its use as main fuel source in nuclear reactors, is one of the most studied elements of the actinide series. Uranium is more complex than thorium in the sense of oxidation states. The different oxidation states of uranium have been identified with XPS and UPS. The off-stoichiometry of $UO_2$ films has been studied both by McLean et al.[24] and Allen et al.[25] on a clean uranium surface exposed to low and high content of oxygen, leaving the surface as $UO_{2+x}$ and $UO_{2-x}$, respectively. Allen et al.[25] showed the uranium´s 4f binding energy increases as a function of oxidation states. Gouder et al. [26] also showed the 5f emission shifting with UPS over the adsorption of oxygen on different temperatures. While U(IV) display $5f^2$ emission at 1.4 eV (above the Fermi level), U(VI) does not display any 5f emission because of the transferred valence electrons to oxygen [27].

Model surfaces synthesized as thin films have shown many advantages for the investigations of surface properties. In this thesis, DC sputtering deposition technique is used to achieve desired surface models[28]. One of the advantages using thin films instead of bulk material for the surface investigations is to handle rather small quantity of actinide material, reducing the cost and waste. Beside that, this technique is quite flexible when it comes to codeposit material from several sources for creating mixed samples. However, the source material should be conductive, therefore for the (mix-) actinide oxide films auxiliary oxygen is required to be introduced into the deposition chamber. This actually allows to control the stoichiometry of the actinide oxide and to observe the evolution of oxidation of the films alongside measuring with XPS and UPS. Miserque et al. [29] has studied uranium oxide thin film to find the adequate conditions to reach the stoichiometric $UO_{2.0}$. In another study [30], $UO_2$ thin films were compared to the bulk $UO_2$ samples to pursue stoichiometric thin layers. It was shown that the further oxidation is limited due to the slow kinetics of deposition of higher oxides. By exposure to gases after the deposition it is also possible to diffuse oxidants ($O_2$, $O^{\cdot}$) and reductants ($H_2$,$H^{\cdot}$) in the material to force oxidition and reduction of the surfaces. Detailed studies were performed for Th, U, Pu, Np and Am films which are perfect examples of oxidation by gas exposure [31–33] at different temperatures and dosages to identify intermediate and stable oxides on the surface. Plutonium is another important key element in spent nuclear fuel research and has been investigated by photoelectron spectroscopy extensively.

Plutonium has two stable oxidation state, (III) and (IV) in the electronic configuration as $5f^5$ and $5f^4$, respectively[23, 34]. Metallic Plutonium reacts with oxygen and easily forms sesquioxide ($Pu_2O_3$) and subsequently forms a dioxide ($PuO_2$)[33]. Neptunium which is present in SNF matrix and is also investigated in this thesis, forms sesquioxide ($Np_2O_3$) and dioxide ($NpO_2$) compounds, with $5f^4$ and $5f^3$ electron configurations, respectively [32, 35].The investigation on Np thin films exposed to atomic oxygen at elevated temperatures also shoed the presence of the stable $Np_2O_5$ bulk oxide[31, 32].

Besides its bonding behaviour with gas molecules such as oxygen, a lot of research has been focussed on the reaction of $H_2O$ with actinide oxides surfaces, in particularly $UO_2$ to mimic the groundwater-like aqueous solutions and moisture to observe the surface corrosion behavior [36–38]. Another approach for studying the interaction of actinide oxide surfaces with water is deposition of ice layers [27, 39]. The main reason of using ice is fact that under the UHV conditions water is not able to hold onto the surface. Also, contamination free, high concentration water would be in contact with the surface. Thin films were also adopted for electrochemical studies[29, 40, 41] where the films were deposited onto conductive substrates and their redox behavior was followed by cyclic voltammetry measurements.

This thesis is motivated by the fact that single uranium dioxide thin films are suitable model systems to study the surface reactions, however other actinides need to be considered when simulating the SNF. Therefore, the main effort has been given into the study of mixed actinide oxide thin films and their surface redox properties. As the studies above mentioned suggest, they can be adopted to many different types of investigations without need of bulk material.

1

## 1.4. AIM OF THE WORK

The consequences of contact between spent nuclear fuel and ground water in a deep geological formation of an ultimate nuclear waste repository are of vital importance for the safety assessment of final storage concepts. SNF contains many elements to be considered in the safety assessment, and particularly fission products mobile in the geological environment need attention. However, $UO_2$ forms the main component of the SNF, and the corrosion of the fuel matrix in contact with groundwater is seen as the initial step in the radionuclide release. $UO_2$ is thus the simplest model material for studying SNF corrosion. In order to understand the cause of corrosion / dissolution this process must be identified in laboratory conditions addressing also different geological formations and radiation-based alterations that can take place during the time of the storage. The problem is that modeling such complex system is quite challenging. Therefore, single effect studies are needed, and this approach is also applied in this study.

While uranium dioxide has been studied extensively in the form of bulk [9, 42–45] as well as thin films [29–31, 40, 46], the effect of other actinides on the the corrosion / dissolution process needs better evaluation. Due to the semiconductor nature of the actinide oxides, measurements especially of the electronic structure are facing challenges. To alleviate this, thin films for model surfaces are used as they overcome the drawbacks related to thickness of bulk samples, such as charging effect.

The research described in this thesis is aimed at understanding the evolution of (mixed-) actinide oxide (namely; thorium, uranium, neptunium, plutonium and cerium as plutonium surrogate and fission product) with respect to oxidation and reduction reactions at the surface. The main goal is to investigate the spent fuel model surfaces over the course of oxidative/reductive conditions to observe the changes which might affect the corrosion/dissolution properties in deep geological formations.

## 1.5. THESIS SYNOPSIS

In this chapter, a summary of the layout of the thesis is presented with the motivation of the studies and essential literature reviews. Throughout this thesis, the chapters are in order starting from the simple system to more complex systems. The work starts with thorium which has only one stable oxide, representing the simplest form of the actinide oxides. It then continues with the effect of thorium on uranium oxidation states in the mixed oxide. Next, Ce (as analogue to plutonium and representing the trivalent and tetravalent cations) is added into uranium dioxide matrix to understand the redox state of uranium in the presence of oxidative and reductive conditions. Finally, the mixed oxides of (U-Th) and (U-Pu), alongside $NpO_2$ are presented for their alterations in contact with water. The chapters with their short abstracts are presented below and the schema of the layout is shown in Figure 1.1.

Chapter 2 examines the electronic structure of Th oxide, which has only one stable oxide formation, (IV), representing itself as a reference material for the subsequent studies. This study aims of following the oxidation of thorium versus the oxygen pressure using two experimental approach. First, by exposing Th metal film to molecular/atomic oxygen and second by altering the oxygen partial pressure during the deposition of the films onto Si substrates. Surface compositions are gradually investigated by XPS / UPS

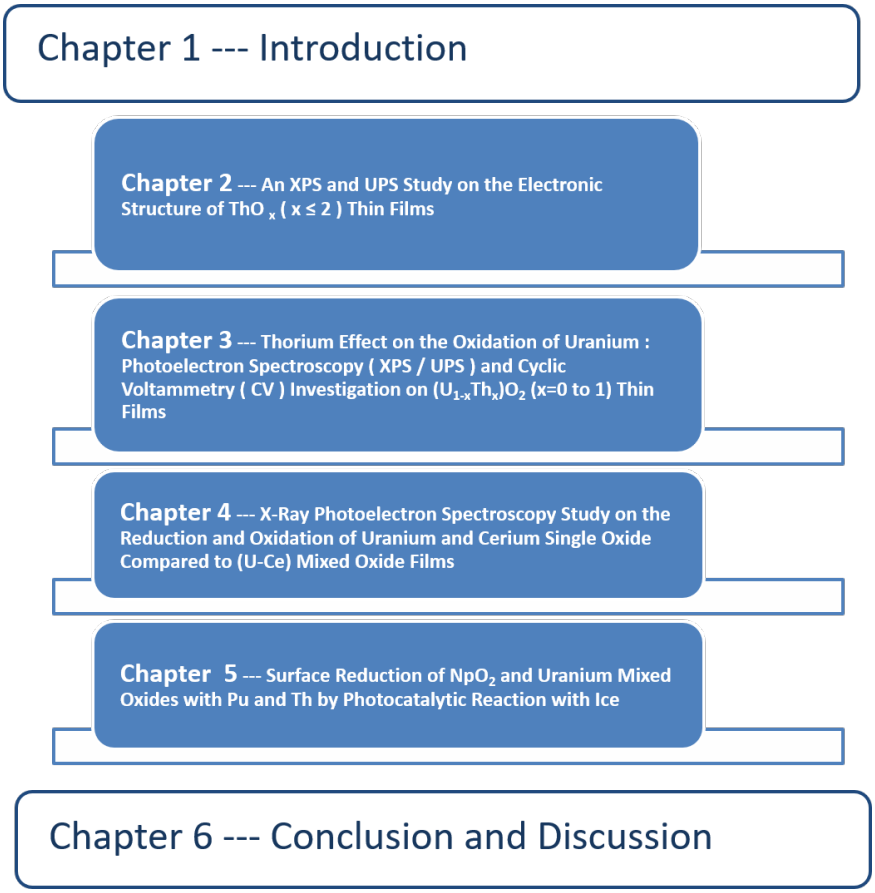


Figure 1.1: Scheme of the thesis layout.

and compared to bulk systems that are represented in literature. The study displays the suitability of using $ThO_2$ thin films as model for bulk materials.

Chapter 3 focuses on the $(U_x,Th_{1-x})O_2$ systems. First the suitability of the thin films to bulk materials is investigated. The question is what is the effect of thorium when substituting uranium in $UO_{2+x}$ on oxidation and reduction behavior. XPS and UPS are used to identify and to quantify the composition/stoichiometry. One of the missing points in the literature was the determination of the redox properties with electrochemical methods of (U-Th) mixed oxides. This method is only allowed when the sample is electrically conductive. However, $UO_2$ is an intrinsic semi-conductor and $ThO_2$ is a classical insulator. Adding Th into the $UO_2$ makes the matrix even less electrically conductive than $UO_2$, and therefore the thick bulk compounds could not be measured electrochemically. The advantage of using thin films helps to fulfill this missing point thanks to the low thickness of the layers. This chapter will examine the redox behaviors of (U-Th) mixed oxides as a function of Th with cyclic voltammetry. It also discusses the end products of

the surface after CV experiments with XPS quantification/qualification features.

Chapter 4 contains the work on ($U_x$,$Ce_{1-x}$) mixed oxides. Cerium exhibits two oxidation states (III) and (IV). The chapter reports the effect of the presence Ce(III) and (IV) in the solid solution on the oxidation and reduction states of uranium by exposing the surfaces to atomic hydrogen and oxygen. It is aimed to follow the contribution of cerium to uranium redox behavior and vice versa. For this purpose, single oxides of cerium and uranium were produced by using sputter reactive (co-)deposition technique, post-treated by reductive/oxidative agents and compared to the mixed oxide form which has gone through the same treatments to evaluate the possible interaction between two component under ambient and high temperature conditions. XPS is used to identify alteration on the surface quantitatively.

Chapter 5 contains the work of ($U_x$,$Pu_{1-x}$)$O_2$, ($U_x$,$Th_{1-x}$)$O_2$ and $NpO_2$ redox behaviour when their surfaces come in contact with water. It is aimed at probing the corrosion products on the surface caused by water interaction under photon radiation enhanced conditions. However, in our experimental work, all the sample preparations and measurements were done under UHV conditions. Therefore, water contact could only be realised in solid form, ice. For the enhanced radiation simulation, Ultra-violet light is used. This chapter will discuss the outcomes on the surface alteration caused by ice contact and Ultra-Violet assisted heating conditions. A mechanism is suggested and will be discussed throughly.

Finally, Chapter 6 provides a general conclusion of the studies conducted in this thesis. Highlights and a discussion of the results alongside a short outlook for possible future studies are presented.

## REFERENCES


[1] H. Kleykamp. The chemical state of LWR high-power rods under irradiation. *Journal of Nuclear Materials*, 84(1-2):109–117, oct 1979.

[2] H. Kleykamp. The chemical state of the fission products in oxide fuels. *Journal of Nuclear Materials*, 131(2-3):221–246, apr 1985.

[3] L. H. Johnson and D. W. Shoesmith. Spent Fuel. In W. B. Lutze and Rodney C. Ewing, editors, *Radioactive Waste Forms for the Future*, chapter 11, page 635. Amsterdam, The Netherlands, 1988.

[4] R. W. Grimes and C. R. A. Catlow. The Stability of Fission Products in Uranium Dioxide. *Philosophical Transactions of the Royal Society A: Mathematical, Physical and Engineering Sciences*, 335(1639):609–634, jun 1991.

[5] R. J. M. Konings, T. Wiss, and O. Beneš. Predicting material release during a nuclear reactor accident. *Nature materials*, 14(3):247–52, mar 2015.

[6] I. Grenthe, J. Fuger, R. J. M. Konings, R.J. Lemire, A. G. Muller, C. Nguyen-Trung Cregu, and H. Wanner. *Chemical thermodynamics of uranium*. North Holland, Amsterdam, 1992.

[7] G. R. Choppin, J. O. Liljenzin, and J. Rydberg. *Radiochemistry and nuclear chemistry*. Butterworth-Heinemann, 2002.

[8] D.W. Shoesmith. Fuel corrosion processes under waste disposal conditions. *Journal of Nuclear Materials*, 282(1):1–31, nov 2000.

[9] D. W. Shoesmith, S. Sunder, and W. H. Hocking. Electrochemistry of UO2 Nuclear Fuel. In J. Lipkowski and N. P Ross, editors, *The Electrochemisty of Novel Materials*, pages 297–337. VCH, New York, 1994.

[10] K. Spahiu, L. Werme, and U. B. Eklund. The influence of near field hydrogen on actinide solubilities and spent fuel leaching. *Radiochimica Acta*, 88(9-11):507–512, 200.

[11] P. Carbol, P. Fors, T. Gouder, and K. Spahiu. Hydrogen suppresses UO2 corrosion. *Geochimica et Cosmochimica Acta*, 73(15):4366–4375, aug 2009.

[12] L. Liu and I. Neretnieks. The Effect of Hydrogen on Oxidative Dissolution of Spent Fuel. *Nuclear Technology*, 138(1):69–78, 2002.

[13] M.E. Broczkowski, J.J. Noël, and D.W. Shoesmith. The inhibiting effects of hydrogen on the corrosion of uranium dioxide under nuclear waste disposal conditions. *Journal of Nuclear Materials*, 346(1):16–23, nov 2005.

[14] D. Cui, J. Low, C. J. Sjostedt, and K. Spahiu. On Mo-Ru-Tc-Pd-Rh-Te alloy particles extracted from spent fuel and their leaching behavior under Ar and H2 atmospheres. *Radiochimica Acta*, 92(9-11):551–555, 2004.

[15] T Gouder and C Colmenares. Actinide Thin Films on the Electronic Structure and Reactivity of Various Elements. Technical report, 1994.

[16] A. Seibert, S. Stumpf, T. Gouder, D. Schild, and M. A. Denecke. Actinide Thin Films as Surface Models. In *Actinide Nanoparticle Research*, pages 275–313. Springer Berlin Heidelberg, Berlin, Heidelberg, 2011.

[17] T. Gouder. Thin layers in actinide research. *Journal of Alloys and Compounds*, 271-273:841–845, jun 1998.

[18] J. R. Naegele and J. Ghijsen. Localisation and hybridisation of 5f states in the metallic and ionic bond as investigated by photo- electron spectroscopy. In L. Manes, editor, *Actinides—chemistry and physical properties, structure and bonding*, page 197. Springer, Berlin, 1985.

[19] C.A. Colmenares. Oxidation mechanisms and catalytic properties of the actinides. *Progress in Solid State Chemistry*, 15(4):257–364, jan 1984.

[20] B. W. Veal and D. J. Lam. X-ray photoelectron studies of thorium, uranium, and their dioxides. *Physical Review B*, 10(12):4902–4908, 1974.

[21] J. C. Fuggle, A. F. Burr, L. M. Watson, D. J. Fabian, and W. Lang. X-ray photoelectron studies of thorium and uranium. *Journal of Physics F: Metal Physics*, 4:335, 1974.

[22] P. R. Norton, R. L. Tapping, D. K. Creber, and W. J. L. Buyers. Nature of the 5f electrons in uranium nitride: A photoelectron spectroscopic study of UN, U, UO2, ThN, and Th. *Physical Review B*, 21(6):2572–2577, 1980.

[23] C.A. Colmenares. The oxidation of thorium, uranium, and plutonium. *Progress in Solid State Chemistry*, 9:139–239, jan 1975.

[24] W. Mclean, C. A. Colmenares, and R. L. Smith. Electron-spectroscopy studies of clean thorium and uranium surfaces. Chemisorption and initial stages of reaction with O2, CO, and CO2. *Physical Review B*, 25(1):8–24, 1982.

[25] G. C. Allen, J. A. Crofts, M. T. Curtis, P. M. Tucker, D. Chadwick, and J. P. Hampson. X-Ray photoelectron spectroscopy of some uranium oxide phases. *Journal of Chemical Society, Dalton Transactions*, (12):1296–1301, 1974.

[26] T. Gouder, C. Colmenares, J. R. Naegele, and J. Verbist. Study of the surface oxidation of uranium by UV photoemission spectroscopy. *Surface Science*, 235:280–286, 1989.

[27] T. Gouder, A. B. Shick, and F. Huber. Surface Interaction of PuO2, UO2+x and UO3 with Water Ice. *Topics in Catalysis*, 56(12):1112–1120, jul 2013.

[28] M. M. Waite, W. Chester, and D. A. Glocker. Sputtering Sources. *Society of Vacuum Coaters*, pages 42–50, 2010.

[29] F. Miserque, T. Gouder, D. H. Wegen, and P. D W Bottomley. Use of UO2 films for electrochemical studies. *Journal of Nuclear Materials*, 298(3):280–290, 2001.

[30] S. Van den Berghe, F. Miserque, T. Gouder, B. Gaudreau, and M. Verwerft. X-ray photoelectron spectroscopy on uranium oxides: a comparison between bulk and thin layers. *Journal of Nuclear Materials*, 294(1-2):168–174, apr 2001.

[31] A. Seibert, T. Gouder, and F. Huber. Formation and stability of actinide oxides: a valence band photoemission study. *Radiochimica Acta*, 97(4-5):247–250, jan 2009.

[32] A. Seibert, T. Gouder, and F. Huber. Reaction of neptunium with molecular and atomic oxygen: Formation and stability of surface oxides. *Journal of Nuclear Materials*, 389(3):470–478, jun 2009.

[33] T. Gouder, A. Seibert, L. Havela, and J. Rebizant. Search for higher oxides of Pu: A photoemission study. *Surface Science*, 601(14):L77–L80, jul 2007.

[34] R. G. Haire and J. M. Haschke. Plutonium Oxide Systems and Related Corrosio n Products. *MRS bulletin*, 26(9):689–696, 2001.

[35] J. R. Naegele, L. E. Cox, and J. W Ward. Photoelectron spectroscopy (UPS/XPS) study of Np203 formation on the surface of neptunium metal. *Inorganica Chemica Acta*, 139:327–329, 1987.

[36] D.W. Shoesmith. Fuel corrosion processes under waste disposal conditions. *Journal of Nuclear Materials*, 282(1):1–31, nov 2000.

[37] S. Cohen, M.H. Mintz, S. Zalkind, a. Seibert, T. Gouder, and N. Shamir. Water chemisorption on a sputter deposited uranium dioxide film — Effect of defects. *Solid State Ionics*, 263:39–45, oct 2014.

[38] H. Idriss. Surface reactions of uranium oxide powder, thin films and single crystals. *Surface Science Reports*, 65(3):67–109, mar 2010.

[39] A. Seibert, T. Gouder, and F. Huber. Interaction of PuO 2 thin films with water. *Radiochimica Acta*, 98(9-11):647–657, nov 2010.

[40] A. Seibert, D.H. Wegen, T. Gouder, J. Römer, T. Wiss, and J.-P. Glatz. The use of the electrochemical quartz crystal microbalance (EQCM) in corrosion studies of UO2 thin film models. *Journal of Nuclear Materials*, 419(1-3):112–121, dec 2011.

[41] S. Stumpf, a. Seibert, T. Gouder, F. Huber, T. Wiss, and J. Römer. Development of fuel-model interfaces: Investigations by XPS, TEM, SEM and AFM. *Journal of Nuclear Materials*, 385(1):208–211, mar 2009.

[42] D. W. Shoesmith, S. Sunder, M. G. Bailey, and G. J. Wallace. The Corrosion of Nuclear Fuel (UO2) in Oxygenated Solutions. *Corrosion Science*, 29(9):1115–1128, 1989.

[43] S. Sunder, D. W. Shoesmith, M. G. Bailey, F. W. Stanchell, and N. S. McIntyre. Anodic oxidation of UO2 Part I. Electrochemical and X-Ray Photoelectron spectroscopic studies in neutral solutions. *Journal of Electroanalytical Chemistry*, 130:163–179, 1981.

[44] S. Sunder, D.W Shoesmith, and N.H Miller. Oxidation and dissolution of nuclear fuel (UO2) by the products of the alpha radiolysis of water. *Journal of Nuclear Materials*, 244(1):66–74, 1997.

[45] T. E. Eriksen, D. W. Shoesmith, and M. Jonsson. Radiation induced dissolution of UO2 based nuclear fuel – A critical review of predictive modelling approaches. *Journal of Nuclear Materials*, 420(1-3):409–423, jan 2012.

[46] T. W. Trelenberg, S. C. Glade, J. G. Tobin, and a. V. Hamza. The production and oxidation of uranium nanoparticles produced via pulsed laser ablation. *Surface Science*, 600:2338–2348, 2006.

# 2

# AN XPS AND UPS STUDY ON THE ELECTRONIC STRUCTURE OF $ThO_x$ ($x \leq 2$) THIN FILMS

**Pelin CAKIR, Rachel ELOIRDI, Frank HUBER, Rudy J. M. KONINGS, Thomas GOUDER**

*Model systems are needed for surface corrosion studies of spent nuclear oxide fuels. For this purpose, $ThO_2$ films have been prepared in-situ by adsorption of molecular and atomic oxygen on Th metal films, and by sputter deposition of Th metal in an $Ar/O_2$ gas mixture. Surface compositions and electronic structure were compared to the bulk oxide and oxygen sub-stoichiometry effects investigated. X-ray and Ultraviolet photoemission spectroscopy (XPS and UPS, respectively) were used to measure to Th-4f, O-1s core levels and the valence band region. The Th-4f line was analysed in terms of the final-state screening model. The evolution of the binding energies with oxygen concentration has been studied. On Th metal, adsorption of molecular oxygen ceased after the formation of a $ThO_2$ surface layer. In the presence of atomic oxygen, the oxidation proceeded into the underlying bulk. The formation of oxygen interstitials was shown by the broadening of the O-2p and O-1s lines and by the increase of the O-1s/Th-4f ratio. Once $ThO_2$ is formed, all photoemission peaks from Th and O undergo a rigid shift to low binding energy (BE).*

Parts of this chapter have been published in Journal of Physical Chemistry C **118**, 24497-24503 (2014)[1]

## 2.1. INTRODUCTION

THORIUM is a potential future nuclear fuel [2]. There is a high natural abundance of the fertile $^{232}Th$ isotope. During operation, a smaller fraction of minor actinides is produced as compared to the U cycle [2], so that it is quasi-inert, making it a candidate as an inert matrix to incinerate plutonium stockpiles. In this context, mixed oxides of Th with other actinides are worth being studied. Comparatively little information exists on thorium fuel, compared to uranium fuel forms [3], because thorium based fuels have not been used commercially so far.

One important aspect for the application of nuclear fuels is the long-term stability of the waste. It depends on the resistance of the waste surface toward corrosion and dissolution in contact with groundwater [4]. To reach a better understanding and prediction of these processes [5, 6], surface science studies are being conducted, mainly on $UO_2$ fuel [4, 7, 8]. Only a few spectroscopy studies have been performed on (U,Th)$O_2$ [9]. Because of the complexity of spent nuclear fuel, systematic studies of surface reaction mechanisms are difficult but can be realized by studying model systems, which focus on single reaction parameters. Fuel model systems can be prepared as thin films, starting with single actinide oxides, then processing to more complex systems, doping with fission products [10]. Such model films can be prepared by reactive sputtering from a series of elemental targets [11]. Thorium is the only actinide without 5f electrons. Its simplified chemistry, with only two oxidation states (0 and 4), makes it a very interesting reference material, indeed.

In this paper we discuss the preparation of $ThO_2$ films starting from the metal. Surface characterization, focusing on surface composition and electronic structure, is provided by photoemission spectroscopy following the core level Th-*4f* and O-*1s* by XPS and the valence band by UPS. The films are compared to bulk oxide compounds already reported in the literature [12, 13] to ensure that there are no differences and that the films can really be used to model the bulk system. McLean et al. [12] performed an XPS and AES study of the surface oxidation of Th metal by $O_2$, CO, and $CO_2$ while Veal et al. [14] looked at both uranium and thorium as metal and dioxide forms. According to their results, the O-*2p* valence band spectra of $UO_2$ and $ThO_2$ are similar, but the 5f electron occupancy in $UO_2$ causes the difference between the two oxides, in particular electrical conductivity, color, and magnetism. Resonant photo- emission spectra of the $ThO_2$ valence band have been compared to LMTO DOS calculations [15]. It was shown that there is a strong hybridization between O-*2p* and Th-*6d* orbitals. Riviera [16] reported the surface potential of thorium films during the exposure of oxygen. His study shows that, once the surface of the film converted to $ThO_2$, oxygen does not diffuse into the metal further.

This paper is divided into two sections. First we investigate the reaction of the surface of thorium metal with oxygen, when exposed to molecular and atomic oxygen. Then, in a second part, we study the deposition of thin films of $ThO_2$ by argon sputtering in the presence of $O_2$. We follow the effect of the oxygen partial pressure on the surface oxidation and electronic structure of the sample. Possible oxygen off-stoichiometry (vacancies or interstitials) are investigated because they often are at the origin of enhanced reactivity. Substoichiometry oxides simulate oxygen vacancies. Their formation is tested by depositing Th in the presence of low oxygen partial pressure. Thorium cannot ox-

idize beyond $Th^{4+}$ because it possesses only four valence electrons ([Rn] $6d^2 7s^2$), and supplementary surface oxygen cannot be incorporated into the lattice. We tested the accumulation of surface oxygen by chemisorption. While many surface characterization studies have been reported on $UO_2$ thin films [17–20], it was important to report the first equivalent study on $ThO_2$ thin films, which will be used as a reference for a forthcoming study on (U,Th)$O_2$ films. The results obtained on ThOx thin films are compared to those obtained previously on $UO_x$ thin films.[17–19]



## 2.2. EXPERIMENTAL

The thin films of thorium metal and thorium oxide $ThO_x$ ($x \leq 2$) were prepared in situ by direct current sputtering from a thorium metal target in Ar (6 N) and in a gas mixture of Ar (6 N) and $O_2$ (6 N), respectively. The oxygen concentration in the films was varied by adjusting the $O_2$ partial pressure ($10^{-8}$- $8 \times 10^{-7}$ mbar), while the Ar pressure was maintained at $5 \times 10^{-7}$ mbar. The thorium target voltage was fixed at -700 V. The thin films were deposited at a rate of about 1 Å/s for 120 s at room temperature on a silicon wafers (111), which have been cleaned by Ar ion sputtering (4 keV) for 10 min, and subsequently annealed at 773 K for 5 min. The plasma in the diode source was maintained by injection of electrons (50-100 eV; triode setup) to work at low Ar pressure in the absence of stabilizing magnetic fields. Atomic oxygen was produced by an electron cyclotron resonance (ECR) Plasma Source Gen I from Tectra GmbH, Frankfurt/M. The atom flux is specified as $>10^{16}$ atoms $cm^{-2}$ s, corresponding to an exposure of roughly 10 langmuirs/s (i.e., $10^{-5}$ mbar of O). After deposition, the thin films were transferred to the XPS-UPS analysis chamber via an interlock without exposing them to air.

Photoelectron spectroscopy data were recorded using a hemispherical analyzer from Omicron (EA 125 U5). The spectra were taken using Mg K$\alpha$ (1253.6 eV) or Al K$\alpha$ (1486.6 eV) radiation with an energy resolution of ~1 eV. A few high- resolution XPS spectra were taken with a SPECS EA300 hemispherical analyzer using monochromated Al K$\alpha$ radiation, yielding an energy resolution of 0.4 eV. UPS measurements were made using He *II* (40.81 eV) and He *I* (21.22 eV) radiation produced by a high-intensity windowless UV rare gas discharge source (SPECS UVS 300). The total resolution in UPS was 0.1-0.05 eV for the high-resolution scans. The background pressure in the analysis chamber was $2 \times 10^{-10}$ mbar. The spectrometers was calibrated by using metallic Au-$4f_{7/2}$ at 83.9 eV BE and metallic Cu-$2p_{3/2}$ at 932.7 eV BE for XPS and on He *I* and He *II* Fermi edges for UPS. Photoemission spectra were taken at room temperature. The O/Th concentration ratio was determined by the ratio of the O-*1s*/Th-$4f_{7/2}$ surface areas, corrected by the atomic sensitivity factors [21]. The Th-*4f* and O-*1s* spectra were fitted by simple Gaussian functions. The inelastic background was subtracted by the Shirley algorithm [22]. The following equation has been used [23]:

$$\frac{n_O}{n_{Th}} = \frac{I_O/S_O}{I_{Th}/S_{Th}}$$

where n is the atomic concentration, I is the surface area of the main peak, O-1s and Th-$4f_{7/2}$, and S is the atomic sensitivity factor of 0.66 and 7.8 for O-*1s* and Th-$4f_{7/2}$, respectively.

An uncertainty of ±10 % must be expected using tabulated values instead of internal references [23].

The X-ray diffraction analyses were made on a conventional Phillips PW3830 powder diffractometer with a Cu anode ($K\alpha_1$ = 0.154056 0 nm). Films of about 360 nm thicknesses were deposited (1 Å/s) at 100 °C on a Si (111) wafer and at room temperature on a Si (100) wafer.



## 2.3. Results and Discussion

### 2.3.1. Oxygen Adsorption on Th Metal Film

Initial Th metal films were produced by sputtering Th onto a Si (111) substrate. The films were then exposed at room temperature to molecular oxygen until saturation and then to atomic oxygen. Figure 2.1 shows the corresponding Th-*4f* core level spectra.

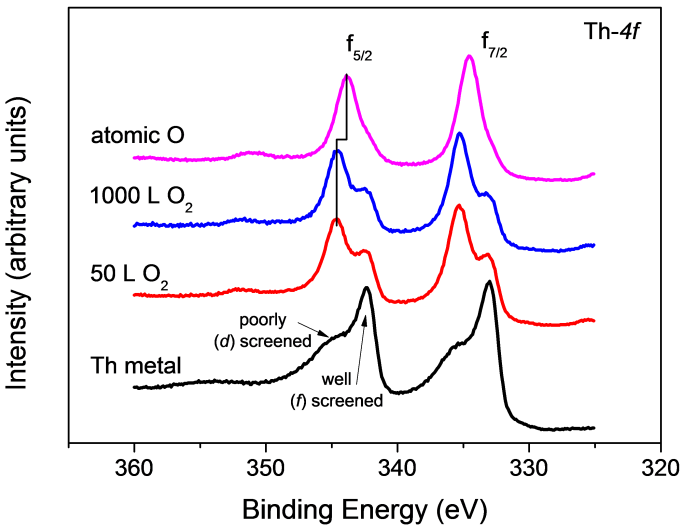


Figure 2.1: Th-*4f* spectra for Th metal film and after exposure to molecular and atomic oxygen.

They are split into the $4f_{5/2}$ and $4f_{7/2}$ components with a BE in the metal of 342.4 and 333.1 eV, respectively. Each peak has two components, associated with two different final states [24, 25]. The well-screened peak (at low binding energy) corresponds to the final state where the 4f core hole of the ionized atom is screened by the population of a 5f-state, called f-screening. The poorly screened peak (at high binding energy) corresponds to the d-screened final state [20]. The well-screened peak occurs in the metal, while in $ThO_2$ oxide, the f-states become so high in energy that they no longer participate in the screening [20, 26].

After an exposure of 50 langmuirs of molecular oxygen (1 langmuir = 1 s x $10^{-6}$ Torr would provide one monolayer of gas particles, if the sticking probability is one) the poorly screened peak becomes dominant at the expense of the well- screened peak, the intensity of which decreases (Figure 2.1). The spectra are the same after exposure of 50 and

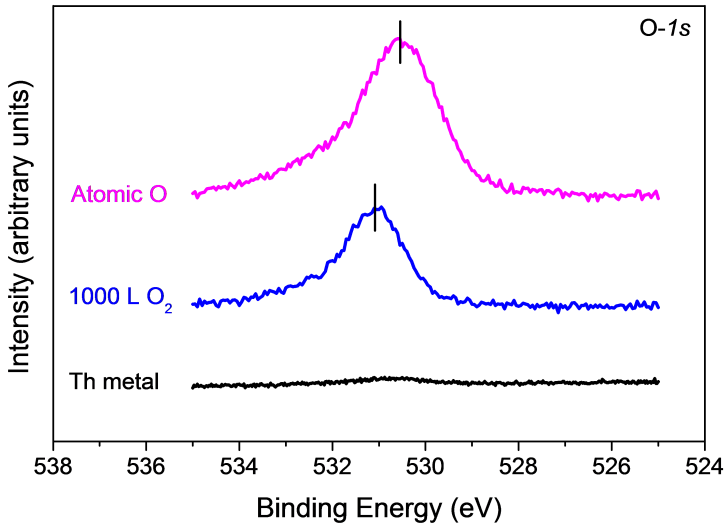


Figure 2.2: O-*1s* spectra of Th metal film and after exposure to molecular.

1000 langmuirs of $O_2$, showing the surface to be saturated. The presence of the well-screened peak indicates the contribution of the metal underneath the oxide layer. Indeed, the 4f spectrum of $ThO_2$ has only one component: the poorly (d) screened peak [20]. Quite remarkably, the 4f level of $ThO_2$ (in the presence of the metal) has the same binding energy as the poorly screened peak of the metal: as displayed in Figure 2.1, there is no shift to higher binding energy, which one would expect after oxidation [27]. The chemical shift links the binding energy to the oxidation state [22], but this relation is not universal, and notably in the heavier actinides Am [28] and Cm [13, 29], the oxides have the same or even lower core level binding energies than the metal. In all these cases, metal and oxide have the screening type (d-screening), and f-screening is minor either because the f-peak is too high in energy (Th) or because it is localized (Am, Cm) [13].

The spectrum after exposure to molecular oxygen (Figure 2.1, red and blue curve) still shows some metal left (at the position of the (f) screened peak). Oxidation is not complete in the region probed by XPS, which obtains a signal not only from the surface but also from deeper layers, which remain still metallic. The top surface, roughly estimated to 4.7 monolayers in our experimental conditions, is completely oxidized, and and on this surface, the dissociation of molecular oxygen is inhibited slowing down the diffusion through the oxide layer. Similar saturation after fast initial reaction has been observed for U metal [12, 30]. After exposure to atomic oxygen (Figure 2.1, purple curve), the f-screened peak disappears completely, indicating all metal is oxidized to the depth probes by XPS. Atomic oxygen adsorbs on the oxide and subsequently diffuses through the oxide layer and reacts with the metal below. Thus, the rate- limiting step in the formation of the thin $ThO_2$ layers is the dissociation of molecular oxygen, not the bulk dif-

fusion. After reaction with atomic oxygen the (d-screened) 4f peak shifts to lower binding energy. We will discuss this below.

In the study by Riviere [16] on the surface potential of oxygen on thorium using the Kelvin method, it was reported that oxygen incorporation in the metallic lattice takes place before transformation of the saturated surface layers into $ThO_2$. Further oxygen cannot dissolve in $ThO_2$ as it does in $UO_2$ and it does not chemisorb on the $ThO_2$ surface at room temperature, so that, once the surface is saturated, oxygen diffusion into the bulk stops. The oxygen can reach the underlying metal by a mechanism of exchange with vacancies and not by interstitial diffusion. Part of this analysis is supported by the present study. Indeed, $O_2$ adsorbs on the Th metal surface transforming it into $ThO_2$, covering the Th metal underneath. Then $O_2$ adsorption stops. Atomic oxygen continues to adsorb and diffuse into the bulk, oxidizing the metal into $ThO_2$.

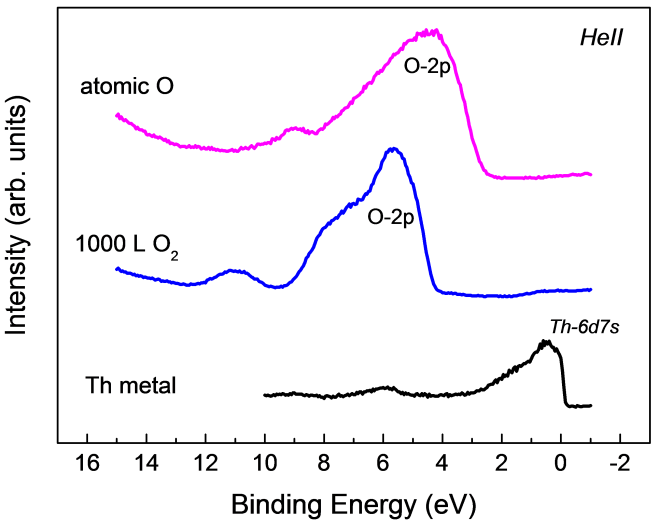


Figure 2.3: He*II* spectra for Th metal film and after exposure to molecular (bottom) and atomic oxygen (top).

The O-*1s* spectra after exposure to molecular and atomic oxygen are shown in Figure 2.2. Exposure to molecular oxygen leads to a sharp O-*1s* peak with a maximum at 531 eV BE and a weak shoulder at 532.5 eV. After exposure to atomic oxygen, the peak broadens considerably and higher BE component increases, which indicate chemisorption of oxygen at the surface because in this chemical form solid state relaxation is less strong [31, 32]. This does not mean further oxidation of Th because similar adsorption was observed for MgO [33–35], which cannot oxidize beyond $Mg^{2+}$ and where the oxygen atoms bond to surface oxygen anions (in $O\text{-}O^-$ entities). The broadening of the peak, too, may be explained by oxygen build-up, resulting in nonequivalent surface oxygen atoms. The O-*1*s/Th-*4f* intensity ratio increases from 0.147 after molecular oxygen exposure to 0.201 after atomic oxygen. This increase indicates accumulation of oxygen, going from

oxygen-deficient stoichiometry, formally ($ThO_{1.73}$), to oxygen-rich stoichiometry, formally ($ThO_{2.37}$), thorium oxide. $ThO_{2.37}$ is not a stable oxide, but this overstoichiometry is due to atomic oxygen chemisorbed on the surface. In addition, the film composition has been determined using general XPS sensitivity factors. Thus, an uncertainty of not better than 10 % should be considered [36].

After exposure to atomic oxygen, the O-*1s* shifts to lower BE. Th-*4f* undergoes the same shift (see Figure 2.1). So it is not a true chemical shift of one species in the crystal. A similar rigid shift has been observed in $UO_2$ upon surface oxidation, when the Fermi energy decreases due to charge carrier depletion [37, 38] or to adsorbate induced band bending at the surface [39]. Since all photoemission lines in the (conductive) solid are referenced to the Fermi energy, a shift of the Fermi-level toward the core levels is seen as a coherent shift of all core-level lines to lower binding energy. $ThO_2$ is an insulator, but the thickness of the oxide layer (~120 Å) seems small enough to allow electrons to tunnel through. Therefore, the Fermi level is still defined and the thin surface oxide film does not experience charging upon photoemission [32].

The He *II* valence band spectra (Figure 2.3) allow studying the electrons levels participating in the oxidation process. The metal film has a peak ranging from the Fermi level to 3 eV BE and corresponding to the Th-*6d7s* conduction band. After 1000 langmuirs of $O_2$, this peak totally disappears, and the O-*2p* valence band appears between 4 and 10 eV. As Th oxidizes to $ThO_2$, the 6d7s electrons are transferred into the O-*2p* band, leaving no states at the Fermi level. The high BE shoulder of the O-*2p* (8-9 eV) corresponds to the bonding part of the band, formed by Th-*6d* states hybridized with O-*2p* states. The maximum at low BE (5-6 eV) corresponds to the nonbonding part of the band [40]. In contrast to the Th-*4f* spectra, the oxidation observed in He *II* is complete and no trace of underlying metal is observed. The He *II* spectra are more surface sensitive than the 4f (the inelastic mean free path is 1 instead of 5 layers [41]), and this confirms that the residual metal signal in the 4f data indeed came from deeper levels, and not from an incomplete reaction in the upper layers. The small signal at 11 eV comes from a small OH contamination, likely to be produced by water desorbed from the chamber walls. A shift of about 1.2 eV to lower binding energy is observed after exposure of the surface to atomic oxygen. As for the core level, it is attributed to the decrease of the Fermi energy concomitant with slight increase of the oxygen concentration. The O-*2p* is broadened, with supplementary intensity appearing at the high BE side, which is explained by supplementary oxygen, chemisorbed on the surface. It appears at high BE because of the lower relaxation energy available for chemisorbed species (less coordination).

Such oxygen is more visible in the surface sensitive UPS-He *II* spectra than in the bulk spectra, therefore the buildup of intensity at the high BE side is more pronounced than for the O-*1s* line.

### 2.3.2. REACTIVE DC SPUTTERING OF $ThO_x$ ($0 \leq x \leq 2$) THIN FILMS

Sputter deposition has been also used to prepare thin oxide films. In contrast to the previous method, there is no concentration gradient between the reacted surface and the bulk, but the films are homogeneous in composition. Thorium is sputtered from a thorium metal target in an $Ar/O_2$ gas mixture. Oxygen reacts with the metal atoms on the target, in the plasma and on the substrate. The oxygen composition of the film depends

on the oxygen partial pressure in the chamber.

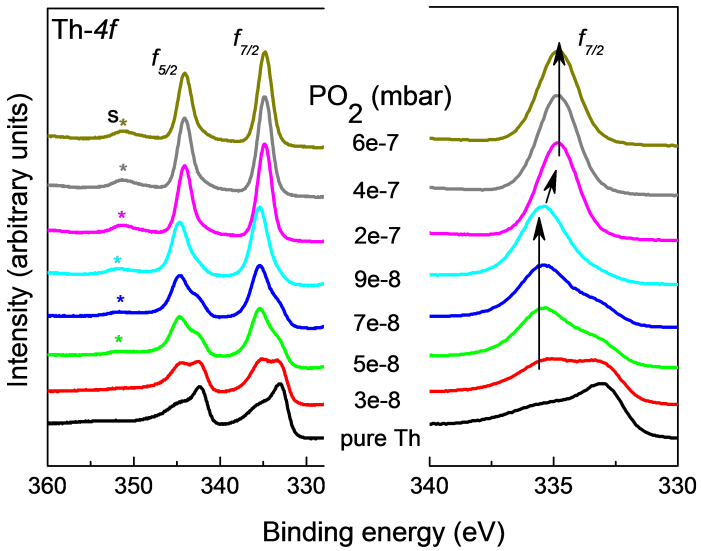


Figure 2.4: Left: Th-*4f* core level spectra of $ThO_x$ ($0 \leq x \leq 2$) thin films versus $O_2$ partial pressure Right: zoom on corresponding Th-$4f_{7/2}$ core level spectra

Figure 2.4 shows the Th-*4f* core level spectra of $ThO_x$ at different $O_2$ partial pressures. In Figure 2.4 left, the spin-orbit split $4f_{7/2}$ and $4f_{5/2}$ peaks can be followed, together with the appearance of a shakeup satellite peak(s) at 7.1 eV higher binding energy than the main peaks. Figure 2.4 right focuses on the Th-$4f_{7/2}$ component to emphasize the evolution of the peak shape and binding energy with oxygen partial pressure. As for $O_2$ adsorption, the f-screened component at low binding energy decreases with increasing oxygen pressure, as the Th metal consumes. The high BE component, consisting of the d-screened metal and oxide peak increases in intensity, replacing the f-screened peak completely at 9 x $10^{-8}$ mbar of $O_2$. Once all metal has reacted, the oxide line shifts to lower binding energy by about 0.7 eV (from 335.4 to 334.7 eV).

Figure 2.5 shows the spectrum of $ThO_2$ thin films obtained with a monochromated Al K$\alpha$ source. The main lines are accompanied by two satellites at 7.5 and 15 eV, appearing at higher binding energy than the $f_{5/2}$ and $f_{7/2}$ peaks. The $f_{5/2}$ component is compared to a REELS (reflection electron energy loss spectroscopy) spectrum obtained with a primary electron beam of 1000 eV. The REELS spectrum indicates a band gap in the $ThO_2$ thin film of about 5.2 eV, which lies in the energy range reported for $ThO_2$ bulk (3.4-5.7 eV) [16]. It also shows a plasmon loss feature at 15 eV and a weaker loss at 10 eV (associated with a surface plasmon: $\omega_s = \omega_b / \sqrt{2}$). The main Th-*4f* satellite at 7.4 eV higher BE than the main line is not a plasmon feature, but either a shake-up or a final-state satellite [42].

The Fermi level shift of 0.7 eV observed at the formation of $ThO_2$ is smaller than the

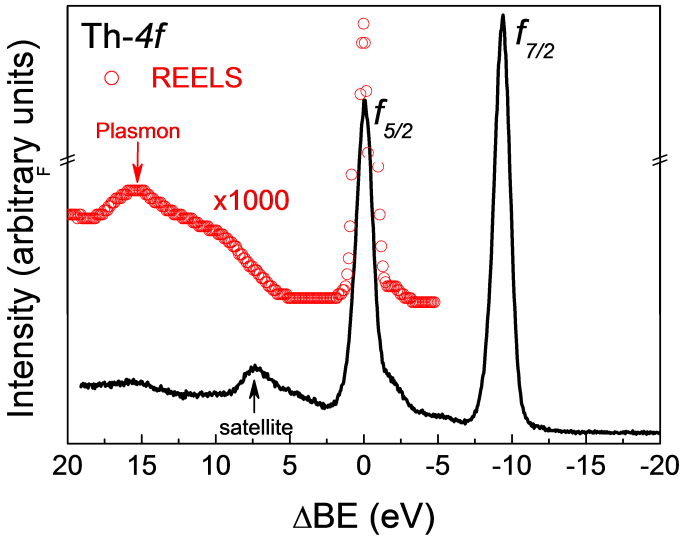


Figure 2.5: Th-*4f* core level spectra of $ThO_2$ thin film and superposition of corresponding plasmon signal measured by REELS. For better comparison, the spectra of Th-*4f*, normalized on the $4f_{5/2}$ component, and REELS are superimposed at same binding energy.

band gap measured by REELS. A similar observation has been reported for $UO_2$ thin film [18]. This has been related to the defects present in the layers produced by dc sputtering, pinning the Fermi level between the valence band and the conduction band. Thus, the Fermi level shift and the band gap cannot be correlated. The band gap for $UO_2$ was determined to be 2.1-2.7 eV [14, 44], which is smaller than the value found in this study for $ThO_2$ film and would be expected by the stronger insulator properties of $ThO_2$.

The O-*1s* spectra of the $ThO_x$ ($0 \leq x \leq 2$) thin films are displayed in Figure 2.6. For pure Th metal, the oxygen peak can be hardly seen, which demonstrates the good sample purity. With increasing oxygen partial pressure the O-*1s* intensity increases. It first shifts to higher binding energy by 1.4 eV, and then at $9 \times 10^{-8}$ mbar of $O_2$, it suddenly shifts back to low binding energy (by 0.7 eV), just as the Th-*4f* oxide peak (see above). The low BE shift occurs at the same oxygen pressure, i.e., once all metal contribution has disappeared. The shape of the peaks is highly symmetric and can be related to the good homogeneity of the films produced by dc sputtering.

Table 2.1 compares the binding energy of the thorium and oxygen core level obtained for $ThO_2$ thin film to the bulk values, obtained in this study and in the literature [14, 43]. The values are in a good agreement emphasizing the interest and the capacity of using thin films as model for bulk samples.

Figure 2.7 shows He *II* valence band spectra of $ThO_x$ ($x \leq 2$) thin films deposited at increasing $O_2$ partial pressure. Th metal has a broad peak from 3 to 0 eV, attributed to the 6d7s conduction band. The small peak around 6 eV is due to the O-*2p* emission of a

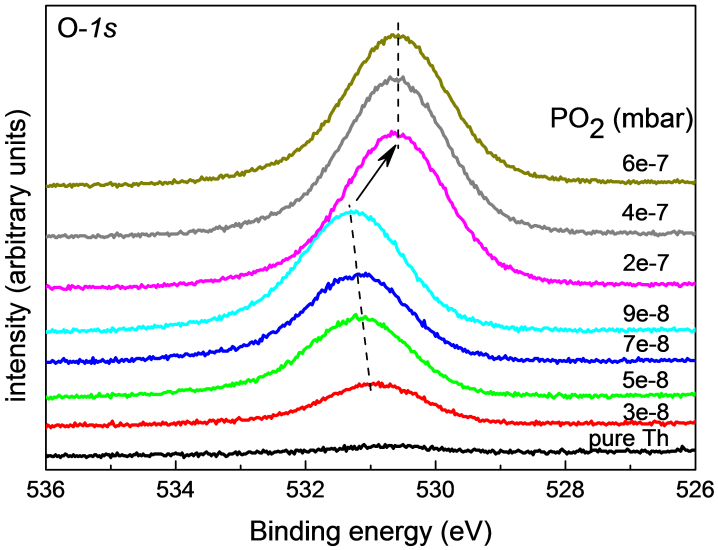


Figure 2.6: O-*1s* core level spectra as a function of $O_2$ partial pressure.

small oxygen contamination at the surface. With increasing $O_2$ pressure the conduction band peak decreases while the O-*2p* valence band peak grows between 5 and 9 eV. At 9 × $10^{-8}$ mbar of $O_2$, when all metal disappears (the emission at the Fermi level vanishes) the O-*2p* peak shifts to lower BE. This is the same shift as for the Th-*4f* and O-*1s* core level spectra, discussed earlier in this paper. The valence band spectra prove it to be associated with the disappearance of the metal. Upon increasing oxygen concentration, the Th-*6d7s* conduction band narrows (Figure 2.7, right). A similar narrowing has been observed for other valence and conduction band peaks upon dilution of metals in a host matrix, e.g., for U diluted in the weakly interacting Ag matrix [45], of Au diluted in Ag [46]. Conversely, the O-*2p* line width of oxygen chemisorbed on metal surfaces increases with surface oxygen concentration. In all these case decrease of the spectral line width seems to reflect the narrowing of the bandwidth, due to spatial restriction or atomic isolation. In the present case a similar isolation of Th in the $ThO_2$ matrix would lead to a narrowing of the Th-*6d7s* band. Oxide formation does not proceed via island growth (leaving large areas of metal unchanged) but proceeds homogeneously on the entire surface, disrupting the metal - metal bond.

In Figure 2.8, we report the X-ray diffraction pattern of a $ThO_2$ film obtained by dc sputtering and deposited on Si (111) at 100 °C. The (111) peak of Si is used as internal reference and despite the film thickness; we consider the sample height relatively to the Si surface negligible. The lattice parameter is calculated from the peak positions adjusted after the (111) Si peak was corrected to $2\theta$ 28.44° [47] and obtained after extrapolation of a = f($\sin^2\theta$). The pattern shows a polycrystalline structure corresponding to the cubic crystal structure expected for $ThO_2$ with a lattice parameter of a = 5.61 Å, which is very

Table 2.1: Binding Energy of Th-*4f* and O-*1s*, Peak Width, and Satellite Position Relatively to Main Peak Th-$4f_{7/2}$ Measured for $ThO_2$ Film and Bulk of This Study and Compared to Literature Data

| | This study | | Literature |
|---|---|---|---|
| | thin fim | bulk | bulk |
| Th-$4f_{7/2}$ | 334.8 | 334.5 | 334.6[14] 334.9[43] |
| fwhm | 1.85 | 2.32 | 1.8[14] |
| Th-$4f_{5/2}$ | 344.0 | 343.7 | 343.9[14] |
| satellite | 7.3 | 7.6 | 7.3[14], 6.9[43] |
| O-*1s* | 530.6 | 530.4 | |

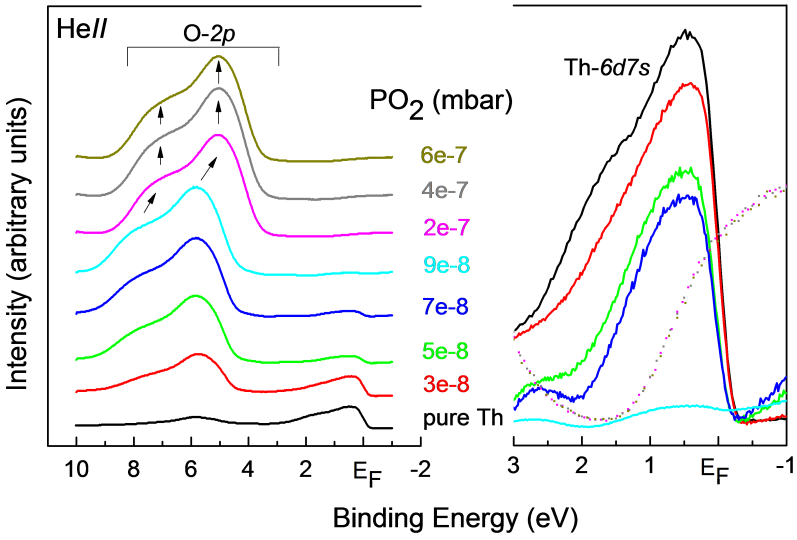


Figure 2.7: Left: He*II* spectra $ThO_x$ ($0 \leq x \leq 2$) thin films versus $O_2$ partial pressure. Right: superposition of density of states of $ThO_x$ ($0 \leq x \leq 2$) at Fermi level.

close with the bulk lattice parameter, a = 5.598 Å [48]. In the inset in Figure 8 the deposition of $ThO_2$ on Si (100) at room temperature is reported, and here we can see an epitaxial growth of the film along the direction (400). As reported for the deposition of UN films [49], the microstructure of the sample is depending on the conditions of deposition, for instance the gas partial pressure, the temperature, and time of deposition. This has been the subject of complete experiments presented in the literature [42, 50], and this is out of the frame of the present study on the electronic structure, which is independent of

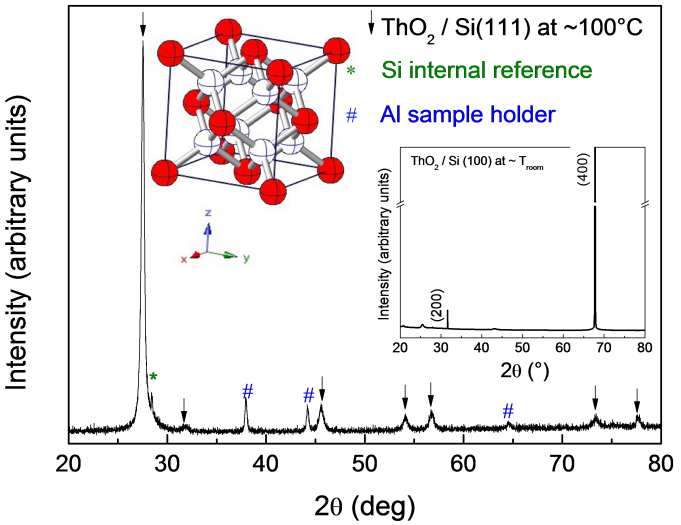


Figure 2.8: X-ray diffraction pattern of $ThO_2$ thin film deposited on Si(111) wafer at 100 °C and in inset on Si(100) at room temperature. Crystallographic structure of $ThO_2$.

the microstructure. However, this aspect is important due to its influence on the electrochemical behavior. Before to study the corrosion properties of $ThO_2$ and (U,Th)$O_2$ films, it is important to characterize their polycrystalline character to be representative as model of the fuel. The use of thin films as model for bulk fuel has the advantages that a large range of microstructure can be obtained going from single crystal to polycrystal, simulating different aspect of the nuclear fuel properties.

## 2.4. CONCLUSION

We have studied the formation and electronic structure of thin films of Th oxides using X-ray and ultraviolet photoemission spectroscopy. Thin films were prepared by exposing metal surfaces to oxygen or by depositing Th in the presence of oxygen (reactive sputtering).

When exposed to molecular oxygen, the thorium metal surface oxidizes quickly reaching saturation, while the subsurface stays metallic, with a characteristic Th-*4f* signal. The saturated surface reacts further with atomic oxygen, and eventually the bulk metal is transformed into oxide at room temperature. It is concluded that molecular oxygen does not dissociate on the oxide while atomic oxygen is still capable of adsorbing and diffusing into the bulk. Atomic oxygen adsorption broadens the O-*2p* valence band. All photoemission peaks underwent a rigid shift to low binding energy, which is consistent with the formation of $O^{2-}$ surface atoms.

Thin films of $ThO_x$ ($0 \leq x \leq 2$) were also produced by dc sputtering in Ar plasma with

the presence of $O_2$. The film was continuously oxidized during formation, and there was no oxygen concentration gradient between surface and bulk. The Th-*4f* core level spectrum could be fitted by two peaks corresponding to f-screened and d-screened peak. While the f-screened peak is the main peak for the thorium metal, its BE shifts and its intensity decreases at the expense of the d-screened peak which is the main peak in $ThO_2$. The Th-*4f* and O-*1s* peaks both increase to higher binding energy until an O/Th ratio of about 2 and then drop suddenly to a lower and constant energy corresponding to the formation of $ThO_2$ which cannot further oxidized. The sudden drop of the binding energy observed for $ThO_2$ thin film is also attributed to the decrease of the Fermi energy. The advantage of working with thin films is that it avoids the charging effect which is observed on isolating bulk material.



Deposition of $ThO_2$ thin film on Si(111) wafer at 100 °C enable to produce a polycrystalline film with a preferential orientation along the $ThO_2$ (111) direction as demonstrated by X-ray diffraction. When the deposition is made at room temperature, an epitaxial growth takes place along the orientation of the support. It is apparent from these results that this method of using of actinide oxide thin films can be used for surface characterization and analysis without having pellets and bulk materials.

## REFERENCES

[1] Pelin Cakir, Rachel Eloirdi, Frank Huber, Rudy J M Konings, and Thomas Gouder. An XPS and UPS Study on the Electronic Structure of ThO x ( x <= 2 ) Thin Films. *Journal of Physical Chemistry C*, 118:24497–24503, 2014.

[2] IAEA. Role of Thorium to Supplement Fuel Cycles of Future Nuclear Energy Systems, IAEA Nuclear Energy Series. Technical report, 2012.

[3] Douglas C. Crawford, Douglas L. Porter, and Steven L. Hayes. Fuels for sodium-cooled fast reactors: US perspective. *Journal of Nuclear Materials*, 371(1-3):202–231, sep 2007.

[4] M.N. Hedhili, B. V. Yakshinskiy, and T. E. Madey. Interaction of water vapor with UO2 ( 001 ). *Surface Science*, 445:512–525, 2000.

[5] Horst Geckeis and Thomas Rabung. Actinide geochemistry: from the molecular level to the real system. *Journal of contaminant hydrology*, 102(3-4):187–95, dec 2008.

[6] Jae-il Kim. Significance of actinide chemistry for the long-term safety of waste disposal. *Nuclear Engineering and Technology*, 38(6):459–482, 2006.

[7] G. C. Allen, P. M. Tucker, and J. W. Tyler. Oxidation of uranium dioxide at 298 K studied by using X-ray photoelectron spectroscopy. *Journal of Physical Chemistry*, 86(2):224–228, 1982.

[8] K. Winer, C. A. Colmenares, R. L. Smith, and F. Wooten. Interaction of water vapor with clean and oxygen-covered uranium surfaces. *Seminars in thoracic and cardiovascular surgery. Pediatric cardiac surgery annual*, 183:67–99, jan 1987.

[9] S. Sunder and N.H. Miller. XPS and XRD studies of (Th,U)O2 fuel corrosion in water. *Journal of Nuclear Materials*, 279(1):118–126, mar 2000.

[10] S. Stumpf, A. Seibert, T. Gouder, F. Huber, T. Wiss, J. Römer, and M.A. Denecke. Development of fuel-model interfaces: Characterization of Pd containing UO2 thin films. *Journal of Nuclear Materials*, 397(1-3):19–26, feb 2010.

[11] T. Gouder. Thin layers in actinide research. *Journal of Alloys and Compounds*, 271-273:841–845, jun 1998.

[12] W. Mclean, C. A. Colmenares, and R. L. Smith. Electron-spectroscopy studies of clean thorium and uranium surfaces. Chemisorption and initial stages of reaction with O2, CO, and CO2. *Physical Review B*, 25(1):8–24, 1982.

[13] B.W. Veal, D.J. Lam, H. Diamond, and H. R. Hoekstra. X-ray photoelectron-spectroscopy study of oxides of the transuranium elements Np, Pu, Am, Cm, Bk, and Cf. *Physical Review B*, 15(6):2929–2942, 1977.

[14] B. W. Veal and D. J. Lam. X-ray photoelectron studies of thorium, uranium, and their dioxides. *Physical Review B*, 10(12):4902–4908, 1974.

[15] W P Ellis, A M Boring, J W Allen, L E Cox, R D Cowan, A J Arko, Los Alamos, and Ann Arbor. Valance-Band Photoemission Intensities in thorium dioxide. *Solid State Communications*, 72(7):725–729, 1989.

[16] J. C. Riviere. The surface potential of oxygen on thorium. *Brit. J. Appl. Phys.*, 16:1507, 1965.



[17] Z. Bao, R. Springell, H. C. Walker, H. Leiste, K. Kuebel, R. Prang, G. Nisbet, S. Langridge, R. C. C. Ward, T. Gouder, R. Caciuffo, and G. H. Lander. Antiferromagnetism in UO_{2} thin epitaxial films. *Physical Review B*, 88(13):134426, oct 2013.

[18] F. Miserque, T. Gouder, D. H. Wegen, and P. D W Bottomley. Use of UO2 films for electrochemical studies. *Journal of Nuclear Materials*, 298(3):280–290, 2001.

[19] S. Van den Berghe, F. Miserque, T. Gouder, B. Gaudreau, and M. Verwerft. X-ray photoelectron spectroscopy on uranium oxides: a comparison between bulk and thin layers. *Journal of Nuclear Materials*, 294(1-2):168–174, apr 2001.

[20] S. Stumpf, a. Seibert, T. Gouder, F. Huber, T. Wiss, and J. Römer. Development of fuel-model interfaces: Investigations by XPS, TEM, SEM and AFM. *Journal of Nuclear Materials*, 385(1):208–211, mar 2009.

[21] C. D. Wagner, L. E. Davis, M. V. Zeller, J. a. Taylor, R. H. Raymond, and L. H. Gale. Empirical atomic sensitivity factors for quantitative analysis by electron spectroscopy for chemical analysis. *Surface and Interface Analysis*, 3(5):211–225, oct 1981.

[22] D. A. Shirley. High-Resolution X-Ray Photoemission Spectrum of the Valence Bands of Gold. *Physical Review B*, 5(12):4709–4714, 1972.

[23] M P Seah. The Quantitative Analysis of Surfaces by XPS : A Review. *Surface and Interface Analysis*, 2(6):222–239, 1980.

[24] O. Gunnarsson, D. D. Sarma, F. U. Hillebrecht, and K. Schonhammer. Electronic structure of the light actinide oxides from electron spectroscopy (invited). *Journal of Applied Physics*, 63(8):3676, 1988.

[25] Kevin T. Moore and G. van der Laan. Nature of the 5f states in actinide metals. *Reviews of Modern Physics*, 81(1):235–298, feb 2009.

[26] S Hufner and G K Wertheim. Systematic of core line asymmetries in XPS spectra of Ni. *Physics Letters*, 51A(5):301–303, 1975.

[27] C.C. Chusuei and D. W. Goodman. X-ray Photoelectron Spectroscopy, 2002.

[28] T. Gouder, P. M. Oppeneer, F. Huber, F. Wastin, and J. Rebizant. Photoemission study of the electronic structure of Am, AmN, AmSb, and Am2O3 films. *Physical Review B*, 72(11):115122, sep 2005.

[29] T. Gouder, G. van der Laan, a. B. Shick, R. G. Haire, and R. Caciuffo. Electronic structure of elemental curium studied by photoemission. *Physical Review B*, 83(12):125111, mar 2011.

[30] T. Gouder, C. Colmenares, J. R. Naegele, and J. Verbist. Study of the surface oxidation of uranium by UV photoemission spectroscopy. *Surface Science*, 235:280–286, 1989.

[31] J. Bloch, U. Atzmony, M. P. Dariel, M. H. Mintz, and N. Shamir. Surface spectroscopy studies of the oxidation behavior of uranium. *Journal of Nuclear Materials*, 105(2-3):196–200, 1982.

[32] H. Over and A. P. Seitsonen. Surface chemistry: Oxidation of Metal Surfaces. *Science*, 297:2003–2005, sep 2002.

[33] J. Ghijsen, H. Namba, P. A. Thiry, J. J. Pireaux, and P. Caudano. Adsorption of Oxygen on the magnesium (0001) surface studied by XPS. *Application of Surface Science*, 8:397–411, 1981.

[34] Jason S Corneille, Jian-wei He, and D Wayne Goodman. XPS characterization of ultra-thin MgO films on a Mo(100) surface. *Surface Science*, 306:269–278, 1994.

[35] G. Fanjoux, H. Fornander Billault, B. Lescop, and a. Le Nadan. Evolution of the magnesium surface during oxidation studied by Metastable Impact Electron Spectroscopy. *Journal of Electron Spectroscopy and Related Phenomena*, 119(1):57–67, jul 2001.

[36] M P Seah. Recent advances to establish XPS as an accurate metrology tool. *Journal of Surface Analysis*, 13(2):136–141, 2006.

[37] A Cros. Charging effects in X-ray photoelectron. *Journal of Electron Spectroscopy and Related Phenomena*, 59:1–14, 1992.

[38] J. Cazaux. Mechanisms of charging in electron spectroscopy. *Journal of Electron Spectroscopy and Related Phenomena*, 105(2-3):155–185, dec 1999.

[39] Zhen Zhang and John T Yates. Band Bending in Semiconductors : Chemical and Physical Consequences at Surfaces and Interfaces. *Chemical Reviews*, 112:5520–5551, 2012.

[40] Anton Teterin, Mikhail Ryzhkov, Yury Teterin, Labud Vukcevic, Vladimir Terekhov, Konstantin Maslakov, and Kirill Ivanov. Valence electronic state density in thorium dioxide. *Nuclear Technology and Radiation Protection*, 23(2):34–42, 2008.

[41] H. Bubert and J. C. Riviere. Photoelectron Spectroscopy. In H. Bubert and H. Jenett, editors, *Surface and Thin film analysis*, chapter 2, pages 6–32. Wiley- VCH, Weinheim, 2002.

[42] A. Kotani and T. Yamazaki. Systematic analysis of core photoemission spectra for actinide di-oxides and rare-earth sesqui-oxides. *Progress of Theoretical Physics Supplement*, 108:117–131, 1992.

[43] Geoffrey C. Allen, Solange Hubert, and Eric Simoni. Optical absorption and X-ray photoelectron spectroscopic studies of thorium tetrabromide. *Journal of the Chemical Society, Faraday Transactions*, 91(17):2767, 1995.

[44] P. W. Winter. The electronic transport properties of UO2. *Journal of Nuclear Materials*, 161:38–43, 1989.

[45] R. Eloirdi, T. Gouder, P.A. Korzhavyi, F. Wastin, and J. Rebizant. Dilution effect on the U-5f states: U in an Ag matrix. *Journal of Alloys and Compounds*, 386(1-2):70–74, jan 2005.

[46] A. Bzowski, M. Kuhn, T. K. Sham, J. A. Rodriguez, and J. Hrbek. Electronic structure of Au Ag bimetallics: Surface alloying on Ru(001). *Physical Review B*, 59(20):13379–13393, may 1999.

[47] W.L. Bond and W. Kaiser. Interstitial versus substitutional oxygen in silicon. *Journal of Physics and Chemistry of Solids*, 16(1):44–45, 1960.

[48] S Hubert, J Purans, G Heisbourg, P Moisy, and N Dacheux. Local structure of actinide dioxide solid solutions Th(1-x)U(x)O2 and Th(1-x)Pu(x)O2. *Inorganic chemistry*, 45(10):3887–94, may 2006.

[49] D. Rafaja, L. Havela, R. Kužel, F. Wastin, E. Colineau, and T. Gouder. Real structure and magnetic properties of UN thin films. *Journal of Alloys and Compounds*, 386(1-2):87–95, jan 2005.

[50] L. Havela, K. Miliyanchuk, D. Rafaja, T. Gouder, and F. Wastin. Structure and magnetism of thin UX layers. *Journal of Alloys and Compounds*, 408-412:1320–1323, feb 2006.

# 3

# TH EFFECT ON THE OXIDATION OF U: XPS/UPS AND CV INVESTIGATION ON $U_{1-x}Th_xO_2$ (X=0 TO 1) THIN FILMS

**Pelin CAKIR, Rachel ELOIRDI, Frank HUBER, Rudy J. M. KONINGS, Thomas GOUDER**

*Thin films of $U_{1-x}Th_xO_2$ (x = 0 to 1) have been characterized by XPS/UPS, XRD and CV in order to understand the effect of Th on the oxidation mechanism. During the deposition, the competition between U and Th for oxidation showed that Th has a much higher affinity for oxygen. Deposition conditions, time and temperature were also examined, to look at the homogeneity and the stability of the films. XRD patterns, core level spectra obtained for $U_{1-x}Th_xO_2$ vs. the composition showed that lattice parameters follow the Vegard's law and the binding energies of U-4f and Th-4f are in good agreement with literature data obtained on bulk compounds. To study the effect of Th on the oxidation of $U_{1-x}Th_xO_2$ films, we used CV experiments at neutral pH of a NaCl solution in contact with air. The results indicated that Th has an effect on the U oxidation as demonstrated by the decrease of the current of the oxidation peak of U. XPS measurements made before and after the CV, showed a relative enrichment of Th the surface, supporting the formation at a longer term of a Th protective layer at the surface of $U_{1-x}Th_xO_2$.*

Parts of this chapter have been published in Applied Surface Science **393**, 204-211 (2017) [1]

## 3.1. INTRODUCTION

THORIUM-Uranium mixed oxides are interesting nuclear fuel materials. Compared to uranium-plutonium mixed oxide, the higher thermal stability and melting temperature results in a larger margin to melting [2]. The use of Thorium-Uranium mixed oxide results in the production of smaller quantities of Transuranium elements [3].

During the geological storage of used nuclear fuel, the radionuclides embedded in the uranium fuel matrix, which are produced during the reactor irradiation, can be released via the dissolution of the fuel matrix. Uranium has two stable oxidation states, (IV) and(VI), and several mixed valence phases (i.e. $U_3O_7$, $U_4O_9$, $U_3O_8$). The solubility of uranium increases several magnitudes as the oxidation state increases from U(IV) to U(VI) in the matrix [4]. On the other hand, $ThO_2$ is chemically stable, having one oxidation state (IV), and its dissolution is reported to be extremely difficult [5].

Since the first contact of the material with the environment happens on the surface, our interest is to observe changes and the evolution of the oxide layer forming at the interface. In this work, thin films of (U, Th) mixed oxides formed by sputter deposition technique [6] are used instead of using bulk material [7–10]. The use of thin films to simulate the surface of bulk compounds results in a high flexibility for compositional changes (O/(U + Th) or U/Th ratios). Moreover, it allows deposition of layers of different thickness onto variable substrates, with different microstructure when changing the temperature and gas pressure during the deposition. Materials such as uranium-thorium oxides, are difficult to study by photoelectron spectroscopy [11], which is due to their semiconductor properties as a result of which the flow of current cannot be achieved properly along the bulk sample thickness. This aspect can be limited or avoided by the use of thin films because the low thickness results in a low resistance and the voltage drop can be neglected [12, 13].

The main goal of this study is to understand the effect of the stable tetravalent actinide Th(IV) onto uranium dioxide and to follow the electronic structure, oxidation state and redox reactions on the surface.

The paper is divided into three sections. The first part investigates the relative oxygen affinity between uranium and thorium, by bringing them into competition. The second part examines the effect of high temperature and low temperature deposition on the surface properties such as oxygen diffusion and atomic segregation. Also in this part, we compare $U_{1-x}Th_xO_2$ (x = 0 to 1) thin films to bulk materials to confirm their use as model, by analysing their electronic structure and lattice parameters versus their composition. The third part consists of electrochemical studies on $U_{1-x}Th_xO_2$ (x = 0 to 1). Electrochemistry, especially cyclicvoltammetry (CV) of $UO_2$ samples has been intensively employed [14–19] however to the best of our knowledge, there has been no CV record on uranium-thorium mixed oxides, probably due to the semiconductor properties. The objective of the current CV studies is to examine the oxidation of $U_{1-x}Th_xO_2$ before and after the CV using XPS, looking at the composition and the oxidation state.

## 3.2. EXPERIMENTAL

The thin films of $U_{1-x}Th_xO_2$ (x = 0 to 1) were prepared in-*situ* by direct current reactive co-sputtering from thorium and uranium metal targets in a gas mixture of Ar (6N) and

$O_2$(6N). The oxygen concentration in the films was adjusted by changing the $O_2$ partial pressure ($10^{-8}$mbar - $6 \times 10^{-6}$mbar), while the Ar partial pressure was maintained at $5 \times 10^{-7}$mbar. The composition of the films is controlled by changing the respective target voltages for U and Th target. The thin films were deposited onto silicon wafer (111) substrates, which were cleaned by Ar ion sputtering (4 keV) for 1 min. The plasma in the diode source was maintained by injection of electrons of 50-100 eV energy (triode setup), allowing working at low Ar pressure in absence of stabilizing magnetic fields. After deposition, the thin films were transferred to the XPS-UPS analysis chamber without exposing them to air.



Photoelectron spectroscopy data were recorded using a hemispherical analyzer from Omicron (EA 125 U5). The spectra were taken using Mg K$\alpha_1$ (1253.6 eV) radiation with an approximate energy resolution of 1 eV. UPS measurements were made using He*II*(40.81 eV) excitation radiation produced by a high intensity windowless UV rare gas discharge source (SPECS UVS 300). The total resolution in UPS was 0.1-0.05 eV for the high resolution scans. The background pressure in the analysis chamber was $2 \times 10^{-10}$mbar. The spectrometer was calibrated by using Au-$4f_{7/2}$ line of metal to give a value at 83.9 eV BE and Cu-$2p_{3/2}$ line of metal at 932.7 eV BE for XPS, and on He*I* and He*II* Fermi-edges for UPS. Photoemission spectra were taken at room temperature. Quantification of the spectra was done using CasaXPS software (version 2.3.13Dev50). As Relative Sensitivity Factors, Scofield cross-sections for Mg-K$\alpha_1$ radiation [20] were taken. An example of peaks deconvolution with the CasaXPS software is reported in Figure 3.1.

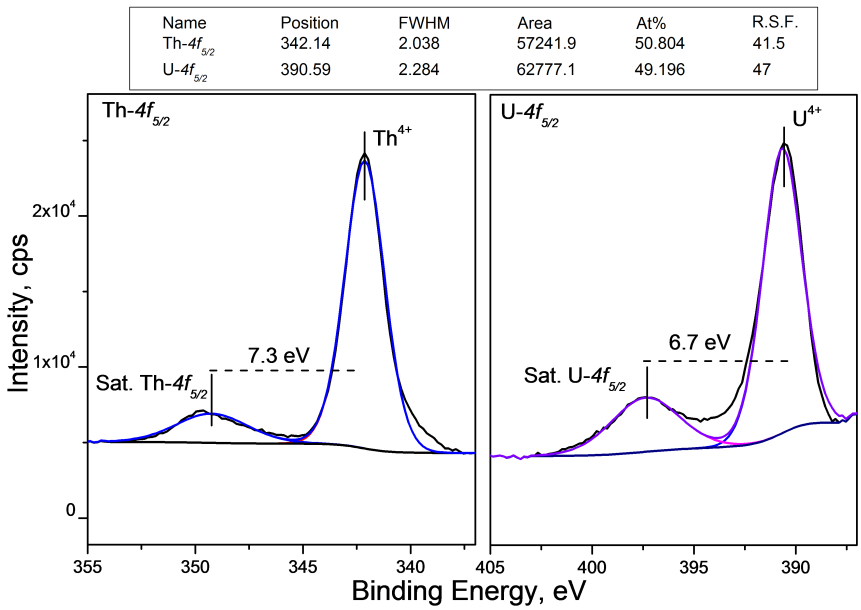


Figure 3.1: Peaks Deconvolution of Th-$4f_{5/2}$ and U-$4f_{5/2}$, with peaks positions, FWHM, peaks area and quantification obtained with CasaXPS software.

For the electrochemical study, a standard 3-electrode setup was used with a working

Table 3.1: Binding energy of $4f_{5/2}$ core level peak for Th metal, U metal, $ThO_2$ and $UO_2$. Substance

| Substance | $4f_{5/2}$ | Satellite |
|---|---|---|
| Th metal | 342.3 [21, 22] | - |
| U metal | 388.4 [23] | - |
| $ThO_2$ | 346.8 [21, 24] | 7.3 |
| $UO_2$ | 390.95 [12, 25] | 6.7 |



electrode composed of $U_{1-x}Th_xO_2$ (x = 0.00,0.10, 0.44, 0.84, 1.00) thin films deposited onto gold foil surface; the reference electrode was an Ag/AgCl (3 M KCl) electrode and a Pt wire as counter electrode. Gold foils were first cleaned with Ethanol/1N $H_2SO_4/H_2O$ then heated till 300°C under ultra-high vacuum (UHV). As adhesion layer, an interface composed of a (U,Th) metal layer was deposited at 300°C between the gold foil and the $U_{1-x}Th_xO_2$ film. All potential values in this paper are versus Ag/AgCl. The measurements were carried out with a stationary electrode in an unstirred solution. The electrolyte was a 0.01 M NaCl solution at neutral pH in contact with air. Experiments were carried out at room temperature (22 ± 3°C) in a closed Teflon electrochemical cell with an electrolyte volume of 3 ml. Applied potentials were not corrected for voltage drop because of the negligible electrode resistance of the film electrodes [12]. Before the scans, the electrodes were preconditioned at the most cathodic potential for 5 min to reduce any higher oxides formed during the transportation. The cyclovoltammetry (CV) measurements were recorded in potential sweep cycles in a first series (15 cycles) from -1.000 $V_{Ag/AgCl}$ up to +0.600 $V_{Ag/AgCl}$, and back to -1.000 $V_{Ag/AgCl}$ and then in a second series (15 cycles) from -1 $V_{Ag/AgCl}$ to 0.8 $V_{Ag/AgCl}$ at a scan rate of 0.010 V $s^{-1}$. Ultra pure water from a MilliQ-system (>18 M Ω) was used. Chemicals were all p.a. grade (Merck, Darmstadt).

The X-ray diffraction analyses were made on a conventional Phillips PW3830 powder diffractometer with a Cu X-ray tube (40 kV, 30 mA, $K\alpha_1$ = 0.1540560 nm). Films of about 360 nm (1 Å/s) thicknesses were deposited at 100°C on a Si (111) wafer. The patterns were recorded at room temperature in a step scan mode over a $2\theta$ range of [10-100]°, with a step size of 0.01° and a count time of 5 s per step.

## 3.3. RESULTS AND DISCUSSION

### 3.3.1. RELATIVE OXYGEN AFFINITY

To measure the relative oxygen affinity of thorium and uranium, a series of thin films were deposited successively by increasing the oxygen partial pressure with a low increment and analyzing them in-*situ* by XPS. The U-*4f* and Th-*4f* core level spectra enable to investigate the oxidation of uranium and thorium through their binding energy (BE) peak, their shape and their satellites. As reference values, Table 3.1 reports the $4f_{5/2}$ BE of thorium and uranium present in the metal and in the dioxide, as well as the corresponding satellite.

Figure 3.2 reports U-$4f_{5/2}$and Th-$4f_{5/2}$ core level spectra of (U,Th)$O_x$(x < 2) thin films obtained successively by co-deposition under slight increase of oxygen partial pressure and (U,Th) metal films pectra are used as reference (red plots). It should be noted that the oxygen partial pressures used in this experiment are not universal values, but vary according to the experimental set-up. The BE and the peak shapes obtained for (U,Th) metal are in agreement with those reported in literature for single and bulk element of uranium and thorium [21, 26].



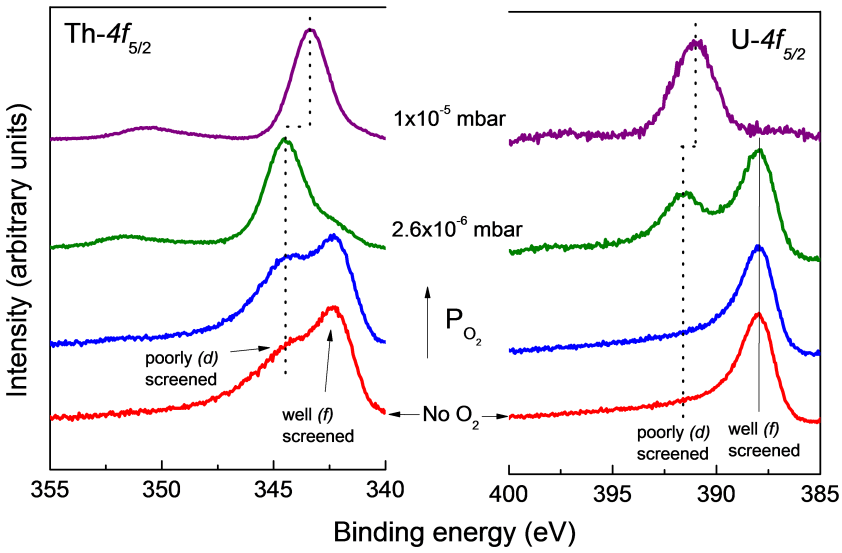


Figure 3.2: Th-$4f_{7/2}$ line (left) U-$4f_{7/2}$ line (right) core level spectra for co-deposited (U,Th) films versus the relative increase of partial pressure of oxygen ($PO_2$).

The initial adding of oxygen during deposition affects first the thorium as shown by the relative increase of the d-screened peak whereas the uranium peak keeps constant in shape and in binding energy. The quicker oxidation of thorium relative to uranium is confirmed by the further and nearly complete oxidation of thorium (green curves) while for uranium the f-screened peak is still the main peak. This simple experiment demonstrates an obvious and much stronger affinity of oxygen for thorium than for uranium, as shown by the oxidation of uranium starting only once thorium is nearly completely oxidized This is in agreement with the higher stability (lower Gibbs energy of formation) of $Th^{4+}$ relatively to $U^{4+}$. The shift to lower binding energy of Th-*4f* and U-*4f* peaks is taking place due to the decrease of Fermi-energy linked to charge carrier depletion [27, 28] in the sample, as reported in a previous study on $ThO_2$ [21]. It is a coherent shift, occurring for all photoemission lines (including O-*1s*). The thickness of the oxide layer is small enough to allow electrons to tunnel through. This avoids the charging upon photoemission and still permits a well-defined Fermi-level [29].

### 3.3.2. INFLUENCE OF DEPOSITION CONDITIONS AND COMPARISON WITH BULK DATA

#### INFLUENCE OF DEPOSITION TIME AND TEMPERATURE ON $U_{0.50}Th_{0.50}O_2$ THIN FILMS

In the following section, we compare the effect of deposition time of films at room temperature on the core level and valence band spectra. The idea behind is to investigate the reproducibility and the homogeneity of the film surface as a function of the film thickness, going from atomic to bulk properties. While XPS probes a depth of about 100 Å, XRD is looking into a sample depth of the order of a $\mu$m. Since we showed that the composition along the thickness of the film (i.e. deposition time) is constant, we consider that the composition of the surface is representative of that of the bulk.



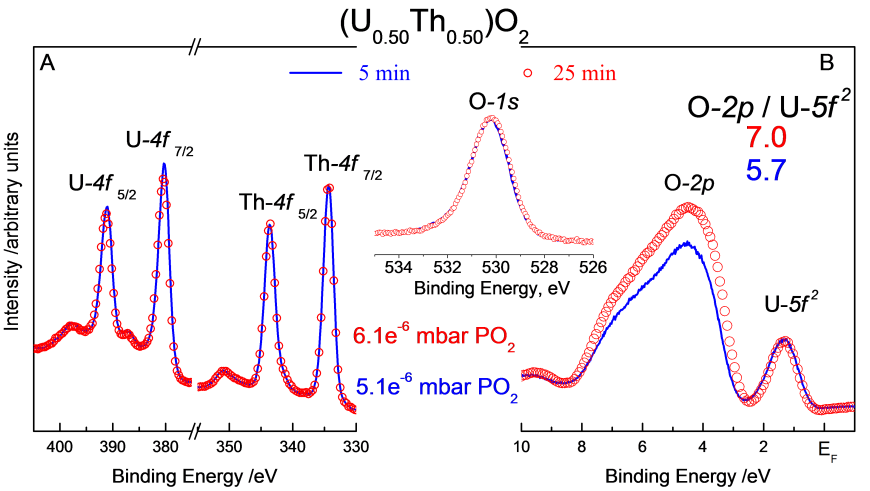


Figure 3.3: The influence of the deposition time on the U-*4f* and Th-*4f* core level spectra (A) and on He*II* valence band spectra (B) for $U_{0.50}Th_{0.50}O_2$.

A film composition of $U_{0.50}Th_{0.50}O_2$ has been chosen for this experiments series. The deposition rate is about 1 Å/s. Figure 3.3 shows the core level spectra U-4f and Th-4f (A), the valence band (B) and the corresponding O–*1s* (middle) of $U_{0.50}Th_{0.50}O_2$ film deposited during 5 min and 25 min corresponding to 30 and 150 nm, respectively. The deposition conditions were kept rigorously the same despite a small difference for the oxygen partial pressure. The Figure 3.3A shows the spin-orbit splits of uranium and thorium $4f_{5/2}$ and $4f_{7/2}$. The binding energies of $4f_{7/2}$ in uranium and thorium are 380.3 eV and 334.3 eV respectively, corresponding to uranium (IV) and thorium (IV) oxidation states. The satellite peaks and the peak positions have been extensively studied in previous papers both on $ThO_2$ [21] and $UO_2$ [12]. The position and the intensity of the satellite peaks are characteristic for the oxidation states of the materials and are linked to the final state occupation. The satellite peak positions for U-Th mixed oxides (6.7 eV for U-$4f_{7/2}$ and 7.3 eV for Th-$4f_{7/2}$) are also those expected for the +IV oxidation state [30]. Within the uncertainty the quantification of the spectral lines, using CasaXPS software, does not indicate any atomic segregation at the surface for both depositions, and

this is also emphasized by the constant full width at half maximum (FWHM) and binding energies. This shows the stability of the deposition technique.

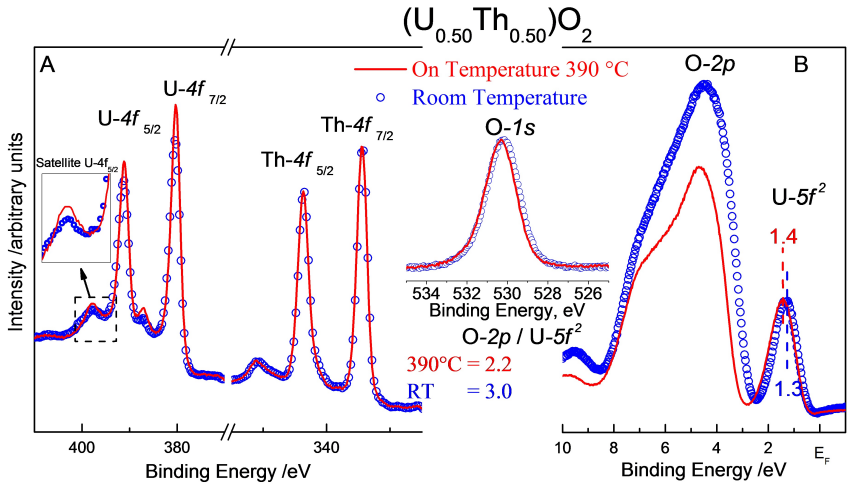


Figure 3.4: The influence of the deposition temperature on the U-*4f* and Th-*4f* core level spectra (A) and on the He*II* valence band spectra (B) for a $U_{0.50}Th_{0.50}O_2$.

The He*II* valence band spectra (Figure 3.3B) are more sensitive to 5f states compared to He*I* (not reported here) and due to the short range of the emitted photoelectrons, UPS is more sensitive to the surface than XPS. As thorium does not have a 5f state, the peakat 1.3 eV below $E_F$ is due to the U-$5f^2$. The peak between 3 and 9 eV is attributed to O-*2p* band emission. While XPS spectra did not show quantitative differences, UPS shows different O-*2p* band intensity and thus different ratio O-*2p*/U-*5f*, going from 5.7 to 7.0 for $5.1 \times 10^{-6}$ and $6.1 \times 10^{-6}$ mbar partial oxygen pressure, respectively.

With the same goal as the previous experiments, we compared the electronic structure of $U_{0.50}Th_{0.50}O_2$ films prepared with the same time of deposition at room temperature and at 390°C. Figure 3.4A reports the U-*4f* and Th-*4f* core level states and the O-*1s* spectra (inset Figure 3.4), while Figure 3.4B shows the corresponding He*II* valence band of $U_{0.50}Th_{0.50}O_2$. First we observed a clear superposition of the Th-*4f* core level peaks for both temperatures, while a small difference appears for the intensity of the U-*4f* peaks and for the shape of their satellites. This shows that temperature does not have an effect on the thorium states once this is completely oxidized, whereas it influences the uranium states due to the diffusion of the oxygen in the film, leading to further oxidation of U. This is also shown in the magnified satellite intensities (inset Figure 3.4A) and by the slight shift towards higher BE observed in inset O–*1s* figure. The composition of the film deposited at 390°C could be quantified as $U_{0.51}Th_{0.49}$ which is within the uncertainty of the technique similar to the composition of the film deposited at room temperature. In Figure 3.4B, the He*II* valence spectra show a main effect of the temperature on the O-*2p* band whose intensity and FWHM decrease, while the $5f^2$ peak shifts slightly to higher BE. The diffusion of the oxygen from the top surface to the inner of the film can explain this effect.

### ELECTRONIC STRUCTURE AND LATTICE PARAMETER VERSUS COMPOSITION OF $U_{1-x}Th_xO_2$ FILMS AND BULK MATERIALS

To validate the use of thin films as model, we proceeded with th edeposition of a series of $U_{1-x}Th_xO_2$ (x = 0 to 1) films monitoring the U-*4f* and Th-*4f* binding energies in-*situ* and also the lattice parameter versus the composition in ex-*situ* by XRD. The corresponding data reported in Figure 3.5A are compared to the data obtained on bulk samples [30–34]. The lattice parameters observed for our thin films are close to the ones reported on bulk sample, following Vegard'slaw expected for this solid solution. The intercept of the linear fit of our work and of Anthonysamy et al. [30] study for $UO_2$ are 5.448 and 5.465 Å, respectively. The smaller lattice parameter found for our film can be explained by the presence of the stress in the films and with the small crystallite size as shown by the broadening of the XRD peaks [35]. Another parameter which may influence the evolution of the lattice parameter is the oxygen content which compared to bulk compounds might be slightly different from our films produced in-*situ*. However, XPS results showed that the films are stoichiometric.

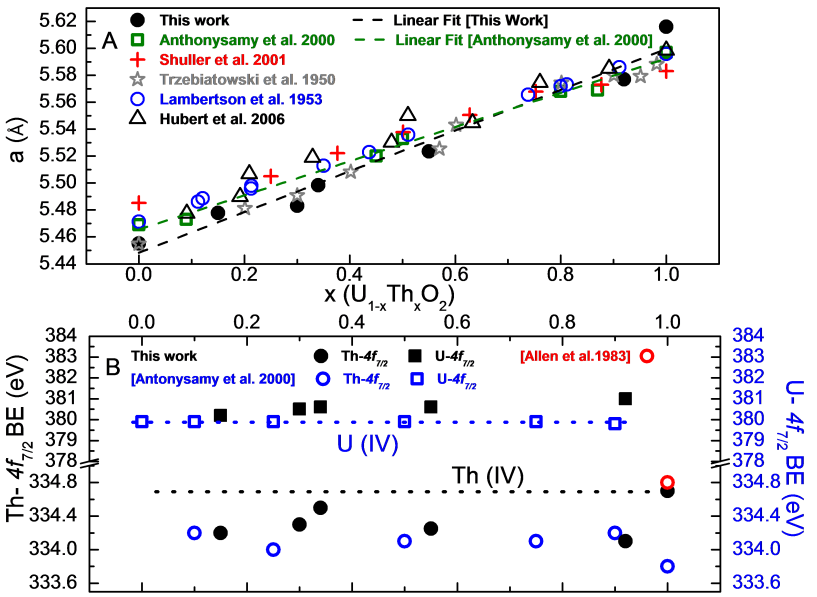


Figure 3.5: Lattice parameter of $U_{1-x}Th_xO_2$ films versus x obtained in this work and compared to literature data obtained on bulk compounds (A). Th-$4f_{7/2}$ and U-$4f_{7/2}$ Binding energy in $U_{1-x}Th_xO_2$ films obtained in this work and compared to literature obtained on bulk compounds (B).

Figure 3.5B shows the BE of U-$4f_{7/2}$ and the Th-$4f_{7/2}$ in $U_{1-x}Th_xO_2$ (x = 0 to 1) versus the compositions and compares with the data obtained on bulk samples [30, 36]. Vael et al. [37] pointed out that the binding energy of U-$4f_{7/2}$ for U(IV) ranges from 379.9 to 380.9 eV. Our results stay in the reported range which shows that U and Th mixed oxides are stoichiometric. Binding energies of Th-$4f_{7/2}$ are also stable in a 0.6 eV range and in a good agreement with data obtained by Allen et al. [36] but different by 1 eV relatively to

the one reported by Anthonysamy et al. [30].

To summarize, $U_{1-x}Th_xO_2$ (x = 0 to 1) mixed oxides films follow Vegard's law and the binding energies are in good relation with the ones obtained for bulk materials. It is apparent from these results that our thin films can be used as model for actinide oxide bulk samples, despite the microstructure which can be different (stress,preferential orientation, . . .).

### 3.3.3. ELECTROCHEMICAL STUDIES



Many studies have been reported on chemical, physical properties and leaching experiments of (U,Th) mixed oxides [7, 10, 38, 39]. Sunder et al. [10] showed that the oxidation process taking place at the surface of (U,Th) mixed oxide samples are similar to pure $UO_2$. However, compared to $UO_2$ the leaching experiments showed that the decrease of the uranium dissolution rate and this has been linked to the lower uranium content present in mixed oxide and in contact with solution. This statement has been supported by Heisbourg et al. [7, 38] who studied the kinetics of dissolution of (U,Th) mixed oxides both thorium- and uranium-rich samples. Also, XPS analyses of samples obtained after leaching experiment demonstrate a surface enriched in thorium, forming a protective layer disabling further dissolution of the uranium [7]. Demkowicz et al.[39] also reported that the uranium dissolution rate in fresh samples of $(U,Th)O_2$ was 10 to 40 times lower than for conventional $UO_2$ fuel.

Thus compared to pure $UO_2$, there is a clear indication for a lower dissolution rate of uranium in (U,Th) mixed oxide, however the oxidation and reduction process is not clear yet. Sunder et al.[10] pointed out that due to the high electrical resistivity, working with electrochemical techniques on such a system as bulk material was not possible. To overcome this difficulty, thin films can be a good alternative as demonstrated by Miserque et al. [12], who reported cyclic voltammetry on $UO_2$ thin films. By comparing CV measurements on $UO_2$ thin film (1 $\mu$m) and bulk $UO_2$ (1 mm), it was confirmed that the films made by DC sputtering technique have much lower resistance than the bulk electrodes and the IR drop for cyclic voltammetry is negligible.

Figure 3.6 shows the first two cycles of $U_{1-x}Th_xO_2$ (x = 0.10, 0.44,0.84, 1.00) electrodes scanned between -1 V to 0.6 V (vs. Ag/AgCl) in 0.01 M NaCl. The first cycles are indicated with solid lines, the second ones are indicated with dashed lines. Roman numbers on the graphs indicate the peak positions of the suggested reactions based on literature [18, 40]. During the first cycle, the $UO_2$ electrode does not show any significant peak in region I. In this potential window it is thermodynamically impossible to oxidize homogeneous $UO_2$ and the previous studies attributed the current change to the different energy sites or inhomogeneity such as grain boundaries and hyperstoichiometry (e.g $UO_{2+x}$) on the surface of the electrode [18, 40]. The first cycle for the $UO_2$, $U_{0.90}Th_{0.10}O_2$, $U_{0.56}Th_{0.44}O_2$ and $U_{0.16}Th_{0.84}O_2$ electrodes does not show any significant peaks, however, the second cycles of $UO_2$ and $U_{0.90}Th_{0.10}O_2$ electrodes show a slight current increase. On the other hand, at lower content of uranium (i.e. $U_{0.56}Th_{0.44}O_2$ and $U_{0.16}Th_{0.84}O_2$ electrodes) we do not observe the increase of the current, which can be explained by alower oxidation on the surface in the first cycles.

In region II, the oxidation of $UO_2$ to $UO_{2+x}$ starts and in the subsequent region III, $UO_{2+x}$ increases to $UO_{2.33}$ by $O^{2-}$ incorporation into the lattice. At higher potentials,

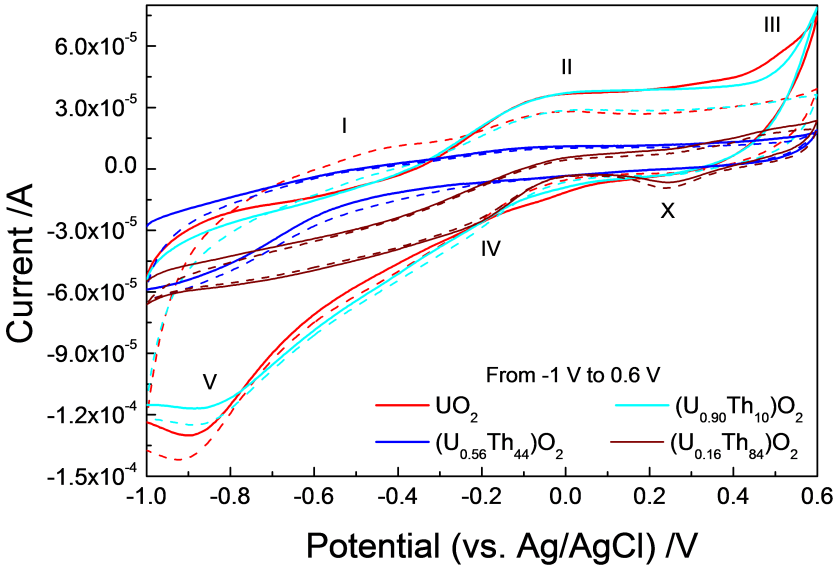


Figure 3.6: Cyclic voltammetry on $U_{1-x}Th_xO_2$ (x = 0, 0.10, 0.44, 0.84, 1) films for the first two cycles.

the oxidation process might lead either to its dissolution as $UO_2^{2+}$ or recrystallization as $UO_{2.5}$ and $UO_{2.66}$ (due to the adsorbed $UO_2^{2+}$). However, in neutral to slightly alkaline electrolytes, $UO_2^{2+}$ in solution might re-precipitateon the electrode either as schoepite ($UO_3{\cdot}H_2O$) or as metaschoepite($UO_3{\cdot}2H_2O$) [18, 40].

In region III, a fast increase of the current is observed for both $UO_2$ and $U_{0.90}Th_{0.10}O_2$ electrodes indicating the onset of dissolution, which is not to such extent the case for $U_{0.56}Th_{0.44}O_2$ and $U_{0.16}Th_{0.84}O_2$ films. This process was studied by monitoring the mass loss from the $UO_2$ electrode in solutions of pH = 5 to pH = 8 using EQCM by Seibert et al. [13].

Region IV and V are the reduction peaks of oxidized layers observed on cathodic potentials. These peaks are usually coupled with the anodic oxidation peaks. The potentials of the peaks are related to the thickness of the oxide layer formed during the anodic scans at the surface [41]. In neutral electrolytes, region IV is observed and attributed to reduction of $UO_3{\cdot}nH_2O$ to $UO_{2+x}$. $UO_3{\cdot}nH_2O$ phases are insulators and thought to precipitate as porous layer and do not interfere with the reduction of the under-lying oxides [42, 43]. Region V is associated to the reduction of underlying oxides such as $UO_{2.33}/UO_{2+x}$ or $UO_{2.5}$, $UO_{2.67}$ created in region III, as stated above [40]. Starting from region IV and going to region V, $UO_2$ and $U_{0.90}Th_{0.10}O_2$ electrodes show higher cathodic currents indicating the reduction of U(VI) to U(IV). This is not the case for $U_{0.56}Th_{0.44}O_2$ and $U_{0.16}Th_{0.84}O_2$. This behavior is also reflected in region V while $UO_2$ and $U_{0.90}Th_{0.10}O_2$ electrodes show reduction to stoichiometric $UO_2$, the other two electrodes does not indicate any compelling current activity. The low current observed at this potential window on the $U_{0.56}Th_{0.44}O_2$ and $U_{0.16}Th_{0.84}O_2$ electrodes can be at-

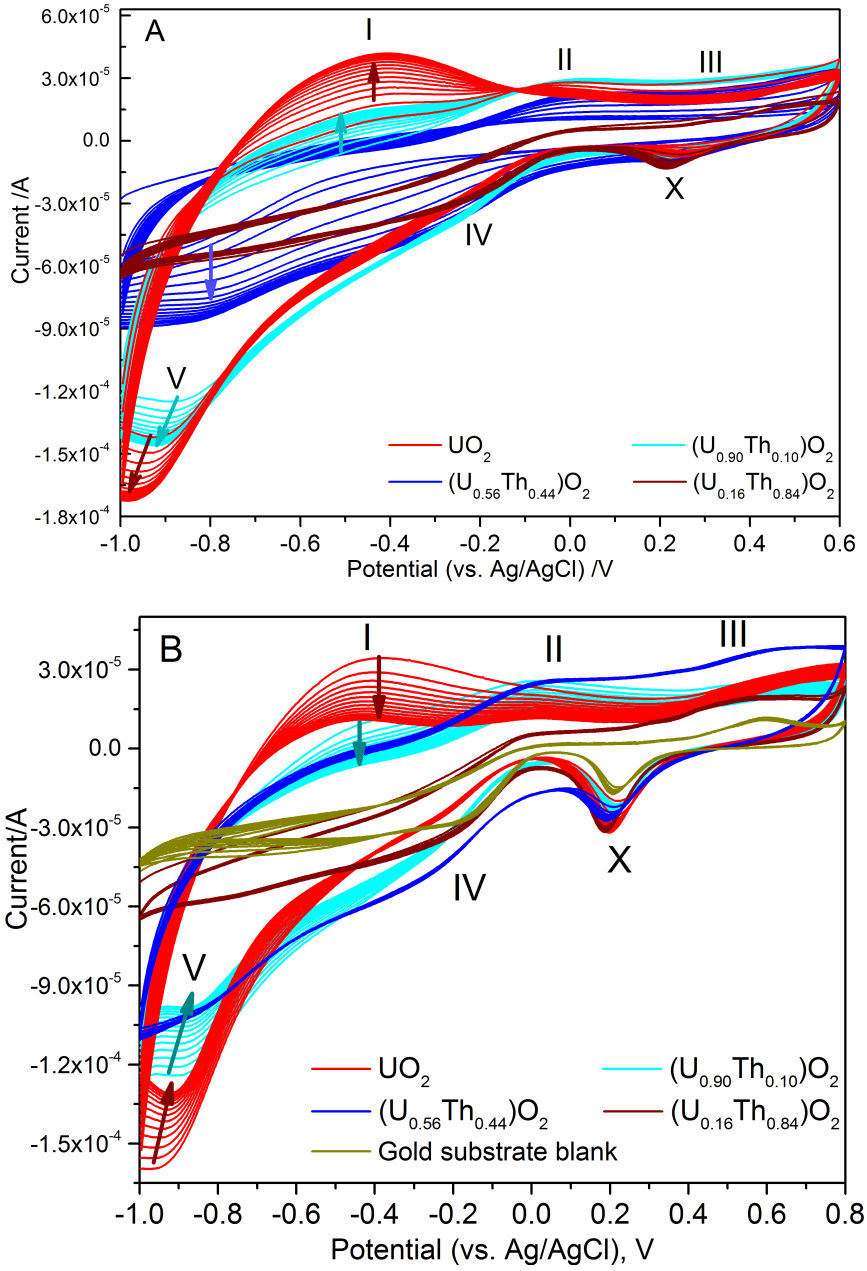


Figure 3.7: Cyclic voltammetry for $U_{1-x}Th_xO_2$ (x = 0, 0.10, 0.44, 0.84, 1) films from the 3rd up to the 15th cycle in the range of -1 V to 0.6 V (A). Cyclic voltammetry for $U_{1-x}Th_xO_2$ (x = 0, 0.10, 0.44, 0.84, 1) films for higher potential window up to 0.8 V (vs. Ag/AgCl) and gold substrate cycles (yellow lines) (B).

tributed to the lower content of uranium in contact with the solution. Also the substitution of uranium by thorium in $UO_2$ lattice leads to the alteration of the electric properties (from semi-conductor $UO_2$ to insulator $ThO_2$) of mixed oxide samples. It decreases the electrical conductivity and thus the dissolution rate of uranium as reported in literature [10, 44].

Figure 3.7A represents the cycles from $3^{rd}$ till $15^{th}$ CV in the range of -1 V to 0.6 $V_{Ag/AgCl}$. In Figure 3.7A, in region V, we do observe that the cathodic current increases with the uranium content. While $U_{0.90}Th_{0.10}O_2$ and, to a lesser extent, $U_{0.56}Th_{0.44}O_2$ behave in a similar way as pure $UO_2$, showing a shifting to higher cathodic potential along the successive cycle, $U_{0.16}Th_{0.84}O_2$ remains constant current in this region. The shifting to lower potential seems to indicate the formation of a thicker oxide layer increasing along the successive cycles (indicated with the arrows). Uncompleted reduction in domain V leads to an increase of oxidation on region I of the current getting higher and higher in each cycle. The same phenomenon is not observed for $U_{0.56}Th_{0.44}O_2$ and $U_{0.16}Th_{0.84}O_2$ electrodes due to the lower amount of uranium. In region II and III, where oxidation of $UO_2$ and $UO_{2+x}$ is taking place, the current increases with the content of the uranium present in the electrodes.

When the scans continued up to 0.8 $V_{Ag/AgCl}$ for another 15 cycles, differences were observed as shown in Figure 3.7B. Looking at the peaks in region V and region I, we do observe an opposite trend compared to Figure 3.7A. The broader scan window to higher anodic potential leads a shifting to lower cathodic potential of region V and to a decrease of current along the cycles in regions V and I. This might be due to fact that higher dissolution rates are achieved at higher anodic potentials. This decrease in intensity of peaks in region V and I may be related to the decrease of the thickness of the hyperstoichiometric oxide layers (region V), thus leading to less different energy sites or grain boundaries on the surface (region I).The reason why this is happening in this bigger potential window is not totally clear.

Gold used as substrate and considered as noble metal does not interfere strongly in the working potential window chosen in this study, as shown in Figure 3.7B in yellow lines. In the potential windows up to 0.6 V (not reported here) it has no effect as demonstrated by the low current value, but when measured up to 0.8 V a peak marked as X on the cathodic potentials is observed. This might be attributed to the electrolyte reduction. The films have a certain porosity enabling the contact of the solution with gold substrate. The intensity peak X increase along the successive cycles and can be related to the oxide layer getting more and more porous while the gold surface increases together with its related current.

The current counts for the $U_{0.56}Th_{0.44}O_2$ and $U_{0.16}Th_{0.84}O_2$ electrodes throughout their consecutive CVs have about the same values, which can be explained by the lower amount of uranium at the surface. The $U_{0.16}Th_{0.84}O_2$ electrode is rather behaving as the gold substrate itself. It has a higher current than gold substrate due to the small amount of uranium on the surface. Nonetheless the current activity should be related to the electrolyte interference because thorium is not expected to show any oxidation on these potential window [45].

Figure 3.8 compares the U-*4f* and Th-*4f* spectra of $U_{0.67}Th_{0.33}O_2$ film obtained before and after CV as an example the general observations. First the U-*4f* peaks shift to

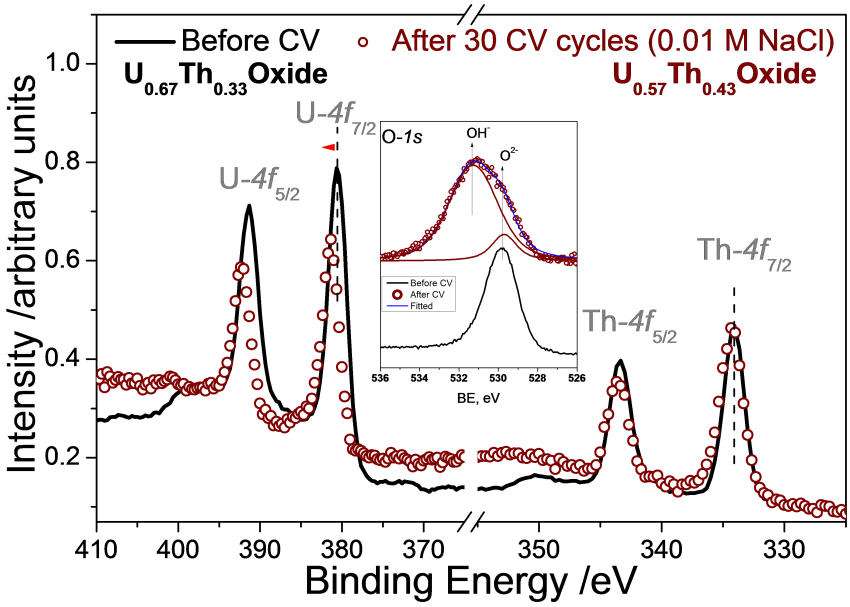


Figure 3.8: U-*4f* and Th-*4f* of $U_{0.67}Th_{0.33}$ oxide film before and after 30 cycles, inset graph represents the corresponding O-*1s* spectra.

higher binding energy indicating further oxidation as $UO_{2+x}$, unlike the Th-*4f* peaks that keep a constant binding energy because no further oxidation than Th(IV) can take place. We also observed the change in the intensity peaks. When the two spectra before and after the CV experiment are normalized to Th-*4f*, the U-*4f* intensity peaks decreased after the CV cycles, indicating a lower uranium content at the surface compared to the initial, as deposited film composition. Also the shift of U-*4f* to higher binding energy after CV experiment indicates a higher oxidation state for uranium at the surface. The quantification using CasaXPS shows that the composition changes from $U_{0.67}Th_{0.33}O_2$ to $U_{0.57}Th_{0.43}O_{2+x}$. In the inset of Figure 3.8 we observe the broadening of the peak O-*1s* which can be deconvoluted in two components, at low BE and one at higher BE, corresponding to $O^{2-}$ and to $OH^-$ respectively [38, 46]. The O-*1s* shift is more pronounced on the films that contain higher amount of uranium on the composition.

To summarize the CV experiment on the mixed oxide films, Table 3.2 reports the compositions and the BE of U-$4f_{5/2}$, Th-$4f_{5/2}$ and O-*1s* core level peaks for the different samples before and after CV cycles. The results show a strong decrease of uranium content relative to thorium, decreasing by about 30 at % (sample 2) compared to the initial composition. The preferential dissolution of uranium at the surface enables to explain this result leading to an enrichment of thorium at the surface which along oxidation and dissolution of U(VI) provides a protection layer inhibiting the further oxidation of the uranium present deeper in the film. The thorium effect has been discussed in literature [7, 10, 38] reporting its role to passivate the surface, limiting further oxidation of uranium and decreasing the dissolution rate of uranium. Our results enable to confirm this

Table 3.2: Composition and U-4f$_{5/2}$, Th-4f$_{5/2}$ and O-1s films before and after 30 cycles of CV in [NaCl]=0.01 M.

| Sample | Before CV | | | | After CV | | | |
|---|---|---|---|---|---|---|---|---|
| | Composition | Binding Energy, eV | | | Composition | Binding Energy, eV | | |
| | | U-$4f_{5/2}$ | Th-$4f_{5/2}$ | O-$1s$ | | U-$4f_{5/2}$ | Th-4f$_{5/2}$ | O-$1s$ |
| 1 | $U_{0.67}Th_{0.33}O_2$ | 380.5 | 334.0 | 529.8 | $U_{0.57}Th_{0.43}O_{2+x}$ | 381.3 | 334.1 | 529.7/531.2 |
| 2 | $U_{0.56}Th_{0.44}O_2$ | 380.5 | 333.9 | 529.8 | $U_{0.40}Th_{0.60}O_{2+x}$ | 381 | 333.9 | 529.8/531.2 |
| 3 | $U_{0.16}Th_{0.84}O_2$ | 380.5 | 333.9 | 529.8 | $U_{0.14}Th_{0.86}O_{2+x}$ | 380.9 | 333.8 | 529.7/531.3 |

process taking place at the surface of the sample in contact with a neutral solution.

## 3.4. CONCLUSION AND SUMMARY

Thin films of $(U_{1-x}Th_x)O_2$ (x = 0 to 1) mixed oxides were investigated by XPS/UPS, XRD and CV to establish the possible influence of thorium on the oxidation/dissolution process.

We first investigated the relative oxygen affinity of Th and U and oxidation of uranium started only once thorium was completely oxidized. This observation is consistent with the higher stability of $ThO_2$ ($\Delta_f G^0$(298 K):-1170 kJ mol$^{-1}$) compared to $UO_2$ ($\Delta_f G^0$(298 K):-1031 kJ mol$^{-1}$ [47]).



Based on core level and valence band spectra, homogeneity of the films could be showed along the deposition. Also deposition temperature (from 25°C to about 400°C) had no influence on thorium oxidation state while uranium undergoes further oxidation, seen by a shift of the U-*4f* satellite and the U-$5f^2$ peak, and by a change of the O-*2p*/U-$5f^2$ intensity ratio.

To determine the suitability of thin films as model system for nuclear fuel we compared the lattice parameters and the U-*4f* and Th-*4f* core level binding energy of films to bulk compounds, for a series of compositions of $U_{1-x}Th_x)O_2$ (x = 0 to 1). The lattice parameters followed the Vegard´ıs law, with a slight deviation attributed to stress present in the films. Also the binding energies of U-*4f* and Th-*4f* core levels were in agreement with those reported on bulk compounds.

Cyclic voltammetry was used to follow the surface redox reactions for different compositions. In the potential window of [-1 to 0.6] V (vs Ag/AgCl), oxidative dissolution of uranium in neutral pH solution suggests the formation of a layer of higher oxide at the surface. Shift of the peaks to the higher negative potentials are observed in the cathodic region V at about -0.9 V (vs Ag/AgCl),as well as in current intensity increase in the anodic region at about -0.5 V (vs Ag/AgCl) in region I, indicating formation of thicker layers hyper-stoichiometric oxides on each cycle performed. The intensity and the position of the peaks showed a proportional relation with the thorium content in $UO_2$ matrix. However, on a larger potential window [-1 to 0.8] V (vs Ag/AgCl), an opposite behaviour is observed, such as lower intensity and adverse direction shifts on each cycles. This change in behavior showed that the successive cycles result in thinner layers of hyper-stoichiometric oxides on the surface. On the other hand, in the higher potential window we observed higher current counts for both anodic and cathodic potentials for films with higher thorium content (going from $U_{0.56}Th_{0.44}O_2$ and $U_{0.16}Th_{0.84}O_2$). This can be explained by the fact that a higher thorium concentration requires higher potentials to oxidise uranium.

The XPS spectra obtained on samples, before and after CV experiments, indicated clearly enrichment in thorium at the surface and a higher oxidation state of uranium. The results also indicated that a higher initial uranium content on the surface leads to a higher shift of U-*4f* binding energies, suggesting a higher oxidation state of uranium. This was supported by the shape of the corresponding O-*1s* spectrum showing higher contribution of oxygen from $OH^-$ groups.

## REFERENCES

[1] P Cakir, R Eloirdi, F Huber, R J M Konings, and T Gouder. Thorium effect on the oxidation of uranium : Photoelectron spectroscopy ( XPS / UPS ) and cyclic voltammetry ( CV ) investigation on (U1-xThx)O2 (x=0 to 1) thin films. *Applied Surface Science*, 393:204–211, 2017.

[2] Y Lu, Y Yang, and P Zhang. Thermodynamic properties and structural stability of thorium dioxide. *Journal of physics. Condensed matter : an Institute of Physics journal*, 24(22):225801, 2012.

[3] J.Stephen Herring, Philip E MacDonald, Kevan D Weaver, and Craig Kullberg. Low cost, proliferation resistant, uranium–thorium dioxide fuels for light water reactors. *Nuclear Engineering and Design*, 203(1):65–85, jan 2001.

[4] I. Grenthe, J. Fuger, R. J. M. Konings, R.J. Lemire, A. G. Muller, C. Nguyen-Trung Cregu, and H. Wanner. *Chemical thermodynamics of uranium*. North Holland, Amsterdam, 1992.

[5] D. Langmuir and J. S. Herman. The Mobility of Thorium in Natural Waters at low Temperatures. *Geochimica et Cosmochimica Acta*, 44:1753–1766, 1980.

[6] A. Seibert, S. Stumpf, T. Gouder, D. Schild, and M. A. Denecke. Actinide Thin Films as Surface Models. In *Actinide Nanoparticle Research*, pages 275–313. Springer Berlin Heidelberg, Berlin, Heidelberg, 2011.

[7] G. Heisbourg, S. Hubert, N. Dacheux, and J. Ritt. The kinetics of dissolution of Th1-xUxO2 solid solutions in nitric media. *Journal of Nuclear Materials*, 321(2-3):141–151, sep 2003.

[8] Erich Zimmer and Erich Merz. Dissolution of thorium-uranium mixed oxides in concentrated nitric acid. *Journal of Nuclear Materials*, 124:64–67, 1984.

[9] Rekha Rao, R K Bhagat, Nilesh P Salke, and Arun Kumar. Raman spectroscopic investigation of thorium dioxide-uranium dioxide (ThO2-UO2) fuel materials. *Applied spectroscopy*, 68(1):44–8, jan 2014.

[10] S. Sunder and N.H. Miller. XPS and XRD studies of (Th,U)O2 fuel corrosion in water. *Journal of Nuclear Materials*, 279(1):118–126, mar 2000.

[11] C.A. Colmenares. The oxidation of thorium, uranium, and plutonium. *Progress in Solid State Chemistry*, 9:139–239, jan 1975.

[12] F. Miserque, T. Gouder, D. H. Wegen, and P. D W Bottomley. Use of UO2 films for electrochemical studies. *Journal of Nuclear Materials*, 298(3):280–290, 2001.

[13] A. Seibert, D.H. Wegen, T. Gouder, J. Römer, T. Wiss, and J.-P. Glatz. The use of the electrochemical quartz crystal microbalance (EQCM) in corrosion studies of UO2 thin film models. *Journal of Nuclear Materials*, 419(1-3):112–121, dec 2011.

[14] D.W. Shoesmith. Fuel corrosion processes under waste disposal conditions. *Journal of Nuclear Materials*, 282(1):1–31, nov 2000.

[15] Linda Wu, Zack Qin, and David W. Shoesmith. An improved model for the corrosion of used nuclear fuel inside a failed waste container under permanent disposal conditions. *Corrosion Science*, 84:85–95, jul 2014.

[16] S. Sunder, N.H. Miller, and D.W. Shoesmith. Corrosion of uranium dioxide in hydrogen peroxide solutions. *Corrosion Science*, 46(5):1095–1111, may 2004.

[17] S. Sunder, D. W. Shoesmith, Robert J. Lemire, M. G. Bailey, and G. j. Wallace. The effect of pH on the corrosion of nuclear fuel (UO2) in oxygenated solutions. *Corrosion Science*, 32(4):373–386, 1991.

[18] S. Sunder, D. W. Shoesmith, M. G. Bailey, F. W. Stanchell, and N. S. McIntyre. Anodic oxidation of UO2 Part I. Electrochemical and X-Ray Photoelectron spectroscopic studies in neutral solutions. *Journal of Electroanalytical Chemistry*, 130:163–179, 1981.

[19] D. W. Shoesmith and S. Sunder. The prediction of nuclear fuel ( UO2) under waste disposal conditions. *Journal of Nuclear Materials*, 190:20–35, 1992.

[20] Neal Fairley. CASA XPS Manual 2.3.15 Introduction to XPS and AES. pages 1–177, 2009.

[21] Pelin Cakir, Rachel Eloirdi, Frank Huber, Rudy J M Konings, and Thomas Gouder. An XPS and UPS Study on the Electronic Structure of ThO x ( x <= 2 ) Thin Films. *Journal of Physical Chemistry C*, 118:24497–24503, 2014.

[22] John C. Fuggle and Santos F. Alvarado. Core-level lifetimes as determined by x-ray photoelectron spectroscopy measurements. *Physical Review A*, 22(4):1615–1624, oct 1980.

[23] J. C. Fuggle, A. F. Burr, L. M. Watson, D. J. Fabian, and W. Lang. X-ray photoelectron studies of thorium and uranium. *Journal of Physics F: Metal Physics*, 4:335, 1974.

[24] M. O. Krause, R. G. Haire, O. Keski-Rahkonen, and J. R. Peterson. Photoelectron spectrometry of the actinides from Ac to Es. *Journal of Electron Spectroscopy and Related Phenomena*, 47(C):215–226, 1988.

[25] G. C. Allen, J. A. Crofts, M. T. Curtis, P. M. Tucker, D. Chadwick, and J. P. Hampson. X-Ray photoelectron spectroscopy of some uranium oxide phases. *Journal of Chemical Society, Dalton Transactions*, (12):1296–1301, 1974.

[26] J. J. Pireaux, J. Riga, E. Thibaut, and C. Tenret-Noel. Shake-up satellites in the X-ray photoelectron spectra of uranium oxides and fluorides. A band structure scheme for uranium dioxides, UO2. *Chemical Physics*, 22:113–120, 1977.

[27] A Cros. Charging effects in X-ray photoelectron. *Journal of Electron Spectroscopy and Related Phenomena*, 59:1–14, 1992.

[28] J. Cazaux. Mechanisms of charging in electron spectroscopy. *Journal of Electron Spectroscopy and Related Phenomena*, 105(2-3):155–185, dec 1999.

[29] G. Fanjoux, H. Fornander Billault, B. Lescop, and a. Le Nadan. Evolution of the magnesium surface during oxidation studied by Metastable Impact Electron Spectroscopy. *Journal of Electron Spectroscopy and Related Phenomena*, 119(1):57–67, jul 2001.

[30] S. Anthonysamy, G. Panneerselvam, Santanu Bera, S.V. Narasimhan, and P.R. Vasudeva Rao. Studies on thermal expansion and XPS of urania–thoria solid solutions. *Journal of Nuclear Materials*, 281(1):15–21, sep 2000.

[31] Lindsay C. Shuller, Rodney C. Ewing, and Udo Becker. Thermodynamic properties of ThxU1-xO2 (0<x<1) based on quantum-mechanical calculations and Monte-Carlo simulations. *Journal of Nuclear Materials*, 412(1):13–21, may 2011.

[32] W. Trzebiatowski and P. W. Selwood. Magnetic Susceptibilities of Urania-Thoria Solid Solutions. *Journal of the American Chemical Society*, 72(10):4504–4506, oct 1950.

[33] W. A. Lambertson, M. H. Mueller, and F. H. Gunzel. Uranium Oxide Phase Equilibrium Systems: IV, UO2-ThO2. *Journal of the American Ceramic Society*, 36(12):397–399, dec 1953.

[34] S Hubert, J Purans, G Heisbourg, P Moisy, and N Dacheux. Local structure of actinide dioxide solid solutions Th(1-x)U(x)O2 and Th(1-x)Pu(x)O2. *Inorganic chemistry*, 45(10):3887–94, may 2006.

[35] Melissa M. Strehle, Brent J. Heuser, Mohamed S. Elbakhshwan, Xiaochun Han, David J. Gennardo, Harrison K. Pappas, and Hyunsu Ju. Characterization of single crystal uranium-oxide thin films grown via reactive-gas magnetron sputtering on yttria-stabilized zirconia and sapphire. *Thin Solid Films*, 520(17):5616–5626, 2012.

[36] G. C. Allen, P. M. Tucker, and J. W. Tyler. Electronic structure of some binary uranium and thorium oxides and halides. *Philosophical Magazine Part B*, 48(1):63–75, 1983.

[37] B.W. Veal, D.J. Lam, H. Diamond, and H. R. Hoekstra. X-ray photoelectron-spectroscopy study of oxides of the transuranium elements Np, Pu, Am, Cm, Bk, and Cf. *Physical Review B*, 15(6):2929–2942, 1977.

[38] G. Heisbourg, S. Hubert, N. Dacheux, and J. Purans. Kinetic and thermodynamic studies of the dissolution of thoria-urania solid solutions. *Journal of Nuclear Materials*, 335(1):5–13, oct 2004.

[39] P. A. Demkowicz, J. L. Jerden, J. C. Cunnane, N. Shibuya, R. Baney, and J Tulenko. Aqueous Dissolution of Urania/Thoria Nuclear Fuel. *Nuclear Technology*, 147:157–170, 2004.

[40] D. W. Shoesmith, S. Sunder, and W. H. Hocking. Electrochemistry of UO2 Nuclear Fuel. In J. Lipkowski and N. P Ross, editors, *The Electrochemisty of Novel Materials*, pages 297–337. VCH, New York, 1994.

[41] B.G. Santos, J.J. Noël, and D.W. Shoesmith. The effect of pH on the anodic dissolution of SIMFUEL (UO2). *Journal of Electroanalytical Chemistry*, 586(1):1–11, jan 2006.

[42] B.G Santos, H.W Nesbitt, J.J Noël, and D.W Shoesmith. X-ray photoelectron spectroscopy study of anodically oxidized SIMFUEL surfaces. *Electrochimica Acta*, 49(11):1863–1873, apr 2004.

[43] S. Sunder, L.K. Strandlund, and D.W. Shoesmith. Anodic oxidation and dissolution of CANDU fuel (UO2) in slightly alkaline sodium perchlorate solutions. *Electrochimica Acta*, 43(16-17):2359–2372, may 1998.

[44] D. E. Grandstaff. A kinetic study of the dissolution of uraninite. *Economic Geology*, 71(8):1493–1506, dec 1976.

[45] B. Kanellakopulus. General Properties of Thorium Atom and Thorium ions. In R. J. Meyer, editor, *Gmelin Handbook of Inorganic Chemistry. Thorium*, pages 1–17. Springer-Verlag, Berlin Heidelberg New York Tokyo, 8th edition, 1989.

[46] Jean-Charles Dupin, Danielle Gonbeau, Philippe Vinatier, and Alain Levasseur. Systematic XPS studies of metal oxides, hydroxides and peroxides. *Physical Chemistry Chemical Physics*, 2(6):1319–1324, 2000.

[47] R. Agarwal and S. C. Parida. Phase Diagrams and Thermodynamic Properties of Thoria, Thoria–Urania, and Thoria–Plutonia. In D. Das and S. R. Bharadwaj, editors, *Thoria-based Nuclear Fuels, Green Energy and Technology*, pages 71–105. Springer-Verlag London, 2013.

# 4

# X-Ray Photoelectron Spectroscopy Study of the Reduction and Oxidation of Uranium and Cerium Single Oxide compared to (U-Ce) Mixed Oxide Films

**Rachel Eloirdi, Pelin Cakir, Frank Huber, A. Seibert, Rudy J. M. Konings, Thomas Gouder**

*Thin films of uranium cerium mixed oxides $U_xCe_{1-x}O_{2\pm y}$ have been prepared by DC sputtering and characterized by X-ray photoelectron spectroscopy (XPS). Reduction and oxidation properties were analysed by exposing the films to atomic hydrogen and to atomic oxygen, respectively. Possible interaction between uranium and cerium were investigated, by comparing the compounds to the single oxides of cerium and uranium. Uranium seems to promote the reduction of cerium. Conversely cerium promotes oxidation of uranium. Under our deposition conditions, it was not possible to produce pure U(IV) together with pure Ce(IV). The synthesis of $U_2O_5$ with U(V) cannot be obtained directly by DC sputtering, whereas with addition of cerium, U(V) seems to be stabilized and obtained more easily. This can be related to a charge transfer between Ce(IV) and U(IV).*

Parts of this chapter have been published in Applied Surface Science **457**, 566-571 (2018) [1]

## 4.1. INTRODUCTION

THE safety assessment of nuclear waste disposal in deep geological repositories requires an understanding of the corrosion behaviour of spent nuclear fuel (SNF). In particular the knowledge about the dissolution of the $UO_{2+x}$ matrix in the groundwater is crucial, as it can be linked to concomitant release of radionuclides produced during fission [2, 3]. The chemical properties of the spent fuel are strongly related to the oxidation state of uranium and thus to any parameter having influence on it [4]. It is well known that the solubility of uranium oxide increases sharply with the oxidation state, but it is also affected by the presence of other elements, transuranium elements or fission products. The effect of plutonium is of particular interest, as mixed uranium-plutonium oxide (MOX) is used as fuel in numerous nuclear reactors, and accumulates as spent nuclear fuel.



In a previous work we focused on the effect of thorium, on $(U_x,Th_{1-x})O_2$ dissolution [5]. Thorium has only one stable oxidation state (IV), therefore, only uranium can change oxidation state, and the system is relatively simple. In the present paper we study the influence of cerium, which has two stable oxidation states, (III) and (IV). Since these oxidation states of cerium are similar to plutonium [6–8] the mixed oxide with uranium can be investigated as surrogate for (U-Pu) mixed oxides. Cerium also forms as a fission product during reactor operation, together with other lanthanide elements, and thus be considered as spent fuel model as well. Cerium oxide is also a candidate for hydrogen production by concentrated solar power using thermochemical cycles for water splitting [9, 10] because of its redox behaviour and high temperature stability. In this frame also (U-Ce) mixed oxides were investigated [11].

In this work, we investigate the interaction of uranium and cerium in mixed oxides using thin film model surfaces produced *in-situ* by DC sputtering. Sputter deposition is a versatile method for producing samples with different U/Ce stoichiometries and oxygen content (O/M ratios). In contrast to real spent fuel, which is very complex, doped films allow focussing on one single element (Ce) and performing a single effect study. Since the interaction of the environment with spent fuel takes place at the surface, this process can be perfectly reproduced by using thin films.

DFT studies have shown that when $CeO_2$ is mixed with $UO_2$, a charge transfer takes place between the U(IV) and Ce(IV) leading to U(V) and Ce(III) [12]. This is corroborated by several experimental studies on (U-Ce) mixed oxide using XPS, in which the surface oxidation states have been analysed. Bera et al. [13] found Ce(III) alongside of U(IV), U(V) and U(VI). XPS measurements and analysis of the oxidized and reduced $Ce_xU_{1-x}O_{2\pm y}$ were performed by Al-Salik et al.[14]. While uranium was reduced from U(VI) to U(V) to U(IV) during $Ar^+$ ions sputtering, cerium was more sensitive to reduction in the mixed oxide than pure $CeO_2$. This shows that uranium promotes cerium reduction.

Even though there have been several studies on the redox behaviour of pure cerium and uranium oxide thin films, research on the uranium cerium mixed oxide thin films has so far not been performed, in contrast to bulk systems [6, 11, 13, 14].

In this work, we study the redox reactions on (U-Ce) mixed oxide surfaces upon exposure to atomic hydrogen and oxygen, respectively. The use of highly reactive atomic species ($O^{\cdot}$ and $H^{\cdot}$) for oxidation and reduction of the film surfaces allows reproducing

redox processes in the repository, triggered by alpha radiolysis of groundwater, creating strong oxidants ($H_2O_2$, $H_2O^{\cdot}$, $O_2$) and reductants ($H_2$, $H^{\cdot}$, $e^-$) [15]. Reaction with the more common molecular species ($O_2$ and $H_2$) under vacuum conditions (where electron spectroscopy is done) fails producing these effects because of the very low reactivity of these species.

In the following, we first discuss reference spectra of $CeO_2$, $Ce_2O_3$, $UO_2$, $U_2O_5$ and $UO_3$ thin films and the deposition of (U-Ce) mixed oxide. Second, reduction by atomic hydrogen at room temperature of $CeO_2$ and $UO_3$ will be compared to (U-Ce) mixed oxide film (ratio U/Ce~ 1), to understand the effect on the redox behavior in the solid solution as claimed in literature [14]. In the third part, oxidation of $Ce_2O_3$, and $U_2O_5$ have been performed by exposure to atomic oxygen at 573 - 673 K, and compared to a (U-Ce) mixed oxide film (ratio U/Ce~ 0.05). The high temperature was chosen to enable diffusion of oxygen into deeper layers and to achieve a homogeneously oxidized film. We will discuss the redox states of uranium and cerium in the mixed oxide and more specifically the effect of Ce(III) on the uranium valence, and compare to other Ln(III) cations [16–19].



## 4.2. EXPERIMENTAL

The thin films of $U_xCe_{1-x}O_{2\pm y}$ (x = 0 to 1) were prepared *in-situ* by direct current reactive co-sputtering from cerium and uranium metal targets in a gas mixture of Ar (6N) and $O_2$ (6N). The oxygen concentration in the films was adjusted by changing the $O_2$ partial pressure ($10^{-4}$ Pa – $5 \times 10^{-3}$ Pa), while the Ar partial pressure was maintained at $5 \times 10^{-3}$ mbar. The composition of the films was controlled by changing the respective target voltages for the uranium and cerium targets.

The thin films were deposited for 120 s with a deposition rate of 1Å/s, at room temperature on silicon wafer (100) substrates, which were cleaned by Ar ion sputtering (4 keV) for 10 min, and subsequently annealed under UHV at 773 K for 5 min. The plasma in the diode source was maintained by injection of electrons of 25-50 eV energy (triode setup), to work at low Ar pressure in absence of stabilizing magnetic fields.

Atomic oxygen ($O^{\cdot}$) and hydrogen ($H^{\cdot}$) were generated in an electron cyclotron resonance (ECR) Plasma Source Gen I from Tectra GmbH, Frankfurt/M. The atom flux is specified to $>10^{16}$ atoms/cm$^2$/s, corresponding to an exposure of roughly 10 Langmuir/s (i.e. 1.33x $10^{-3}$ Pa/s).

High resolution X-ray photoelectron spectroscopy (XPS) measurements were performed using a Phoibos 150 hemispherical analyser. Al K$\alpha$ (E = 1486.6 eV) radiation was produced by a XRC-1000 micro-focus source, equipped with a monochromator and operating at 120 W. The background pressure in the analysis chamber was around 2 x $10^{-10}$ mbar. The spectrometer was calibrated using the Au-$4f_{7/2}$ line (83.9 eV) and Cu-$2p_{3/2}$ (932.7 eV) of metallic gold and copper standards. Photoemission spectra were taken at room temperature. Data analyses were performed using CasaXPS software.

All the films produced and used for this study are never in contact with the laboratory atmosphere. The transfer of the different films from preparation chamber to analyses chamber is made under UHV and by remote control using the Labstation developed at JRC Karlsruhe.

## 4.3. RESULTS

### 4.3.1. REFERENCE SPECTRA OF THE CERIUM AND URANIUM SINGLE OXIDES, AND (U-CE) MIXED OXIDE DEPOSITION

The two cerium oxides $CeO_2$ and $Ce_2O_3$ were obtained by sputter deposition at the appropriate $O_2$ partial pressure.

The Ce-*3d* spectra are rather complex [20–22] due to the coexistence of different final states, well screened, poorly screened and unscreened peaks are observed at different binding energies (BE). The ground state configurations of cerium are $[Xe]4f^1(5d6s)^3$ for $Ce^0$, $[Xe]4f^1(5d6s)^0$ for $Ce^{3+}$ and $[Xe]4f^0(5d6s)^0$ for $Ce^{4+}$. The photoemission process then leads to the typical final state screening picture, where the core hole is screened by population of the 4f states (good screening), 5d6s (poor screening) and no population at all (non-screening). The corresponding photoemission peaks for Ce(III) and Ce(IV) are summarized in Table 4.1. These values are in very good agreement with spectra obtained in literature [20, 22–25].

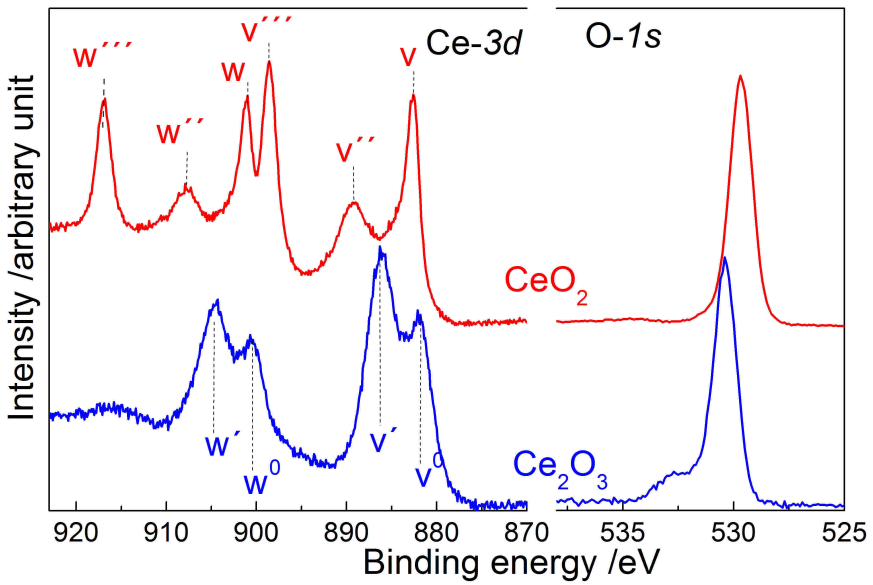


Figure 4.1: Ce-*3d* and O-*1s* core level spectra present in $CeO_2$ (red) and in $Ce_2O_3$ (blue) films

Figure 4.1 shows the Ce-*3d* spectra together with the O-*1s* spectra corresponding to $Ce_2O_3$ (blue curves) and $CeO_2$ (red curves) films. $Ce_2O_3$ displays four peaks for Ce-*3d*, labelled $W^0$, W´ and $V^0$, V´ assigned to $3d_{3/2}$ and $3d_{5/2}$ respectively. In $CeO_2$ the six peaks, W, W´´, W´´´ and V, V´´,V´´´ are assigned to $3d_{3/2}$ and $3d_{5/2}$ respectively. The peak at 916.5 eV BE (W"') is a clear indicator for Ce(IV) because it does not superimpose with any Ce(III) line - it is not present in the spectrum of $Ce_2O_3$. It corresponds to the unscreened Ce-$3d_{3/2}$ final state of Ce(IV). However, there is no clear linear dependence between $Ce^{4+}$ concentration and W"' intensity [26].

Table 4.1: Binding energy of Ce-*3d* peaks present in $Ce_2O_3$ and $CeO_2$.

| **Ce(III)** | Initial → Final State | Binding Energy [eV] | **Ce(IV)** | Initial → Final State | Binding Energy [eV] |
|---|---|---|---|---|---|
| **V**$^0$ | $3d^{10}4f^1$ → $3d^94f^2(5d6s)^0$ | 881.6 | **V** | $3d^{10}4f^0(5d6s)^0$ → $3d^94f^1(5d6s)^0$ | 882.3 |
| **W**$^0$ | | 900.0 | **W** | | 900.7 |
| **V'** | $3d^{10}4f^1$ → $3d^94f^1(5d6s)^1$ | 886.0 | **V"** | $3d^{10}4f^0$ $(5d6s)^0$→ $3d^94f^0(5d6s)^1$ | 889.0 |
| **W'** | | 904.6 | **W"** | | 907.3 |
| | | | **V"'** | $3d^{10}4f^0$ $(5d6s)^0$→ $3d^94f^0(5d6s)^0$ | 898.1 |
| | | | **W"'** | | 916.5 |

The corresponding O-*1s* main line of $CeO_2$ and $Ce_2O_3$ lie at 529.7 eV and 530.4 eV BE, respectively. The O-*1s* line of $Ce_2O_3$ has a shoulder on its high binding energy side while for $CeO_2$, the peak is relatively symmetric. Although this shoulder could a priori be explained by the oxygen from the oxidized silicon substrate interface [20] which is in contact with the $Ce_2O_3$ thin film, this has been rejected because the BE difference with the main peak is too low relatively to the expected value for O-Si substrate lines in the present study. The shoulder has also been attributed to $H_2O$ adsorbed on defect sites [24, 27]. In general, water chemisorbed on oxides gives such high BE shoulder [28]. However, it has been shown that even at a temperature of 645 K the shoulder does not totally disappear [24]. Pfau et al. [22] have linked this shoulder to vacancies or disorder induced by the presence of Ce(III) in the sample. $Ce_2O_3$ deposition at ambient temperature leads to more defects, because of the absence of thermal annealing, as the atoms do not have the energy to diffuse and organize at the surface of the substrate. In this study we always observe this shoulder when $Ce_2O_3$ is present in the mixed oxide.

Figure 4.2 compares the U-*4f* and O-*1s* core level spectra of $UO_2$, $U_2O_5$ and $UO_3$ films. Unlike $UO_2$, $Ce_2O_3$ and $CeO_2$ which can be produced directly by DC sputtering by varying the $O_2$ partial pressure, thin films of $U_2O_5$ and $UO_3$ require further oxidation and reduction treatment with atomic oxygen and atomic hydrogen to be produced. To get $UO_3$, post-deposition exposure to atomic oxygen at high temperature, 673 K, is necessary. $U_2O_5$ is obtained by reducing with atomic hydrogen the $UO_3$ films, kept at the same temperature of 673 K [29].

Spectra show the spin-orbit split final states of U-$4f_{5/2}$ and U-$4f_{7/2}$ with ΔE=10.8 eV. The main lines undergo a strong chemical shift between $UO_2$ and $U_2O_5$ (ΔE=0.8 eV) and a weaker one between $U_2O_5$ and $UO_3$ (ΔE=0.2 eV). The main lines are accompanied by characteristic satellites at higher binding energy. Table 4.2 summarizes the binding energy of the main peaks and the linked satellite peaks for U(IV), U(V) and U(VI). The satellite peaks play an important role in the assignment of the oxidation state of uranium. The energy difference (ΔE) between satellite and main line steadily increase with the oxidation state. The satellite has been attributed to the energy loss of the photoelectrons due to excitation of an O-*2p*→U-$5f_{unoccupied}$ electron transition. However, the correlation

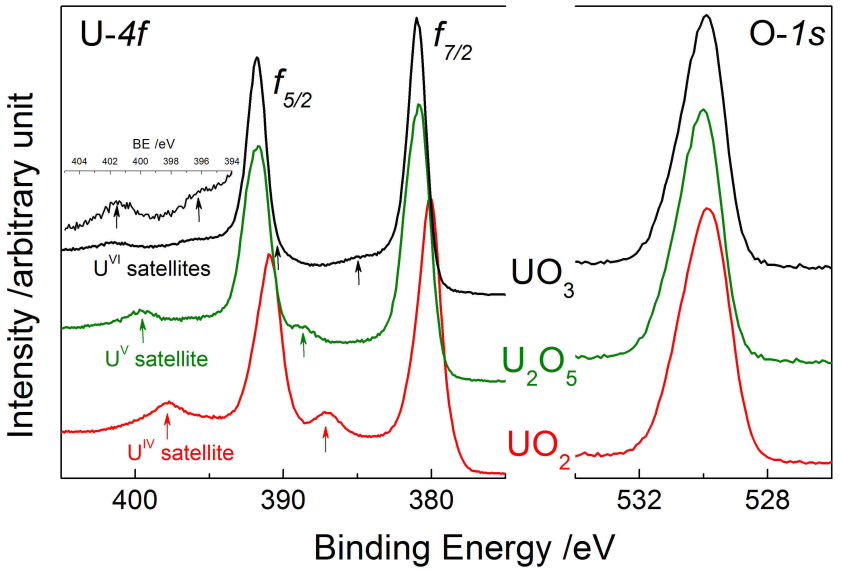


Figure 4.2: U-*4f* and O-*1s* core level spectra present in $UO_2$ (red), $U_2O_5$ (green) and in $UO_3$ (black) films -insert: Satellite peaks of $UO_3$.

between the satellite energies and intensities and inter-atomic effects or environmental condition is still not clear..

Figure 4.3 shows the U-*4f*, Ce-*3d* and O-*1s* spectra of uranium rich $U_{0.8}Ce_{0.2}O_{2-x}$ films co-deposited at low (traces of oxygen) and at high oxygen partial pressure. The fitting of Ce-*3d* and U-*4f* peaks was done by using CasaXPS. Shirley algorithm for inelastic background subtraction [30] and Gaussian-Lorentzian profile were applied for the fitting of the peaks. U/Ce and M/O were calculated using the ratios between the respective peaks. Deposition at zero oxygen pressure still produces oxide films (Figure 4.3, black curves), because of the residual oxidation of the targets from previous depositions and we did not especially seek producing metal films. The film contains U(IV), as shown by the 4f-satellite at ΔE=6.8 eV (Table 4.2), and Ce(III), as shown by the characteristic 3d spectrum (compare to Figure 4.1). The corresponding O-*1s* spectrum has the main line together with the high BE shoulder, which was previously observed for $Ce_2O_3$. At higher oxygen partial pressure, uranium oxidizes further as shown by the appearance of a U-*4f* satellite at ΔE=7.8 eV, characteristic for U(V) (Table 4.2). Cerium is partially oxidized into Ce(IV). The O-*1s* peaks shifts to lower binding energy and the high BE shoulder tends to disappear, resembling again the spectra of $CeO_2$. The shift, which also occurs for Ce-*3d* and U-*4f* (rigid shift), is attributed to the decrease of the Fermi-energy as result of further surface oxidation.

It was not possible to obtain solely Ce(IV) together with U(IV). Even partial oxidation of Ce(III) only takes place when $U^{4+}$ also oxidizes. This seems to reflect the chemical equilibrium situation at the surface, because during sputter deposition the impinging

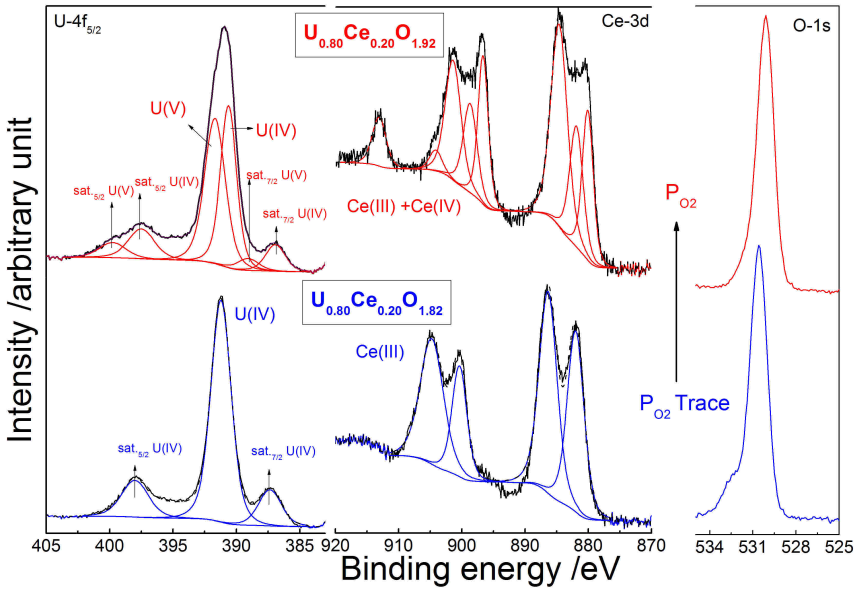


Figure 4.3: U-*4f*, Ce-*3d* and O-*1s* of $U_{0.80}Ce_{0.20}$Oxide, effect of $PO_2$ increase during co-deposition. Peaks were deconvoluted using Shirley background correction and the Gaussian-Lorentzian function

Table 4.2: . Binding energy of O-*1s*, U-$4f_{7/2}$, U-$4f_{5/2}$ and satellite peak present in $UO_2$, $U_2O_5$ and $UO_3$.

| | O-*1s* [eV] | U-$4f_{7/2}$ [eV] | U-$4f_{5/2}$ [eV] | ΔE [eV] U-*4f*-satellites | |
|---|---|---|---|---|---|
| $UO_2$ | 529.9 ± 0.1 | 380.1 ± 0.1 | 390.9 ± 0.1 | 6.9 ± 0.2 | |
| $U_2O_5$ | 530.0 ± 0.1 | 380.8 ± 0.1 | 391.7 ± 0.1 | 7.8 ± 0.1 | |
| $UO_3$ | 529.9 ± 0.1 | 381.0 ± 0.1 | 391.8 ± 0.1 | 9.7 ± 0.1 | 4.1 ± 0.1 |

clusters bring enough energy with them to be organized in a stable configuration.

### 4.3.2. REDUCTION PROCESS WITH ATOMIC HYDROGEN

Reduction of $CeO_2$ and uranium higher oxides, as bulk materials and thin films, are described in detail in the literature [14, 20, 31]. Reduction may occur by thermal decomposition (oxygen desorption), $Ar^+$ sputtering (preferential removal of oxygen) or reaction with hydrogen (water formation and desorption).

In Figure 4.4, spectra of Ce-*3d*, U-*4f* and O-*1s* along the reduction of pure $CeO_2$ (Figure 4.4A) and pure $UO_3$ (Figure 4.4B) films are reported and compared to the reduction of $U_{0.45}Ce_{0.55}O_{2+x}$ by atomic hydrogen (Figure 4.4C).

Figure 4.4A displays the spectra of $CeO_2$ obtained after deposition (black curve), and after exposure to atomic hydrogen at room temperature (green curve) and subsequent heating at 473 K (blue curve). Exposure to atomic hydrogen at ambient temperature has

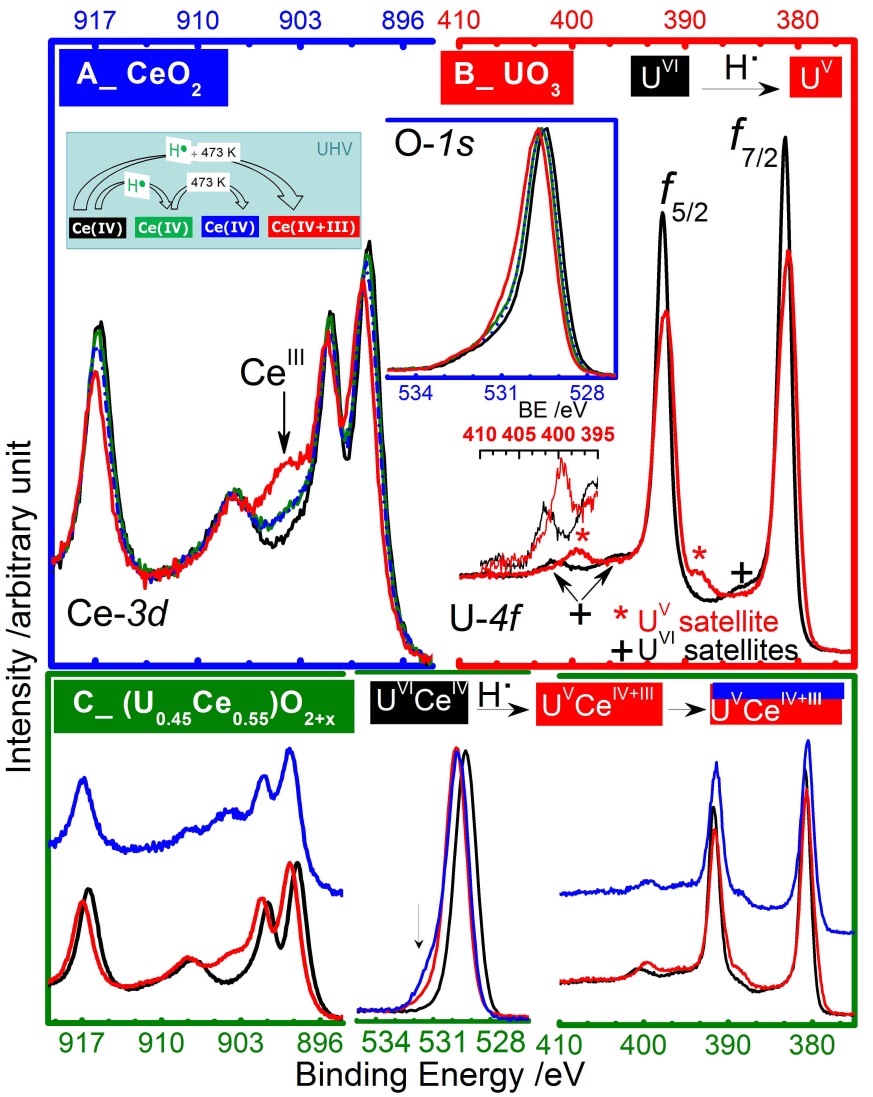


Figure 4.4: Ce-*3d* and U-*4f* before and after reduction with atomic hydrogen obtained on A- $CeO_2$, B- $UO_3$ and C- $U_{0.45}Ce_{0.55}O_{2+x}$. Insert- O-*1s* of $CeO_2$

only a slight effect on the $Ce^{4+}/Ce^{3+}$ ratio measured by XPS (10 atomic layers): the intensity of the $Ce^{4+}$ signal at 916 eV does not decrease and conversely the intensity of the $Ce^{3+}$ line at about 904.6 eV (W´) does not increase. Subsequent heat treatment at 473 K did not change much the $Ce^{4+}/Ce^{3+}$ ratio either. Another interesting sign of reduction on surface is the shoulder at higher BE appearance on the O-*1s* spectrum (inset Figure 4.4A). This has been discussed many times in literature [24, 32]. It is concluded that the surface hydroxyl appears as sign of oxygen vacancy and result of the reduction via break

of M-O bond. The existence of $OH^-$ emission was also found in reductions of $PuO_2$ to $Pu_2O_3$ [33]. In our study, we can say is that the peak intensity of the shoulder in O-*1s* signal does not change much during the reduction process at room temperature followed by heating at 473 K. Surface reduction thus takes place more efficiently when the sample is simultaneously heated to 473 K and exposed to atomic hydrogen (Figure 4.4A, red curve). Decrease of the $Ce^{4+}$ signal at 916.5 eV signal is in this condition stronger. We explain the stronger reaction by the enhanced mobility of hydrogen and/or oxygen. Diffusion of H in the bulk has been confirmed by XPS measurements made on grazing incidence (not reported here) showing a constant intensity peak of Ce(III) for room and for higher temperature. The limiting step for the lower near surface layers reduction is linked to the diffusion of hydrogen and/or oxygen through the lattice.

Figure 4.4B shows U-*4f* core level spectra of $UO_3$ before and after exposure to atomic hydrogen at ambient temperature. The changing U-*4f* satellite energies (see Table 4.2) show that U(VI) is reduced into U(V), i.e. $UO_3$ into $U_2O_5$. Reduction to $U_2O_5$ is complete with the information depth of XPS, with a mean information depth of 10 monolayers.

Figure 4.4C shows the reaction of a mixed (U-Ce) oxide when exposed to atomic hydrogen at room temperature. In the mixed oxide both elements can change their oxidation state and the question is whether uranium can promote the reduction of cerium. The initial deposition (black curve) shows the characteristic U-*4f* peaks of U(VI) with some trace of U(V) and a Ce-*3d* peak typical for Ce(IV). The O-*1s* peak is of symmetrical shape. Deposition was performed at highest possible oxygen partial pressure. The high limit is imposed by the oxidation of the targets during sputter deposition, which eventually disrupts the plasma. It should be noticed that for uranium deposition alone (see above), the highest uranium oxidation that could be reached in the films was $UO_{2+x}$ with a mixture of U(IV)+U(V). In presence of cerium, U(VI) is obtained as main valence state. Co-deposition with cerium as Ce(IV) thus seems to enhance uranium oxidation further to U(VI) after deposition by DC sputtering. The presence of both trivalent and tetravalent states of cerium is expected by the charge transfer reaction between U and Ce as proposed by Griffiths et al. [34] as follows.

$Ce^{4+} + U^{4+} \rightarrow Ce^{3+} + U^{5+}$

A charge-transfer process or orbital hybridization [35–37] has also been reported for the known "cerium-uranium blue" colour of some $CeO_2$-$UO_2$ solid solutions. Magnetic studies [37] of $CeO_2$-$UO_2$ solid solutions were interpreted in terms of partial charge transfer.

When the surface is exposed to atomic hydrogen at room temperature (RT), uranium is fully reduced into U(V) (red curve), as for pure $UO_3$. Also, Ce(IV) is reduced into Ce(III) even though to a lesser extent. This stands in contrast to pure $CeO_2$, which was hardly reduced. Obviously, cerium reduction is enhanced by uranium. Upon reduction the Ce-*3d* peaks shift to higher BE by 0.5 eV. A similar shift is observed for the O-*1s* peak. It is attributed to the increase of the Fermi-energy upon formation of $Ce_2O_3$ and reduction of $UO_3$, and as consequence of negative charging of the surface. As after effect all photoemission peaks rigidly shift to higher binding energy (Ce-*3d*, O-*1s*). For the U-*4f* peak, this shift is compensated by the reduction of U(VI) to U(V) which leads to a chemical shift of the U-*4f* line to about 0.2-0.5 eV lower binding energy. When spectra are taken at grazing incidence (blue curves), the Ce(III) signal at about 904.6 eV increases slightly

showing reduction to take place mainly at the top surface. Also, the high BE shoulder of the O-*1s* peak is increasing (arrow O-*1s* Figure4.4C), pointing to the presence of $Ce_2O_3$.

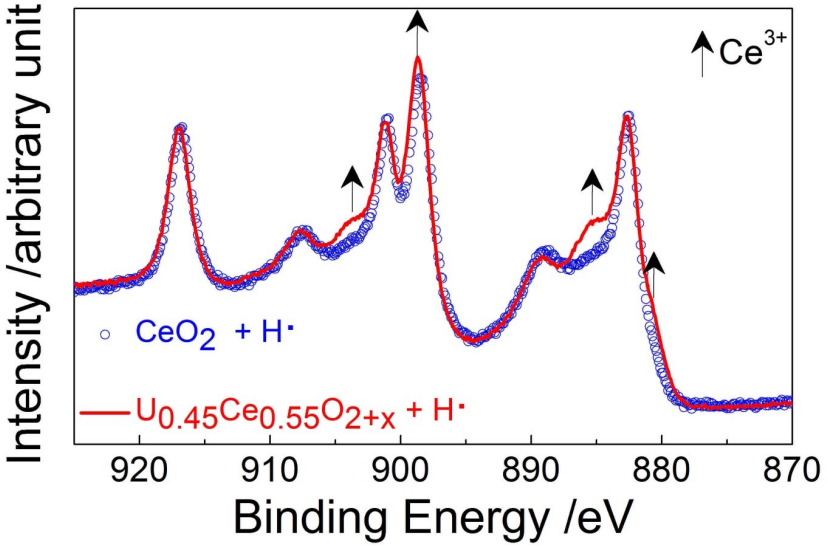


Figure 4.5: Ce-*3d* core level spectra of $CeO_2$ and $U_{0.45}Ce_{0.55}$ after the exposure to atomic hydrogen at room temperature

For better comparison, the Ce-*3d* spectra of $CeO_2$ and $U_{0.45}Ce_{0.55}O_{2+x}$ after reaction with hydrogen are superposed with normalized intensities in Figure 4.5. The mixed oxide has a more reduced Ce(III) signal. The presence of uranium seems to facilitate the reduction of cerium at room temperature. The grazing incidence measurement shows that the cerium reduction is more pronounced at the surface. The corresponding reduction of uranium from U(VI) into U(V) is well extending into the layers underneath.

Similar results are obtained by other authors for bulk samples of mixed uranium-cerium oxides who observed that cerium is more prone to reduction when mixed with uranium [11, 14].

### 4.3.3. OXIDATION PROCESS WITH ATOMIC OXYGEN

Figure 4.6 displays the Ce-*3d* and U-*4f* core level spectra along the oxidation with atomic oxygen of $Ce_2O_3$ (Figure 4.6A) and $UO_{2+x}$ (Figure 4.6B) compared to the oxidation of $U_{0.05}$ $Ce_{0.95}O_2$ (Figure 4.6C). $U_{0.05}Ce_{0.95}O_2$ film is deposited at the highest possible oxygen pressure (limited by U and Ce target oxidation).

The oxidation of $Ce_2O_3$ by atomic oxygen at 623 - 673K leads to pure $CeO_2$ as indicated by the characteristic Ce-*3d* spectrum and by the absence of Ce-*4f* at about 1 eV (Figure 4.6A-insert). Oxidation of $UO_{2+x}$ by atomic oxygen leads to the formation of $UO_3$. The absence of $U^{IV}$ or $U^{V}$ is demonstrated by the absence of the localized U-*5f* emission[29].

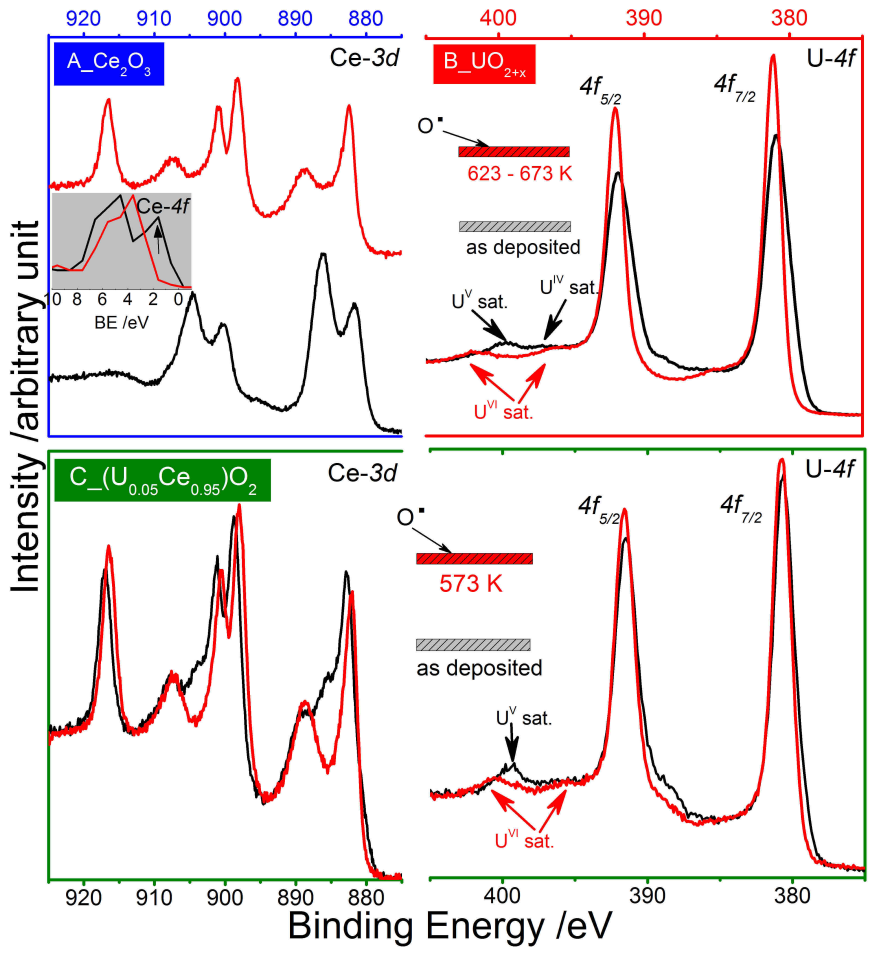


Figure 4.6: Ce-*3d* and U-*4f* before and after oxidation with atomic oxygen at about 600 K obtained on A- $Ce_2O_3$, B- $U_2O_5$ and C- of $U_{0.05}Ce_{0.95}O_2$ after deposition and after oxidation with atomic oxygen at 573 K

After deposition of $U_{0.05}Ce_{0.95}O_2$ (black curves), cerium is present as a mixture with mostly $Ce^{4+}$, while uranium is exclusively U(V), as shown by the satellite at ΔE=7.8 eV. While we cannot obtain directly $U_2O_5$ by DC sputtering, it is interesting to see that in addition to cerium, a single oxidation state of uranium as U(V) can be directly obtained by DC sputtering. This can be due to charge transfer between uranium and cerium, stabilizing U(V) at the extent of pure and single U(IV) together with Ce(IV).

After oxidation of $U_{0.05}Ce_{0.95}O_2$ with atomic oxygen, cerium is completely oxidised into $Ce^{4+}$ as shown by the absence of Ce-*4f* peak at about 1 eV [38] while uranium is oxidised in $U^{+6}$ with still some trace of $U^{5+}$ as observed by a weak shoulder at low BE of U-$4f_{5/2}$ linked to $U^{+5}$ satellite peak. Compared to binary uranium oxide $UO_{2+x}$ (Figure 4.6B) which oxidized completely to U(VI) in the mixed oxide, the oxidation of uranium

into U(VI) is not complete, which may be linked to the presence of Ce(III) present initially as it has been reported in literature relatively to Ln(III) [16–18] which decrease the trend of uranium to oxidise into U(VI).

## 4.4. CONCLUSION

We studied the surface reactivity of (U-Ce) mixed oxides towards atomic hydrogen and atomic oxygen. The redox behaviour of the mixed oxides was compared to that of the binary cerium and uranium oxides. Goal was to detect a possible mutual influence between uranium and cerium on their reactivity. Two questions were addressed, first if uranium has an influence on the reduction of Ce(IV) into Ce(III), second, whether Ce(III) could inhibit uranium oxidation to U(VI) formation, as was reported in literature for other Ln(III) cations[16–19].



Reference spectra of the single oxides were taken using $CeO_2$, $Ce_2O_3$, $UO_2$, $U_2O_5$ and $UO_3$ thin films. Both cerium oxides could be deposited directly by sputter deposition using the appropriate oxygen pressure. In the U-O system only $UO_2$ can be prepared directly by DC sputtering. At maximum oxygen partial pressure, deposition of $UO_{2+x}$ is obtained, containing a mixture of $U^{4+}$ and $U^{5+}$. The higher uranium oxides $U_2O_5$ and $UO_3$ representing the single state U(V) and U(VI) valence states, need post-deposition treatment with atomic oxygen at 673 K.

In mixed oxide films uranium, with mainly $U^{6+}$ or mainly $U^{5+}$ could be deposited directly without post-deposition oxidation necessary for single uranium oxide. This shows a higher reactivity of uranium towards oxygen when co-deposited with cerium and which can be linked to charge transfer between uranium and cerium.

Surface reaction with atomic hydrogen at room temperature was studied. $CeO_2$, $UO_3$ were compared to (U-Ce) mixed oxide system (ratio U/Ce~1). It was shown that uranium promotes the reduction of cerium, as claimed in literature: at room temperature cerium is partially reduced to Ce(III) while in the same condition pure $CeO_2$ hardly reduces. Measurements at grazing incidence of the MOX showed that the cerium reduction is more pronounced at the surface. The corresponding reduction of uranium from U(VI) into U(V) is well extending into the layers underneath. The reduction of the (U-Ce) mixed oxide is thus a complex and incongruent process.

Surface oxidation with atomic oxygen at 573 K - 673 K of (U-Ce) mixed oxide system (ratio U/Ce~ 0.05) was compared to binary oxides $Ce_2O_3$ and $U_2O_5$ films. It was demonstrated that while uranium in $U_2O_5$ is completely oxidised to $UO_3$ as expected, uranium in mixed oxide present initially as U(V) was not completely oxidised to U(VI), keeping some traces of U(V). The result might be linked to the temperature which was kept at about 600 K.

It was so far not possible to form mixtures of U(IV) and Ce(IV) by co-deposition: U(V) always formed together with Ce(III), while Ce(IV) only formed in presence of U(V) or U(VI).

## REFERENCES

[1] R. Eloirdi, P. Cakir, F. Huber, A. Seibert, R. Konings, and T. Gouder. X-ray photoelectron spectroscopy study of the reduction and oxidation of uranium and cerium single oxide compared to (U-Ce) mixed oxide films. *Applied Surface Science*, 457(April):566–571, 2018.

[2] H. Kleykamp. The chemical state of the fission products in oxide fuels. *Journal of Nuclear Materials*, 131(2-3):221–246, apr 1985.

[3] L. H. Johnson and D. W. Shoesmith. Spent Fuel. In W. B. Lutze and Rodney C. Ewing, editors, *Radioactive Waste Forms for the Future*, chapter 11, page 635. Amsterdam, The Netherlands, 1988.

[4] I. Grenthe, J. Fuger, R. J. M. Konings, R.J. Lemire, A. G. Muller, C. Nguyen-Trung Cregu, and H. Wanner. *Chemical thermodynamics of uranium*. North Holland, Amsterdam, 1992.

[5] P Cakir, R Eloirdi, F Huber, R J M Konings, and T Gouder. Thorium effect on the oxidation of uranium : Photoelectron spectroscopy ( XPS / UPS ) and cyclic voltammetry ( CV ) investigation on (U1-xThx)O2 (x=0 to 1) thin films. *Applied Surface Science*, 393:204–211, 2017.

[6] K. Suresh Kumar, T. Mathews, H. P. Nawada, and N. P. Bhat. Oxidation behaviour of uranium in the internally gelated urania–ceria solid solutions – XRD and XPS studies. *Journal of Nuclear Materials*, 324(2-3):177–182, jan 2004.

[7] P. Martin, M. Ripert, T. Petit, T. Reich, C. Hennig, F. D'Acapito, J. L. Hazemann, and O. Proux. A XAS study of the local environments of cations in (U,Ce)O2. *Journal of Nuclear Materials*, 312(1):103–110, 2003.

[8] D. I. R. Norris and P. Kay. Oxygen Potential and Lattice Parameter Measurements in (U, Ce)O2-x. *Journal of Nuclear Materials*, 116:184–194, 1983.

[9] H. Kaneko, T. Miura, H. Ishihara, S. Taku, T. Yokoyama, H. Nakajima, and Y. Tamaura. Reactive ceramics of CeO2–MOx (M=Mn, Fe, Ni, Cu) for H2 generation by two-step water splitting using concentrated solar thermal energy. *Energy*, 32(5):656–663, 2007.

[10] S. Abanades and G. Flamant. Thermochemical hydrogen production from a two-step solar-driven water-splitting cycle based on cerium oxides. *Solar Energy*, 80(12):1611–1623, dec 2006.

[11] I. Al-Shankiti, F. Al-Otaibi, Y. Al-Salik, and H. Idriss. Solar thermal hydrogen production from water over modified CeO2 materials. *Topics in Catalysis*, 56(12):1129–1138, 2013.

[12] B. E. Hanken, C. R. Stanek, N. Grønbech-Jensen, and M. Asta. Computational study of the energetics of charge and cation mixing in U1-xCexO2. *Physical Review B*, 84(8):085131, aug 2011.

[13] S. Bera, V. K. Mittal, R. Venkata Krishnan, T. Saravanan, S. Velmurugan, K. Nagarajan, and S. V. Narasimhan. XPS analysis of UxCe1-xO2+y and determination of oxygen to metal ratio. *Journal of Nuclear Materials*, 393(1):120–125, 2009.

[14] Y. Al-Salik, I. Al-Shankiti, and H. Idriss. Core level spectroscopy of oxidized and reduced CexU1-xO2 materials. *Journal of Electron Spectroscopy and Related Phenomena*, 194:66–73, 2014.

[15] G. R. Choppin, J. O. Liljenzin, and J. Rydberg. *Radiochemistry and nuclear chemistry*. Butterworth-Heinemann, 2002.

[16] N Liu. Electrochemical and Modelling Studies on Simulated Spent Nuclear Fuel Corrosion under Permanent Waste Disposal Conditions. *Electronic Thesis and Dissertation Repository*, feb 2017.

[17] J. Kim, Y. Ha, S. Park, K. Jee, and W. Kim. Effect of a trivalent dopant, Gd3+, on the oxidation of uranium dioxide. *Journal of Nuclear Materials*, 297(3):327–331, sep 2001.

[18] M. Razdan and D. W. Shoesmith. Influence of Trivalent-Dopants on the Structural and Electrochemical Properties of Uranium Dioxide (UO2). *Journal of the Electrochemical Society*, 161(3):H105–H113, dec 2013.

[19] H. He, K. O 'Neil, O. Semenikhin, and D. W. Shoesmith. The Influence of Rare-Earth Doping and Non- Stoichiometry on the Corrosion of Uranium Dioxide. Technical report, 2012.

[20] P. Bera and C. Anandan. Growth, Structural Characterization and Interfacial Reaction of Magnetron Sputtered CeO2 Thin Films On Different Substrates. *Surface Review and Letters*, 21(04):1450054, aug 2014.

[21] D. D. Koelling, A. M. Boring, and J. H. Wood. The electronic Structure of CeO2 and PrO2. *Solid state Communications*, 47(4):227–232, 1983.

[22] A Pfau and K D Schierbaum. The electronic structure of stoichiometric and reduced CeO , surfaces : an XPS , UPS and HREELS study. *Surface Science*, 6028(94):71–80, 1994.

[23] M. A. Henderson, C. L. Perkins, M. H. Engelhard, S. Thevuthasan, and C. H F Peden. Redox properties of water on the oxidized and reduced surfaces of CeO2(1 1 1). *Surface Science*, 526(1-2):1–18, 2003.

[24] S. M. F. Shahed, T. Hasegawa, Y. Sainoo, Y. Watanabe, N. Isomura, A. Beniya, H. Hirata, and T. Komeda. STM and XPS study of CeO2(111) reduction by atomic hydrogen. *Surface Science*, 628:30–35, oct 2014.

[25] D. R. Mullins. The surface chemistry of cerium oxide. *Surface Science Reports*, 70(1):42–85, 2015.

[26] M. Romeo, K. Bak, J. El Fallah, F. Le Normand, and L. Hilaire. XPS Study of the reduction of cerium dioxide. *Surface and Interface Analysis*, 20(6):508–512, may 1993.

[27] Y. Lykhach, V. Johánek, H. A. Aleksandrov, S. M. Kozlov, M. Happel, T. Skála, P. Petkov, N. Tsud, G. N. Vayssilov, K. C. Prince, K. M. Neyman, V. Matolín, and J. Libuda. Water Chemistry on Model Ceria and Pt/Ceria Catalysts. *The Journal of Physical Chemistry C*, 116(22):12103–12113, jun 2012.

[28] S. Benkoula, O. Sublemontier, M. Patanen, C. Nicolas, F. Sirotti, A. Naitabdi, F. Gaie-Levrel, E. Antonsson, D. Aureau, F. X. Ouf, S. Wada, A. Etcheberry, K. Ueda, and C. Miron. Water adsorption on TiO2 surfaces probed by soft X-ray spectroscopies: bulk materials vs. isolated nanoparticles. *Scientific Reports*, 5(1):15088, dec 2015.

[29] T. Gouder, R. Eloirdi, and R. Caciuffo. Direct observation of pure pentavalent uranium in U2O5 thin films by high resolution photoemission spectroscopy. *Scientific Reports*, 8(1):8306, dec 2018.

[30] D. A. Shirley. High-Resolution X-Ray Photoemission Spectrum of the Valence Bands of Gold. *Physical Review B*, 5(12):4709–4714, 1972.

[31] R. J. McEachern and P. Taylor. A review of the oxidation of uranium dioxide at temperatures below 400°C. *Journal of Nuclear Materials*, 254:87–121, 1998.

[32] B. Chen, Y. Ma, L. Ding, L. Xu, Z. Wu, and Q. Yuan. Reactivity of Hydroxyls and Water on a CeO 2 ( 111 ) Thin Film Surface : The Role of Oxygen Vacancy. *The Journal of Physical Chemistry C*, 2(111):5800–5810, 2013.

[33] A. Seibert, T. Gouder, and F. Huber. Interaction of PuO 2 thin films with water. *Radiochimica Acta*, 98(9-11):647–657, nov 2010.

[34] T. R. Griffiths, H. V. St. A. Hubbard, and M. J. Davies. Electron transfer reactions in non-stoichiometric ceria and urania. *Inorganica Chimica Acta*, 225(1-2):305–317, oct 1994.

[35] Y. Hinatsu and T. Fujino. Studies on magnetic properties of UO2-CeO2 solid solutions: I. Magnetic susceptibilities of solid solutions with low cerium concentrations. *Journal of Solid State Chemistry*, 73(2):348–355, apr 1988.

[36] Y. Hinatsu and T. Fujino. Studies on magnetic properties of UO2-CeO2 solid solutions III: Magnetic susceptibilities of solid solutions with high cerium concentrations. *Journal of the Less Common Metals*, 149:197–205, apr 1989.

[37] M. R. Antonio, U. Staub, J. S. Xue, and L. Soderholm. Comparison of the Cation Valence and Coordination in Ce2UO6 and Ce2MoO6. *Chemistry of Materials*, 8(11):2673–2680, jan 1996.

[38] Konstantin I. Maslakov, Yury A. Teterin, Aleksej J. Popel, Anton Yu. Teterin, Kirill E. Ivanov, Stepan N. Kalmykov, Vladimir G. Petrov, Peter K. Petrov, and Ian Farnan. XPS study of ion irradiated and unirradiated CeO2 bulk and thin film samples. *Applied Surface Science*, 448:154–162, aug 2018.

# 5

# SURFACE REDUCTION OF $NpO_2$ AND U MIXED OXIDES WITH PU AND TH BY PHOTOCATALYTIC REACTION WITH ICE

**Pelin CAKIR, Rachel ELOIRDI, Frank HUBER, Rudy J. M. KONINGS, Thomas GOUDER**

*The surface reaction of neptunium dioxide ($NpO_2$) and two mixed oxides of uranium with plutonium and thorium (U-Pu-$O_2$ and U-Th-$O_2$, respectively) with adsorbed water ice were studied by XPS and UPS. The oxides were produced as thin films by reactive sputter deposition. Water was condensed as thick ice overlayer on the surface at low temperature. Subsequent warming led to the desorption of the ice. When warmed up under UV light (HeI and HeII radiation), the surface was reduced. $NpO_2$ was reduced to surface $Np_2O_3$. In the U-Pu mixed oxide, MOX, Pu was reduced from $PuO_2$ to $Pu_2O_3$. In U-Th mixed oxide, MOX, the Uranium was reduced from hyperstoichiometric $UO_{2+x}$ to stoichiometric $UO_2$ but not to lower oxides: the lowest thermodynamically stable oxides are formed. In the mixed oxides, U reduction seems to be activated both for oxides with Th and with Pu. Surface reduction is explained as a photocatalytic reaction of the surface, triggered by the excitation of electrons from the valence (or impurity) band into the conduction band. The enhancement of reactivity of the mixed oxides compared to pure U is explained by the higher band gap of $ThO_2$ and $PuO_2$ compared to $UO_2$.*

Parts of this chapter have been published in Journal of Physical Chemistry C **119**, 1330-1337 (2015)[1]

## 5.1. INTRODUCTION

THE chemical stability of surfaces plays an important role in the safety case of nuclear fuel and waste. In particular the intermediate and long term storage properties of spent fuel depend on corrosion reactions of the surface in contact with gas atmosphere and with water [2]. Most nuclear fuels consist of an oxide matrix, mainly uranium dioxide ($UO_2$) but also uranium-plutonium mixed oxides ($U_xPu_{1-x}O_2$), into which fission products are incorporated. Under corrosive conditions, e.g. in contact with ground water, the $UO_2$ can oxidize, which enhances its solubility by many orders of magnitude [3]. Dissolution of the fuel matrix results in the release of the contained radionuclides into the environment [4]. The resistance of the surface towards corrosion depends on fuel properties (composition, structure, morphology) [5] and on the environment (water composition, pH, redox potential, ...) [6]. A reliable prediction of the reactivity necessitates detailed understanding of the corrosion mechanism, which is difficult because of the complexity of the system. To avoid this, research can be done on simplified model systems such as doped thin films, focussing on a few parameters.



Much attention has been given to the chemically driven corrosion reactions. The influence of radiation enhanced reaction focussed on the aqueous radiolysis products formed in the vicinity of the surface-water interface [7]. This paper addresses another radiation enhanced reaction, occurring at the oxide surface itself, in contact with an aqueous phase. The oxides investigated were neptunium dioxide ($NpO_2$) and mixed oxides of uranium with plutonium or of uranium with thorium (U-Pu MOX and U-Th MOX, respectively). Photoexcitation of the surface was performed by Ultraviolet (UV) light. The UV light was simultaneously used for performing valence band photoemission spectroscopy. To create an aqueous phase under the ultra-high vacuum conditions required by this spectroscopy, water was fixed as a thick ice film at low temperature. In a previous paper, the surface reactions of $UO_{2+x}$ and $PuO_2$ were studied and it was found, that $PuO_2$ [8] is reduced to $Pu_2O_3$ while hyperstoichiometric $UO_{2+x}$ was reduced to $UO_2$ [9]. This stood in sharp contrast to the surface reaction with atomic hydrogen (H·), where $UO_{2+x}$ was readily reduced while $PuO_2$ was not. Reduction of the oxides by water is not feasible thermodynamically, because the water would have to be oxidised to $H_2O_2$ or $O_2$. But under UV light the reaction takes place. It was shown that the reduction does not proceed via direct photolysis of the bulk ice, because the main reducing agent produced, (H·), does not reduce $PuO_2$. It was concluded, that the reaction is driven by activation of surface oxide layers by the UV light (photocatalysis). Such surface reduction in a radiation field would suppress the oxidative dissolution of nuclear waste [2,3] thereby increasing the stability of the waste. The possible impact of this effect needs to be investigated.

In the following, we report first Ultraviolet Photoemission And X-Ray Photoemission Spectroscopy (UPS and XPS, respectively) analyses on the effect of the water adsorption on $NpO_2$ film, in a second part on $U_xPu_{1-x}O_2$ (x 0.33) film and then in a third part on the $U_xTh_{1-x}O_2$ ( x 0.29 and 0.61) film compositions. In the discussion, the respective roles of UV light and ice on the photoreduction of the actinide oxides thin films will be given making a parallel with the observations made on standard materials, for instance transition metal.

## 5.2. EXPERIMENTAL

OXIDES Oxides were produced as thin films (50 to 100nm thickness) by direct-current (dc) sputter deposition from metallic targets. $Ar/O_2$ mixtures were used as sputter gas. Variation of the O2 partial pressure allowed variation of the oxygen content in the films. Films were deposited on silicon wafer plates (111), cleaned in situ by argon ion sputtering before the deposition. The plasma in the diode source was maintained by injection of electrons of 30-60 eV energy. This allowed operating at relatively low sputter gas pressures below 1 Pa. The background pressures in the preparation and in the analysis chamber of the system were around 3x10-7 Pa or better.

The following metallic actinide targets were used: Th: a disc of 1 cm diameter, U: a disc of 6 mm diameter, Np and Pu: metal rods of 6 mm length and 2 mm diameter. Argon and oxygen were 99.9999% grade. Deposited films were clean, disregarding small OH contaminations introduced into the preparation chamber during the water adsorption experiments; within the detection limit of XPS (2 at. %), no other impurities could be detected. Water vapour was introduced into the preparation chamber by a leak valve, which was connected to a stainless steel pressure container filled with water from a Millipore MilliQ system for ultrapure water (with 18MΩcm resistivity). Ultra-Violet and X-Ray Photoelectron Spectra (UPS and XPS, respectively) were recorded in an analysis chamber directly connected to the preparation chamber using a Specs Phoibos 150 hemispherical analyzer. Mg K$\alpha$ (1253.6 eV) excitation radiation was used for the XPS experiments. UPS spectra were taken with He*II* (40.81 eV) UV light, produced by a high intensity windowless discharge lamp. Taking advantage of the different mean free paths ($\lambda$) for He*II* and Mg K$\alpha$, surface and bulk properties were accessed [10]. In addition, the energy dependent photoionisation cross sections [11] allowed identification of the orbital character (p, d, or f ) of the valence levels.



## 5.3. RESULTS

### 5.3.1. $NpO_2$

A $NpO_2$ film was cooled down to 80 K, covered by ice and then gradually warmed up. The He*II* valence band spectra are shown in Figure 1. The initial spectrum (Figure 1a) is typical for $NpO_2$ [12]. At 2.7 eV binding energy (BE), the Np-$5f^3$ peak is observed. The peak system between 4 and 9 eV is attributed to the O-*2p* band. It is composed of a main peak at low BE and a shoulder at the high BE side. This shape is similar for all actinide dioxides. The peak at 10-11 eV BE is assigned to surface hydroxyl species, which originate from water contamination in the preparation chamber introduced during the ice adsorption experiments.

After the film has been exposed to 50 L (Langmuir) of water at 80 K, all the emission lines of Np disappear and a set of three lines between 8 and 20 eV BE appear. The lines persist when the surface is warmed to 178 K (Figure 5.1b). These are the molecular emission lines from water physisorbed on the surface. They are attributed to the $1b_2$, $3a_1$, $1b_1$ molecular orbital emission of water, composed mainly of the O-*2p* orbitals ($1b_1$ corresponds to the non-bonding O-$2p_x$ orbital). The binding energy differences are the same as in water gas, showing the water to be unperturbed and simply physisorbed (condensed) [13]. The lines are shifted to higher BE due to the charging of the insulating ice

film after ejection of the photoelectrons. The surface is covered by a thick ice overlayer (approximately 50 L water forming a layer of 1 $\mu$m thickness) masking the underlying oxide. When the sample is warmed up to 198 K (Figure 5.1c) the pressure in the chamber increases, and the residual gas analyzer (RGA) indeed shows water to be desorbed. The ice signal becomes smaller. The lines shift to lower BE, Figure 5.1c. This is due to less surface charging, because of the thinning of the overlayer (lower resistance for given resistivity) and to the increased mobility of the water molecules and ions in the ice film. Still no oxide substrate lines are observed, and it has to be assumed that the layer is still thick so that only physisorbed water is observed. At 218 K, Figure 5.1d, all ice is desorbed and the only remaining adsorbed surface species is OH.

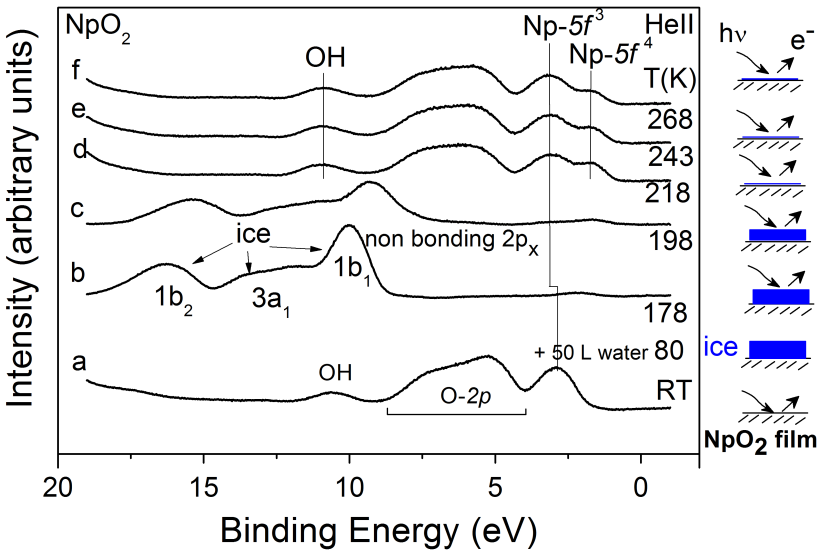


Figure 5.1: He*II* valence band spectra of a $NpO_2$ film (a) cooled down, then covered by ice (b) and warmed up (b-f). After ice desorption, the $5f^4$ emission of reduced $Np_2O_3$ appears (d).

After water desorption, the spectral features of the underlying oxide appear again, the O-*2p* and Np-*5f*$^3$. In addition a new peak appears at 2 eV binding energy, 5.1d. A similar line has been observed at the early oxidation stage of Np metal [12] and was attributed to the $5f^4$ emission of $Np_2O_3$. Its lower binding energy compared to the $5f^3$ line of $NpO_2$ is well consistent with the lower oxidation state of $Np_2O_3$. In contrast to $Pu_2O_3$ and the heavier actinide sesquioxides, $Np_2O_3$ is stable only at the top surface but not in the bulk. It is e.g. produced when $NpO_2$ is bombarded by $Ar^+$ ions, sputtering off the top surface layers and removing the lattice oxygen atoms (preferential sputtering). Its appearance after water desorption shows that water reduced the surface of $NpO_2$ to $Np_2O_3$ – even though this oxide is less stable than $Pu_2O_3$. The O-*2p* emission changes its shape from the asymmetrical peak in $NpO_2$ to a more symmetrical shape, Figure 5.1d-f, due to the superposition of the OH emission formed by the decomposition of water ($3\sigma$ and

$1\pi$, respectively, 10.7 and 7.4 eV) .12 A similar change in O-*2p* shape was observed after reduction of $PuO_2$ to $Pu_2O_3$.7

Formation of $Np_2O_3$ by reduction confirms it to be a stable species. Before it was not clear, whether the $Np_2O_3$ appearing at the early oxidation of Np metal was a metastable intermediate in the oxidation of the Np (0) to Np (4+). The present finding shows that under appropriate conditions $NpO_2$ can be reduced back to $Np_2O_3$. Even though being a photon driven reaction, this points to the stability of the lower oxide.

### 5.3.2. $(U_xPu_{1-x})O_2$

Initial films were produced by co-deposition of U and Pu in presence of oxygen. To estimate the relative strength of oxidation/reduction of the two elements, films were first deposited at low oxygen pressure, so that U and Pu compete for the oxygen (Figure 5.2a).

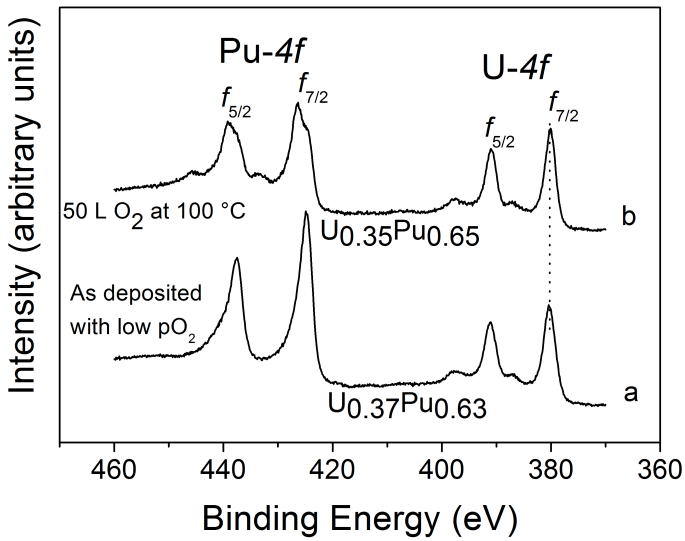


Figure 5.2: U-*4f* and Pu-*4f* core level spectra of U-Pu oxide after deposition (a) and after further oxygen exposure (b).

In sputter deposition, surface adatoms are mobile because of their high energy of impact [14]. They form a two dimensional gas, from which atoms condense and organize into the most stable configuration, i.e. bonding either to U or to Pu. The question then is in what sequence the various oxidation states appear. The 4f core level spectra of uranium and plutonium (Figure 5.2a) show that $UO_2$ is formed together with $Pu_2O_3$ at the surface. The $UO_2$ is close to stoichiometry, as indicated by the U-$4f_{5/2}$ binding energy of 391.1 eV (substoichiometric $UO_{2-x}$ lies around 391.5-392 eV). $Pu_2O_3$ formation is shown by the sharp Pu-*4f* emission ($4f_{5/2}$ at 437.6 eV) without satellite [15]. When exposed to 50 L $O_2$ (Figure 5.2b) new Pu-*4f* lines appear at 1.2 eV higher binding energy. They are due to $PuO_2$ and account for 52% of the Pu-*4f* signal. $PuO_2$ and $Pu_2O_3$ do not form a ho-

mogeneous mixture, but $PuO_2$ is located at the surface, where $O_2$ adsorbs, while $Pu_2O_3$ comes from the bulk. The $UO_2$ changes only slightly. The U-*4f* line shifts to lower BE by 0.25 eV. The shift could be due to oxidation of substoichiometric $UO_{2-x}$ (a n-type semiconductor) to $UO_2$, which is p-type. The concomitant decrease of the Fermi-energy would produce a shift of all photoemission lines to low BE. The oxidation is, however, not very pronounced: The $UO_2$ satellite at 397.7 eV, which is very sensitive to the U oxidation state, is not affected. It would decrease in intensity and change its shape when the oxygen content increases [16]. Yet it stays characteristic for $UO_2$ [17]. The sequence of oxide formation is thus $UO_2$, $Pu_2O_3 \rightarrow UO_2$, $PuO_2 > UO_{2+x}$, $PuO_2$. The Pu/U ratio is not affected by $O_2$ adsorption, as shown by the unchanged U-*4f*/Pu-*4f* intensity ratio (Figure 5.2). There is no surface segregation of one of the actinides as showed by the constant intensity ratio Pu-*4f*/U-*4f*.

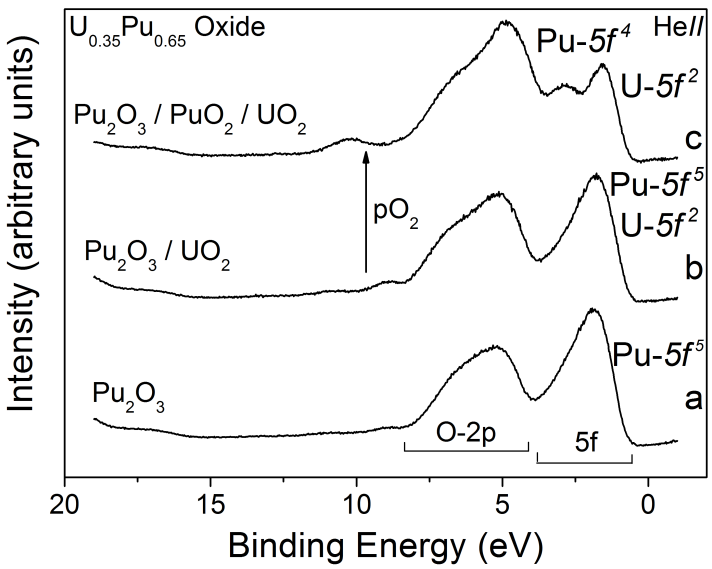


Figure 5.3: He*II* valence band spectra of $Pu_2O_3$ (a); $Pu_2O_3$-UO2 after deposition (b); $PuO_2$-$UO_2$ formed by $O_2$ exposure (c) of the film.

The corresponding He*II* spectra are shown in Figure 5.3. For comparison, a He*II* spectrum of pure $Pu_2O_3$ is shown in Figure 5.3a. The spectrum of the freshly deposited film (Figure 5.3b) looks similar to the $Pu_2O_3$ spectrum, except for the higher 5f intensity (in $Pu_2O_3$) compared to the O-*2p*.

The same holds true for the He*I* spectra, which are more bulk sensitive. This is simply explained by the fact that the 5f emissions of $Pu_2O_3$ and $UO_2$ have the similar binding energies (Pu-$5f^5$: 1.9 eV, U-$5f^2$:1.8 eV for $UO_{2-x}$). The intensity of the Pu-*5f* emission is higher than that of the U-*5f*, because of the larger 5f count, 5 instead of 2. After exposure to $O_2$ (Figure 5.3c), the 5f signal splits into a narrow component at 1.4 eV, typical for stoichiometric $UO_2$, and a small peak at 2.7 eV, attributed to the $5f^4$ level of $PuO_2$. As

shown above, the U/Pu concentration probed by XPS does not change. The loss in 5f intensity is thus mainly due to the removal of Pu-*5f* states and their transfer to the O-*2p* band by oxidation, either by charge-transfer but also by hybridization [18]. This explains the surprisingly low 5f intensity in $PuO_2$ [19]. Probably all surface Pu has been oxidised to $PuO_2$ by reaction with the adsorbed $O_2$. It can thus be assumed that the entire 5f signal of $Pu_2O_3$ has disappeared from the He*II* spectrum and that emission at 1.8 eV binding energy is entirely due to the $5f^2$ level of $UO_2$. This is corroborated by the narrow line width of the f-emission, which is typical for the multiplet structure ($f^2$) of the 5f emission in $UO_2$ [20], while the $5f^5$ emission of the Pu-*5f* has a broader multiplet shape [21].

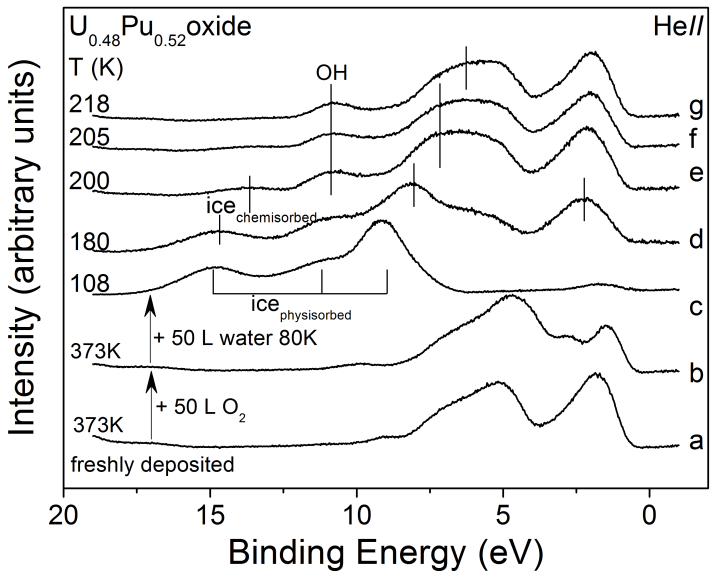


Figure 5.4: Interaction of ice on $U_{0.48}Pu_{0.52}$ oxide film under UV light. (a) Freshly deposited film, (b) exposure to oxygen forming the dioxides, (c) coverage by ice film, (d) immediately after desorption, and (e-g) after further warming up: surface $PuO_2$ is reduced to $Pu_2O_3$.

The surface interaction with ice under UV light was tested on a $U_{0.48}Pu_{0.52}$ oxide film (Figure 5.4). The initial film was composed of $UO_2$ and $Pu_2O_3$, as shown by the single 5f peak at about 1.8 eV binding energy, due to the superposition of Pu-$5f^5$ and U-$5f^2$ lines (Figure 5.4a). Exposure to 50 L $O_2$ at 373 K leads to oxidation of $Pu_2O_3$ to $PuO_2$ (Figure 5.4b), with the corresponding Pu-$5f^4$ line at 2.2 eV binding energy. The surface is then exposed to 50 L of water at 108 K (Figure 5.4c). A thick ice film deposits and all the underlying oxide emission lines disappear. Only the molecular emission lines of water ($1b_2$, $3a_1$ and $1b_1$) are observed. When the surface is warmed up (Figure 5.4d) the water emission lines shift to lower binding energy, again due to the reversal of the charging effect, as for $NpO_2$. Then the lines disappear: ice desorbs and the underlying oxide becomes visible (Figure 5.4e). During warming up the ice lines do not shift by the same amount: the lower lying lines shift more than the higher ones. This is due to fact

that the measurement is scanning from high to low BE and thus the higher lines have been recorded earlier in time, i.e. at higher BE (less shifted) and the lower lines later (more shifted). Upon reaching the final position, the effect vanishes. Desorption of the ice is also shown by the drastic increase of the partial pressure of $H_2O$ in the chamber. The desorption process is complete at 200 K (Figure 5.4e, g). It leaves a surface with a 5f peak, which looks again like that of initial, reduced film. In addition, two peaks appear at 10.7 and 7.4 eV binding energy. They are attributed to the $3\sigma$ and $1\pi$ level of surface hydroxyl (OH) formed by the decomposition of water.

In Figure 5.5 the surface reaction on an irradiated (yellow sun symbol) and a non-irradiated (black solid circle) area are compared. The surface spot left in the dark during warming up is not reduced but retains the initial, high oxidation state (Figure 5.5b). The surface spot warmed up under UV light was reduced (Figure 5.5a). To ensure that the phenomenon was only due to the influence of light and that there was no time and/or temperature dependence, the irradiated spot was analysed before and after the dark spot (Figure 5.5c). Time and temperature played no role and only the light was responsible for surface reduction. It should be noted, that in the time scale used for the measurement, UV light alone has no effect: Actinides oxides are stable during UPS measurements [9, 22]. Hours long of UV light radiation is needed to be effective for the photoreduction of some metal oxide [23].



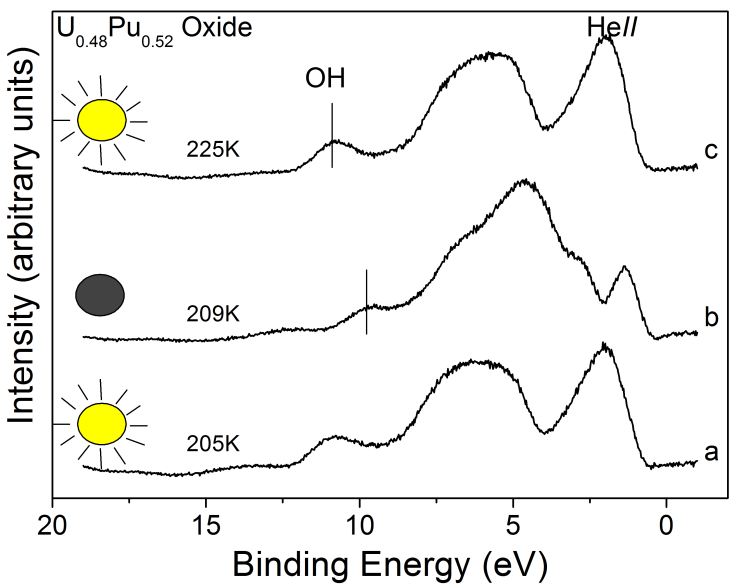


Figure 5.5: He*II* valence band comparison of irradiated and dark areas of $U_{0.48}Pu_{0.52}$ oxide.

Finally, it should be noted that the $3\sigma$ signal of chemisorbed OH is generally more intense on the reduced than on the oxidized surfaces. This could mean that OH adsorption and surface reduction are related. It is not possible to make a quantitative estimation of the amount of OH because there is no reference line. But the light intensity and analyser

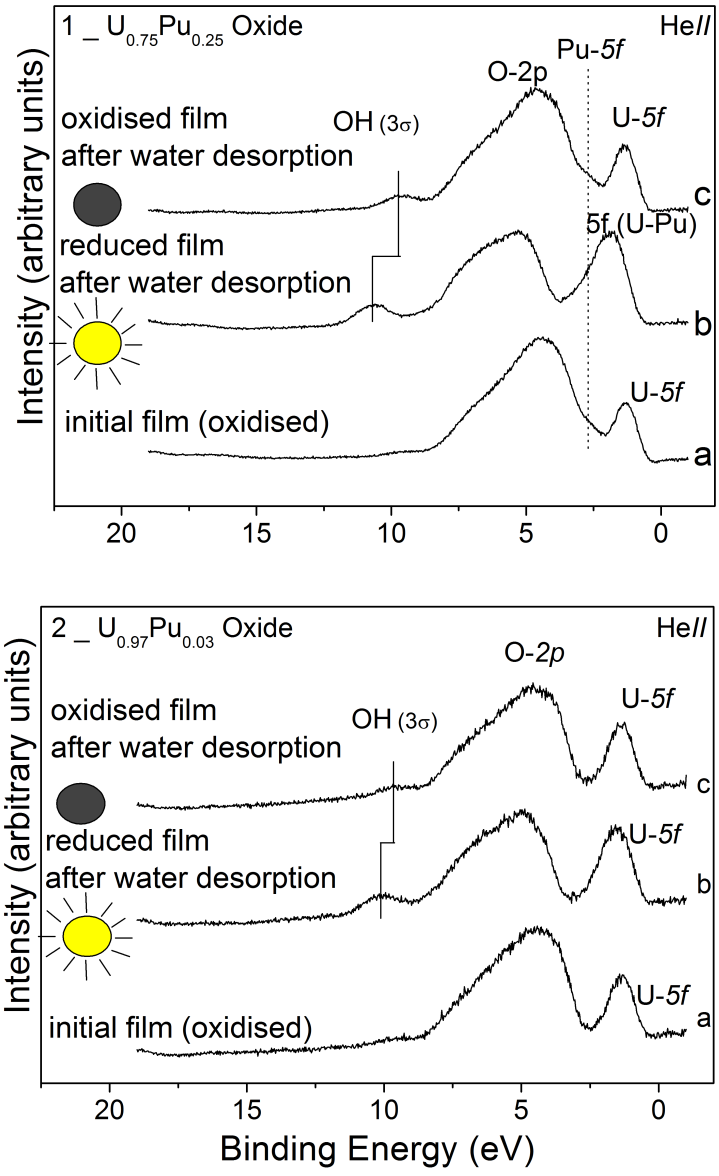


Figure 5.6: He*II* valence band spectra comparison of irradiated and dark areas of (1) $U_{0.75}Pu_{0.25}$ oxide and (2) $U_{0.97}Pu_{0.03}$ oxide thin films after ice desorption.

settings were kept constant, so that the spectra should had roughly the same intensity. On the basis of these arguments, the absolute intensities of the OH lines can be analysed and show that there is clearly more chemisorbed OH on the reduced than on the oxi-

dised surface. One simple explanation would be that broken O-Pu bonds upon surface reduction are replaced by O-H bonds. The surface reduction was also tested for oxide

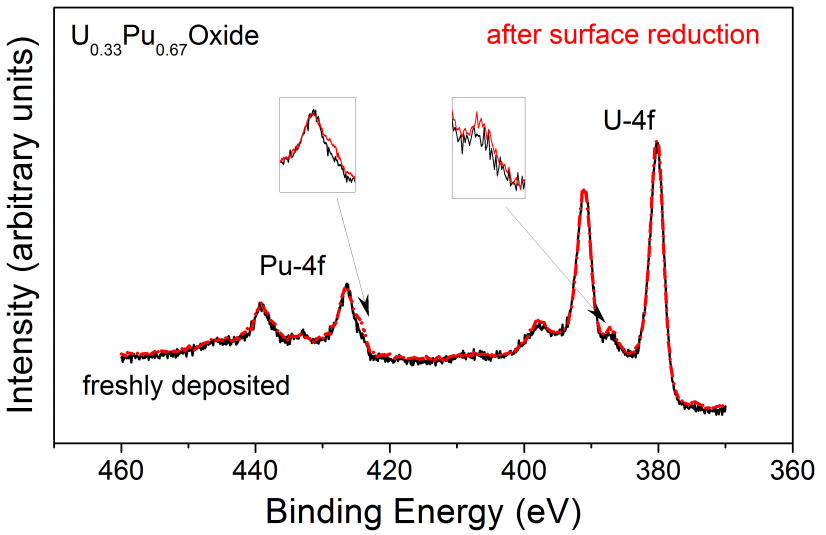


Figure 5.7: U-*4f* and Pu-*4f* core level spectra confirm the reduction of $PuO_2$ and $UO_2$ at the surface.

films of the composition $U_{0.75}Pu_{0.25}$ (Figure 5.6.1 (top panel)) and $U_{0.97}Pu_{0.03}$, (Figure 5.6.2(bottom panel)). For $U_{0.75}Pu_{0.25}$ oxide the Pu-$5f^4$ line in the initial, oxidised sample (Figure 5.6.1a) is smaller than in the previous sample, but still detectable.

When ice is desorbed under UV light the surface is again reduced (Figure 5.6.1b). As for the previous film, the OH-3$\sigma$ signal is more pronounced for the reduced film. The $U_{0.97}Pu_{0.03}$ oxide film (Figure 5.6.2) can be considered as $UO_2$ doped by a small amount of $PuO_2$. The He*II* spectrum of the initial film (Figure 5.6.2a) is typical for $UO_2$, with the broad, asymmetrical O-*2p* line and the U-$5f^2$ peak. The U-*5f*/O-*2p* intensity ratio shows the presence of hyper-stoichiometric $UO_{2+x}$. Also the U- $5f^2$ binding energy of 1.3 eV is typical for $UO_{2+x}$. Again the surface is reduced, when ice is desorbed under UV light (Figure 5.6.2b). The 5f line increases in intensity and shifts to higher BE (1.53 eV), while without light (Figure 5.6.2c) the intensity ratio U-*5f*/O-*2p* is similar as the initial oxidized film (Figure 5.6.2a). The Pu-*4f* and U-*4f* core level spectra of freshly deposited $Pu_{0.67}U_{0.33}$ oxide and after being covered with ice and lighted with UV are displayed in Figure 5.7.

The result confirms the photoreduction made in deeper layer of the film. Indeed, the shoulder appearing at lower binding energy (see inset) representative of the Pu(III) increases in intensity. Also the sharpening of the satellite of U-*4f* is an indication of the presence of stoichiometric $UO_2$ in the film.

Surface reduction was confirmed by XPS core level measurements (Figure 5.7). The Pu-$4f_{7/2}$ line develops supplementary intensity at the low BE side, at the position of

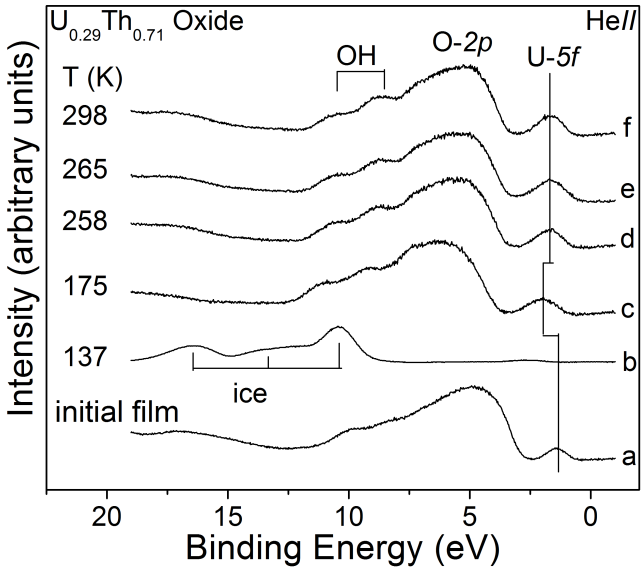


Figure 5.8: He*II* valence band spectra of $U_{0.29}Th_{0.71}$ oxide after ice adsorption and desorption under UV light.

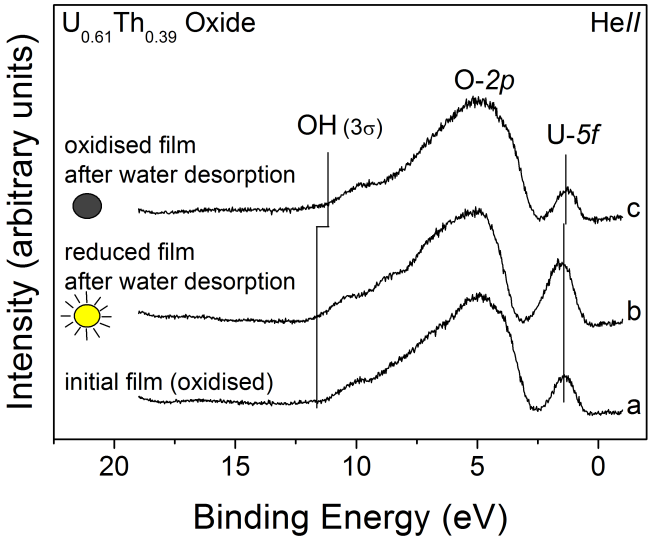


Figure 5.9: He*II* valence band comparison of irradiated and dark areas of $U_{0.61}Th_{0.39}$ oxide.

$Pu_2O_3$. The same effect is reproduced on the weaker Pu-$4f_{5/2}$ emission. Also the satellite

of the U-*4f* line increases slightly. This would be characteristic for formation of stoichiometric $UO_2$, which has higher satellite intensity than the hyper- stoichiometric $UO_{2+x}$. Both effects are weak, however, and compatible with top surface reduction without reaction of the bulk. This is not surprising, because reduction takes place at low temperature (around or below 220 K), and under these conditions the reaction cannot proceed into the bulk because atomic diffusion is too slow. To have bulk reduction, bulk oxygen would need to diffuse to the surface where it would react with the ice.

### 5.3.3. $(U_xTh_{1-x})O_2$

Two thin films of U-Th MOX have been studied, a U poor ($U_{0.29}Th_{0.71}$) oxide and a U rich ($U_{0.61}Th_{0.39}$) oxide. Figure 5.8 shows the $U_{0.29}Th_{0.71}$ MOX. Since Th has no 5f states, the peak at 1.37 eV BE is solely due to U-$5f^2$ emission. It is small compared to the O-*2p* because of the low U concentration and because the oxide hyper-stoichiometric composition ($UO_{2+x}$). Again, after ice adsorption, a thick ice overlayer suppresses all emission from the underlying oxide. After desorption at 175 K (Figure 5.9c) the oxide lines appear again. The U-$5f^2$ signal increases by a factor 2.0 compared to the O-*2p* line. Figure 5.9 compares the surface reduction of irradiated and non-irradiated surface areas for $U_{0.61}Th_{0.39}$ oxide. As previously, the surface warmed up in darkness stays oxidized (Figure 5.9c), while in the irradiated part the U-*5f* peak strongly increases in intensity (Figure 5.9b).

The U-*5f*/O-*2p* ratio increases by a factor 2.1. This is more than that in pure U, where factors around 1.5 were observed under identical conditions [17]. On the other hand, the extent of surface reduction depends on the initial oxidation state: a strongly hyper-stoichiometric $UO_2$ would be more reduced than a less hyper-stoichiometric $UO_2$. So, control of the initial oxidation state is very important. This has not been done systematically.

## 5.4. DISCUSSION

### 5.4.1. PHOTOCATALAYSIS OR SIMPLE PHOTOLYSIS

We first address the question of whether reduction of the surface is really a photocatalytic process driven by the photoexcited surface, or whether it may be due to photolysis of ice and reaction of the products with the surface. The ice is exposed to UV light of mainly 20-50 eV (He*I* to He*II**). The reaction enthalpy for $H_2O \rightarrow H\cdot + \cdot OH$ is 5.1 eV [24]. Direct photolysis is thus energetically possible. However, such photolysis, which is also observed when water is exposed to radioactive solids (mainly $\alpha$, $\beta$, and $\gamma$ emitters), tends to produce oxidative conditions ($\cdot$OH and $H_2O_2$, dissolved in the water) because the main reducing agent, atomic hydrogen ($\cdot$H), forms $H_2$ and escapes from the water. Even if the hydrogen is caged by the ice layer and hindered from escaping, it is a very stable, nonpolar (and non-polarizable) molecule which is inert and does not interact with oxide surfaces at room temperature. In addition, direct reduction of the oxides by hydrogen is thermodynamically unfavorable. We showed previously that even the reactive atomic hydrogen does not reduce $PuO_2$ to $Pu_2O_3$ [9]. This can be understood on the basis of the stability of the oxide: The enthalpy of formation for the various actinide oxides and for the reaction enthalpy for

Table 5.1: Calculated Energy of Reduction of An(IV) to An(III), Formation Enthalpy of An(III) in Solution and in Solid

| | $AnO_2 \longrightarrow AnO1.5 + \frac{1}{4} O_2$[25] | $\Delta H_f 298°(M^{+3},aq)/(M^{+3},s)$[26] |
|---|---|---|
| $UO_2$ | 3.5 | -489.1 / -728 |
| $NpO_2$ | 3.4 | -527.2 / -761 |
| $PuO_2$ | 2.6 | -592.2 / -828 |

$AnO_2 \longrightarrow AnO1.5 + \frac{1}{4} O_2$
is shown in Table 5.1.

Reduction of dioxides becomes more unfavorable from Pu to Np and U. Also the enthalpy of formation evolves in the same direction. And indeed, $Pu_2O_3$ is stable as bulk phase while $Np_2O_3$ only forms on the surface of Np metal and $U_2O_3$ does not form at all. Since atomic hydrogen is not capable of reducing $PuO_2$ at room temperature [9], it does not reduce $NpO_2$ or $UO_2$.

It may now be inquired whether UV radiation can lead surface reduction by direct decomposition of the oxide. Photoreduction of transition and noble metal oxide by UV light has indeed been reported in literature [23]. Spontaneous reduction of $PuO_2$ to $Pu_2O_3$ has been reported for $PuO_2$ films grown on $\delta$-Pu metal [27]. These films indeed reduce with time when stored under vacuum at room temperature. But this is due to the reaction of oxygen with the underlying metal and not decomposition with loss into the vacuum. In the present study, homogeneous oxide films are used and it has been well confirmed (also by previous work) that the films do not react with the underlying silicon substrate, even on time scale much longer than those of the experiment (weeks and months). In addition, reduction in this experiment occurs at low temper- ature where diffusion processes are slow. It is thus concluded that reduction of the surface is not a consequence of direct photolytic decomposition of water or the oxide but a photocatalytic reaction driven by solid excitation.



### 5.4.2. PHOTOCATALYSIS ON BAND GAP OF $AnO_2$

Photocatalysis on semiconductors and insulators occurs, respectively, when photons with energy equal to or higher than the band gap excite electrons from the valence to the conduction band. The energetic electrons ($e^-$) and holes ($h^+$), respectively, reduce or oxidize the adsorbed molecules [28]. This mechanism is responsible for the photosplitting of water on $TiO_2$ electrodes [29, 30] under sunlight. The rate of photocatalized reactions depends on the rate of formation of the excited states (depending on photon flux), their energy (depending on the band gap), their lifetime (before recombination), and also of the potential levels of conduction band and valence band. Table 5.2 shows the band gap of the $AnO_2$ series [31, 32].

The band gap of $ThO_2$ is larger than that of the higher actinides. $NpO_2$ and $PuO_2$ have band gaps similar to that of $TiO_2$ (3.05 eV), and also their thermodynamic potential [25, 26] enables to initiate photolysis of the water adsorbed on the surface. The band

Table 5.2: Band Gap of the $AnO_2$ Series

| | |
|---|---|
| $ThO_2$ | 3.85 eV [32] |
| $UO_2$ | 2.30 eV [31] |
| $NpO_2$ | 2.85 eV [31] |
| $PuO_2$ | 2.80 eV [31] |

gap of $UO_2$ is smaller. It should also be noted that the value of the gap changes with the oxygen content of the surface [31, 33].

Surface photolysis is similar to surface radiolysis (the solid being excited by $\alpha$, $\beta$,or $\gamma$ radiation) which also proceeds via energy transfer via an exciton. Radiolysis of water by $\gamma$-rays was studied for water adsorbed on $CeO_2$ and $ZrO_2$. Yields were highly enhanced for adsorbed molecules compared to bulk liquid water [34]. It was discussed that the effects are strongest in wide band gap solids and almost nonexistent in small band gap semiconductors. The dependence between the energy and band gap would point to the involvement of excitons. This shows the possible relevance of the photochemical reaction for radiolytic processes occurring during long terms storage of spent fuel. It also indicates, that the effect may be enhanced for U oxides, when these are mixed with other actinides with a higher band gap (Th or Pu). The enhancement of U surface reduction in mixed oxide, observed in this work, may be explained by this.

### 5.4.3. ROLE OF ICE

The ice form itself may play an import role in the photoreduction process. In the present experiments, ice was chosen to fix water in sufficiently high concentration on the surface under ultrahigh vacuum. The low temperatures (desorption takes place around 200 K) suppresses conventional chemical reaction with a thermal activation barrier and favors nonthermal (e.g., photochemical) reactions. In addition, the structure of ice differs from that of liquid water. The effect of ice on the photoreduction of a metal oxide [35] has been reported for iron [36], trapped in ice particle polar regions. It was observed that in ice photoreduction occurs more rapidly than in liquid water. This was explained by caging effect, where organic donor molecules (pollutants) are concentrated on the surface. But enhanced photoreduction was also observed in the absence of electron donors which implies, that there must be a reaction with the water. The photoreduction under an ice film was observed for Fe(III) particles (hematite, maghemite $\gamma$-$Fe_2O_3$, and goethite $\alpha$-FeOOH) exposed to UV light [37]. It was attributed to electrons excited by photons of higher energy than the band gap (2.2 eV or 565 nm) followed by trapping of the conduction electrons on Fe(III) lattice sites:

$Fe^{III}{}_2O_3 + h\nu \longrightarrow e^-_{CB} + h^+_{VB}$

$Fe(III)_{surf} + e^-_{CB} + \longrightarrow Fe(II)_{surf}$ (Fe-O bond is broken)

The similarity between Fe and actinide oxides consists in the fact that the solid itself is transformed (reduced) by reaction with the water. It is thus a photocatalyst and reactant in one. This is in contrast to conventional photocatalysts which drive the reaction in

the liquid phase (e.g., radiolysis of water) without being altered. An interesting example is photochemical reduction of dissolved U(VI) to U(IV) in aqueous suspensions of $TiO_2$ which was observed and the kinetics determined [38]. Reduction takes places on species adsorbed on the surface of $TiO_2$ through photogeneration of charge carriers ($h^+$,$e^-$) at the solid-water interface. $TiO_2$ has a band gap of 3.05 eV (corresponding to 390 nm). On the surface both photoreduction and oxidation take place with, as net result, a reduction of the U even in oxygenated environment. Similar mechanisms were also expected for other minerals with semiconducting properties such as iron or zinc oxides. Interband transitions provide the necessary energy. Photon energies in excess of the band gap are required.

### 5.4.4. MECHANISM

Photoreduction of the oxide by water implies that the water itself is oxidized. Photooxidation of water is a common reaction [39] on oxide surfaces used in environmental remediation (oxidation of organic pollutants). The end product is $O_2$. While the exact mechanism depends on morphology, chemistry, and electronic structure of the surface, the overall mechanism is related to the breaking of an M-O bond by a hole in the valence band:

$$M-O-M + h^+ \longrightarrow M-O^\bullet + M^+$$

The $M^+$ cation reacts with water (nucleophilic attack of a Lewis base) with liberation of a proton and chemisorption of a hydroxyl group.

$$M^+ + H_2O \longrightarrow M-OH + H^+$$

The $M-O^\bullet$ reacts with a neighboring M-OH group to form a surface peroxide

$$M-O^\bullet + M-OH + h^+ \longrightarrow M-O-O-M + H^+$$

The reaction can continue until formation of molecular oxygen.

$$M-O-O-M + h^+ \longrightarrow M-O-O^\bullet + M^+$$

$$M-O-O^\bullet + h^+ \longrightarrow M + O_2$$

This is a commonly accepted mechanism for water oxidation on $TiO_2$ [40]. The oxidation products are highly reactive and can oxidize organic pollutants. This makes this process interesting for environmental remediation. In this process, water consumes the oxidizing holes and prevents the surface from being reoxidized. Simultaneously, the photoexcited electrons reduce the oxide:

$$M^{n+} - O^{2-} - M^{n+} + e^- + H^+ \longrightarrow M^{n+} - (OH)^{1-} + M^{(n-1)+}$$

This mechanism explains also why products of bulk water radiolysis (H·) do not reduce the surface: it is the photoexcited surface which reacts with water (oxidizing it) and not the photoexcited (reduced) water which reacts with the surface. A similar mechanism could also occur for the actinide oxides. The reduced surface often show an increase hydroxyl signal (Figure 6), and this would be consistent with the above-described mechanism.

## 5.5. SUMMARY

SURFACE reduction of $NpO_2$ and two mixed oxides of $(U,Pu)O_2$ and $(U,Th)O_2$ thin films under an ice film irradiated by UV light were investigated. The oxidation state of the surface before ice adsorption and after ice desorption where compared with UPS and

XPS. $NpO_2$ is reduced to $Np_2O_3$ at its top surface. While up to now $Np_2O_3$ had only be observed during the early oxidation of Np metal, it was now shown to be stable also on $NpO_2$. It is a stable surface compound and not a metastable reaction intermediate.

Surface reduction of mixed U-Pu and U-Th oxides was also investigated. Prior, the relative stabilities of the oxides were tested by codepositing the metals under low oxygen partial pressure. XPS showed $UO_2$/U metal to coexist with $Pu_2O_3$. Only when all U metal was oxidized $PuO_2$ started to form. Ice interaction under UV light led to the reduction of $PuO_2$ to $Pu_2O_3$ and of $UO_{2+x}$ to $UO_2$. Surface reduction was witnessed by the appearance of the $5f^5$ peak of $Pu_2O_3$ and the increase of the U-$5f^2$ in $UO_2$. UV light was essential for surface reduction: a surface warmed up in the dark was not reduced after ice desorption. Only the irradiated surface area with UV light was reduced. Surface reduction has also been observed for (U,Th) mixed oxides. While Th did not change its oxidation state (+4), $UO_{2+x}$ was reduced as shown by the increase of the U-$5f^2$ emission.

## 5.6. CONCLUSIONS



SURFACE reduction is explained as a photoactivated reaction of the surface with the surrounding water phase. The UV light excites electrons from valence band to the conduction band of the actinide oxides. The holes in the valence band oxidize the water while the electrons in the conduction band ultimately reduce the surface (lattice oxygen desorbs as water). The presence of the ice, preventing the photolysis products from escaping, may increase the reaction rate. It is planned to study the reaction of liquid water under ambient pressure/temperature conditions with doped surfaces to see the possible significance for waste under repository conditions. The reduction of the surface would indeed inhibit oxidative surface dissolution and hence contribute to the long-term stability of waste. But the significance and robustness of the process needs to be assessed.

## REFERENCES

[1] Pelin Cakir, Rachel Eloirdi, Frank Huber, Rudy J. M. Konings, and Thomas Gouder. Surface Reduction of Neptunium Dioxide and Uranium Mixed Oxides with Plutonium and Thorium by Photocatalytic Reaction with Ice. *The Journal of Physical Chemistry C*, 119:1330–1337, jan 2015.

[2] D.W. Shoesmith. Fuel corrosion processes under waste disposal conditions. *Journal of Nuclear Materials*, 282(1):1–31, nov 2000.

[3] I. Grenthe, J. Fuger, R. J. M. Konings, R.J. Lemire, A. G. Muller, C. Nguyen-Trung Cregu, and H. Wanner. *Chemical thermodynamics of uranium*. North Holland, Amsterdam, 1992.

[4] R.S. Forsyth and L.O. Werme. Spent fuel corrosion and dissolution. *Journal of Nuclear Materials*, 190:3–19, aug 1992.

[5] C. N. Wilson and W. J. Gray. Measurement of soluble nuclide dissolution rates from spent fuel. In *Scientific for Nuclear Waste Management XIII*, page 489, Boston, MA (USA), 1990. Material Research Society.

[6] J. K. Bates, B. S. Tani, E. Veleckis, and D. J. Wronkiewicz. Identification of secondary phases formed during unsaturated reaction of uranium dioxide with water. In *Scientific for Nuclear Waste Management XIII*, page 499, Boston, MA (USA), 1990. Material Research Society.

[7] L. Werme and R.S. Forsyth. Radiolytically induced oxidative dissolution of spent nuclear fuel. Technical report, Swedish Nuclear Fuel and Waste Management Company, SKB TR 90-08, 1990.

[8] A. Seibert, T. Gouder, and F. Huber. Interaction of PuO 2 thin films with water. *Radiochimica Acta*, 98(9-11):647–657, nov 2010.

[9] T. Gouder, A. B. Shick, and F. Huber. Surface Interaction of PuO2, UO2+x and UO3 with Water Ice. *Topics in Catalysis*, 56(12):1112–1120, jul 2013.

[10] M P Seah and W. A. Dench. Quantitative electron spectroscopy of surfaces: A standard data base for electron inelastic mean free paths in solids. *Surface and Interface Analysis*, 1(1):2–11, 1979.

[11] J. J. Yeh and I. Lindau. Atomic subshell photoionization cross sections and asymmetry parameters: 1 <Z< 103. *Atomich Data and Nuclear Data tables*, 32(1):1–155, 1985.

[12] J. R. Naegele, L. E. Cox, and J. W Ward. Photoelectron spectroscopy (UPS/XPS) study of Np203 formation on the surface of neptunium metal. *Inorganica Chemica Acta*, 139:327–329, 1987.

[13] Michael A Henderson, Amsterdam London, New York, Oxford Paris, and Shannon Tokyo. The interaction of water with solid surfaces : fundamental aspects revisited. *Surface Science Reports*, 46:1–308, 2002.

[14] W. D. Westwood. *Sputter Deposition*. New York: AVS, New York, vol. 2 edition, 2003.

[15] D. Courteix, J. Chayrouse, and L. Heintz. XPS study of plutonium oxides. *Solid State Communications*, 39:209–213, 1981.

[16] G. C. Allen, P. M. Tucker, and J. W. Tyler. Oxidation of uranium dioxide at 298 K studied by using X-ray photoelectron spectroscopy. *Journal of Physical Chemistry*, 86(2):224–228, 1982.

[17] S. Van den Berghe, F. Miserque, T. Gouder, B. Gaudreau, and M. Verwerft. X-ray photoelectron spectroscopy on uranium oxides: a comparison between bulk and thin layers. *Journal of Nuclear Materials*, 294(1-2):168–174, apr 2001.

[18] J. R. Naegele, J. Ghijsen, and L. Manes. Localization and Hybridization of 5f States in the Metallic and Ionic Bond as Investigated by Photoelectron Spectroscopy. In L. Manes, editor, *Actinides - Chemistry and Physical Properties*, chapter Chapter E, pages 197–262. Berlin Heidelberg New York Tokyo, 56/60 edition, 1985.

[19] A. B. Shick, J. Kolorenč, L. Havela, T. Gouder, and R. Caciuffo. Nonmagnetic ground state of PuO2. *Physical Review B*, 89(4):041109, jan 2014.

[20] J. R. Naegele. Surface analysis of actinide materials. *Journal of Nuclear Materials*, 166:59–67, 1989.

[21] T Gouder, F Wastin, J Rebizant, and L Havela. 5f-electron localization in PuSe and PuSb. *Physical review letters*, 84(15):3378–81, apr 2000.

[22] A. Seibert, T. Gouder, and F. Huber. Reaction of neptunium with molecular and atomic oxygen: Formation and stability of surface oxides. *Journal of Nuclear Materials*, 389(3):470–478, jun 2009.

[23] T. H. Fleisch, G. W. Zajac, and J. O. Screiner. An XPS study of the UV photoreduction of transition and noble metal oxides. *Applied Surface Science*, 26:488–497, 1986.

[24] Akihiro Yabushita, Daichi Kanda, Noboru Kawanaka, Masahiro Kawasaki, and Michael N R Ashfold. Photodissociation of polycrystalline and amorphous water ice films at 157 and 193 nm. *The Journal of chemical physics*, 125(13):133406, oct 2006.

[25] L. Petit, A. Svane, Z. Szotek, W. M. Temmerman, and G. Stocks. Electronic structure and ionicity of actinide oxides from first principles calculations. *Physical Review B*, 81(4):045108–1/045108–12, 2010.

[26] J. Fuger and F. L. Oetting. The Chemical Thermodynamics of Actinide Elements and Compunds, part 2. In *The Actinide Aqueous Ions*. International Atomic Energy Agency, Vienna, 1976.

[27] Harry G García Flores and David L Pugmire. The growth and evolution of thin oxide films on $\delta$-plutonium surfaces. *IOP Conference Series: Materials Science and Engineering*, 9:012038, mar 2010.

[28] Jean-Marie Herrmann. Photocatalysis fundamentals revisited to avoid several misconceptions. *Applied Catalysis B: Environmental*, 99(3-4):461–468, sep 2010.

[29] A. Fujishima. Electrochemical Photolysis of Water at a Semiconductor Electrode. *Nature*, 238:37–38, 1972.

[30] J. T. Yates. Photochemistry on TiO2: Mechanisms behind the surface chemistry. *Surface Science*, 603(10-12):1605–1612, jun 2009.

[31] T. Mark McCleskey, Eve Bauer, Quanxi Jia, Anthony K. Burrell, Brian L. Scott, Steven D. Conradson, Alex Mueller, Lindsay Roy, Xiaodong Wen, Gustavo E. Scuseria, and Richard L. Martin. Optical band gap of NpO2 and PuO2 from optical absorbance of epitaxial films. *Journal of Applied Physics*, 113(1):013515, 2013.

[32] Safwat a. Mahmoud. Characterization of thorium dioxide thin films prepared by the spray pyrolysis technique. *Solid State Sciences*, 4(2):221–228, feb 2002.

[33] Heming He, David a. Andersson, David D. Allred, and Kirk D. Rector. Determination of the Insulation Gap of Uranium Oxides by Spectroscopic Ellipsometry and Density Functional Theory. *The Journal of Physical Chemistry C*, 117(32):16540–16551, aug 2013.

[34] J. A. Laverne and L. Tandon. H2 Production in the Radiolysis of Water on CeO2 and ZrO2. *Journal of Physical Chemistry B*, 106:380–386, 2002.

[35] Kitae Kim and Wonyong Choi. Enhanced redox conversion of chromate and arsenite in ice. *Environmental science & technology*, 45(6):2202–8, mar 2011.

[36] D. Jeong, K. Kim, and W. Choi. Accelerated dissolution of iron oxides in ice. *Atmospheric Chemistry and Physics*, 12(22):11125–11133, nov 2012.

[37] K. Kim, W. Choi, M. R. Hoffman, H. Yoon, and B.-K. Park. Photoreductive dissolution of iron oxides trapped in ice and its environmental implications. *Environmental Science Technology*, 44(11):4142–4148, 2010.

[38] W P Ellis, A M Boring, J W Allen, L E Cox, R D Cowan, A J Arko, Los Alamos, and Ann Arbor. Valance-Band Photoemission Intensities in thorium dioxide. *Solid State Communications*, 72(7):725–729, 1989.

[39] A. Imanishi, O. Tomoaki, N. Ohashi, R. Nakamura, and Y. Nakato. Mechanism of water photooxidation reaction at atomically flat TiO2 (rutile) (110) and (100) surfaces: dependence on solution pH. *Journal of Americal Chemical Society*, 129(37):11569–11578, 2007.

[40] Chenghua Sun, Li-Min Liu, Annabella Selloni, Gao Qing (Max) Lu, and Sean C. Smith. Titania-water interactions: a review of theoretical studies. *Journal of Materials Chemistry*, 20(46):10319, 2010.

# 6

# CONCLUSION AND DISCUSSION

*In science there are no "depths";*
*there is surface everywhere.*

Rudolf Carnap

*There's something that doesn't make sense.*
*Let's go and poke it with a stick.*

Stephan Moffat- Doctor Who "Amy´s Choice"

Spent nuclear fuel (SNF) is a complex system and the requirement for safety assessments of its disposal under deep geological conditions for a very long time have resulted in many studies concerning corrosion and dissolution scenarios. Most of the research related to SNF corrosion is done by using different environmental conditions to look at the consequences for the safety assessment of the SNF. Also different model systems are used, going from bulk materials to computational studies and as represented in this thesis thin films model systems.

The aim of the research described in this thesis is to evaluate the electronic structure of actinide oxide (Th, U, Np, Pu and Ce as Pu surrogate and fission product) and mixed oxide thin films. In addition, their surface interaction with gas ($O_2$, $O^{\cdot}$, $H_2$, $H^{\cdot}$), liquid (water) and solid (ice) was investigated to follow oxidation / reduction couples as spent fuel model systems for the safety assessments. The studies in this thesis have been done using thin films to model the spent fuel surfaces, starting from simple system to more complex systems.

## 6.1. SUMMARY OF THE RESULTS

In the first part (Chapter 2), $ThO_2$ thin films have been investigated due to its simplified chemistry since it only contains one stable oxidation state. This makes it a very interest-

ing reference material for investigating the potential use of thin films and understanding the oxidation process inside of the Ultra-High Vacuum systems. Th metal was exposed to molecular and atomic oxygen and the thin films were analysed by XPS and UPS on each exposure. It was shown that molecular oxygen results in limited oxidation on the surface, but that atomic oxygen could penetrate all the way to the lower layers. XPS is capable of measuring deeper layers (up to 10 monolayers) compared to UPS is limited to the most upper layers. When Th metal was exposed to molecular oxygen, XPS showed signals that still contain metal, whereas UPS showed full oxidation. During further exposure to atomic oxygen, XPS and UPS both showed tetravalent features corresponding to $ThO_2$ as illustrated in Figure 6.1.

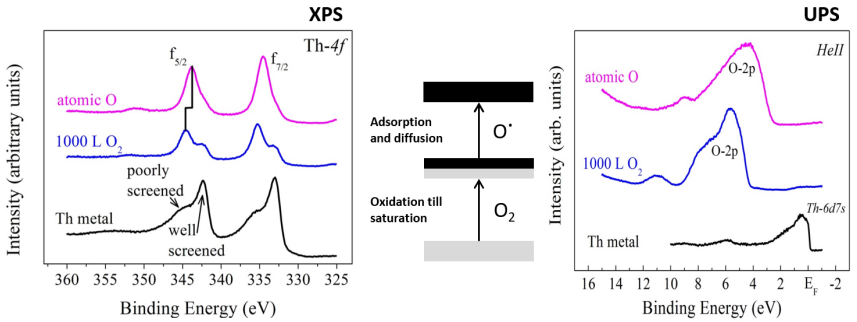


Figure 6.1: XPS core level spectra and UPS valence band spectra of thorium oxidation with molecular and atomic oxygen (Chapter 2 )

A second set of experiments was performed using reactive sputter depositions technique in which during the sputtering of Th metal, oxygen was introduced into the deposition chamber from very low to high oxygen partial pressure as illustrated in Figure 6.2.

In this method, the films are homogeneously oxidized along their thickness. When thorium reached its final oxidation state, the stability of the measured binding energies is one indicator that no further oxidation is possible. In the lower partial pressure oxygen range, we did observe some off-stoichiometry suggested by both the position of binding energies and the peak areas between thorium and oxygen peaks in core level spectra. This is one of the advantages of XPS which can be used for quantitative and qualitative analysis. Even though UPS has no quantitative analysis features, it gives an indication about the density of state of the samples. Since thin films are used as model to simulate the bulk systems, it is important to examine whether the lattice parameters and binding energies are in agreement with bulk materials. The produced $ThO_2$ films have shown good agreement with the literature, indicating that our films are good model materials.

It was important to perform the studies on thorium similar to uranium [1], as both systems form the basis of (U-Th) mixed oxide. Thus, after the assessment of $ThO_2$ films, (U-Th) mixed oxide thin films has been deposited to observe the effect of thorium on the oxidation. Thorium has been chosen as reference material to investigate the effect on oxidation of uranium in a solid solution with an actinide that has a simplified chemistry. Thorium contains only one stable oxidation state, whereas uranium has (IV), (V)

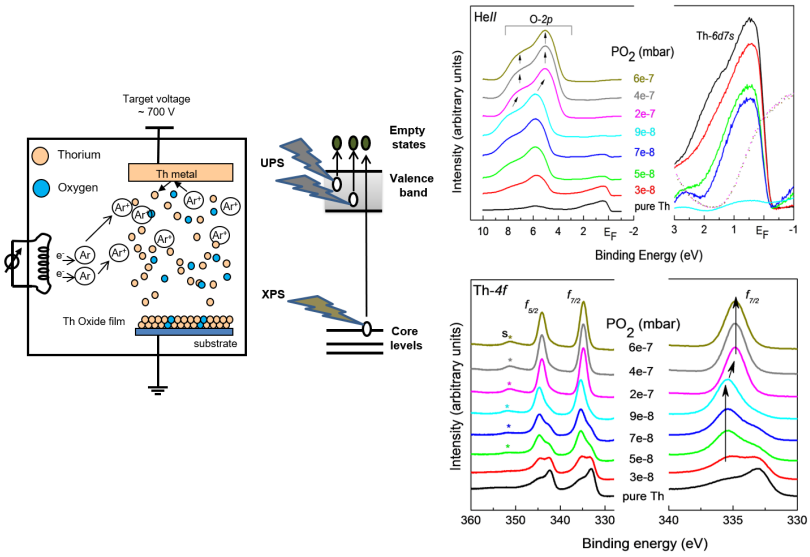


Figure 6.2: Scheme of film deposition by DC sputtering and process of XPS and UPS. Th-*4f* core level and He*II* valence band spectra obtained during the oxidation of thorium (Chapter 2 )



and (VI) oxidation states and forms a series of stable oxides, some with off-stoichiometry compositions. The mixed oxide films deposited onto substrates were also investigated for their capability to replace or mimic bulk materials. As also mentioned in chapter 2, the films are relatively thin as a result of which it is easier to tunnel the electrons during the measurements. This aspect is quite important for reliable electronic structure investigations, and shifts or charging effects which are common in semiconductor and insulator materials, do not occur. In Chapter 2, $ThO_2$ thin film were measured without any disturbance although the materials is an electric insulator. Considering that uranium dioxide (intrinsic semiconductor) mixed with thorium dioxide finds a place between intrinsic semiconductor and insulator, the mixed oxide will be more difficult to measure by any means of spectroscopic techniques used for surface characterization. In Chapter 3, the results of co-deposition of uranium and thorium with different deposition conditions such as low oxygen partial pressure and different temperatures were reported. Co-deposition starting from low partial oxygen pressure to higher amounts showed that the oxygen affinity of thorium is higher than uranium, which was deduced from consecutive measurements via XPS. The reproducibility of the films was examined by depositing over different time periods, and it was concluded that films composition and electronic state kept identical along their deposition. However, deposition at different temperatures affected the oxygen diffusion. The films deposited at high temperatures showed that thorium has a high oxygen affinity, being present in its highest oxidation state, and did not display any change and that uranium indicated slight hyper-stoichiometry due to the increased diffusion of oxygen induced by heating. As was the case in Chapter 2,

lattice parameters and binding energies determined for uranium-thorium mixed oxides versus the composition agree with literature data obtained on bulk, and it was concluded that also the mixed oxide films are suitable surface model materials.

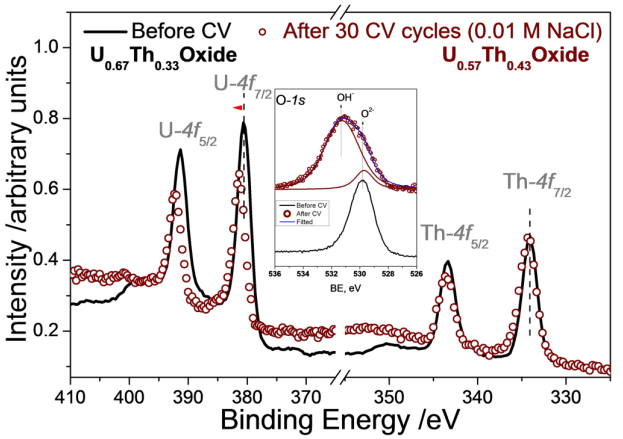


| Sample | Before CV | | | | After CV | | | |
|---|---|---|---|---|---|---|---|---|
| | Composition | Binding Energy, eV | | | Composition | Binding Energy, eV | | |
| | | U-$4f_{5/2}$ | Th-$4f_{5/2}$ | O-*1s* | | U-$4f_{5/2}$ | Th-$4f_{5/2}$ | O-*1s* |
| 1 | $U_{67}Th_{33}O_2$ | 380.5 | 334.0 | 529.8 | $U_{57}Th_{43}O_{2+x}$ | 381.3 | 334.1 | 529.7/531.2 |
| 2 | $U_{56}Th_{44}O_2$ | 380.5 | 333.9 | 529.8 | $U_{40}Th_{60}O_{2+x}$ | 381 | 333.9 | 529.8/531.2 |
| 3 | $U_{16}Th_{84}O_2$ | 380.5 | 333.9 | 529.8 | $U_{14}Th_{86}O_{2+x}$ | 380.9 | 333.8 | 529.7/531.3 |

Figure 6.3: U-*4f* and Th-*4f* core level spectra of $U_{0.67}Th_{0.33}$ oxide film before and after 30 cycles, inset graph represents the corresponding O-*1s* spectra. Table: Composition and U-$4f_{5/2}$, Th-$4f_{5/2}$ and O-1s films before and after 30 cycles of CV in [NaCl]=0.01 M.(Chapter 3)

Previous studies of uranium dioxide thin film materials have explored their possible use in electrochemical analysis, in particularly cyclic voltammetry [1, 2], which examines the corrosion behavior as a function of potential energy. This provides finger-print-like results on the oxidation/reductions properties in aqueous environment to model possible contact with groundwater. Cyclic voltammetry (CV) was applied thanks to the advantages of the thin films mentioned above. In this work CV was applied to uranium-thorium mixed oxides for the first time, to the best to our knowledge. Successful cycles have been performed, and the results showed that thorium slows down the corrosion of uranium. After the cyclic voltammetry investigations XPS measurements have been performed to prove that thorium forms a protective oxide layer, as the results show a thorium enrichment on the surface. It was also observed that if the initial amount of uranium is high in the mixed oxide matrix, the end product of the cyclic voltammetry exhibits itself higher uranium oxidation states (Figure 6.3). This fact also provides an explanation why stronger dissolution was observed in uranium-rich films compared to uranium-poor mixed oxides (as shown in the inset table in Figure 6.3), and why the uranium dissolution increased by many orders of magnitude [3].

After the investigation of the effect of tetatravalent thorium on the redox behavior of uranium in mixed oxides, the next step was to incorporate an element into uranium which has both trivalent and tetravalent stable oxidation states. For that purpose cerium was chosen to form (U-Ce) mixed oxide thin films (Chapter 4). Cerium is easy to handle as it is not a radioactive material, and is mostly used as surrogate for plutonium due to their chemical similarities. The redox properties of uranium and cerium mixed oxides were investigated using the highly reductive (atomic hydrogen, $H^{\cdot}$) and oxidative (atomic oxygen, $O^{\cdot}$) exposure under ultra-high vacuum conditions to fully comprehend the reduction and oxidation in their single and mixed forms. For this purpose, first cerium oxides ($Ce_2O_3$, $CeO_2$) and uranium oxides ($UO_2$, $U_2O_5$ and $UO_3$) thin films were used as reference for the uranium-cerium mixed oxide experiments. Next, $CeO_2$ and $UO_3$ were exposed to atomic hydrogen ($H^{\cdot}$) while $UO_2$ and $CeO_2$ were exposed to atomic oxygen ($O^{\cdot}$). The same procedures were also applied to (U-Ce) mixed oxides to understand the influence of cerium on the oxidation state of uranium.

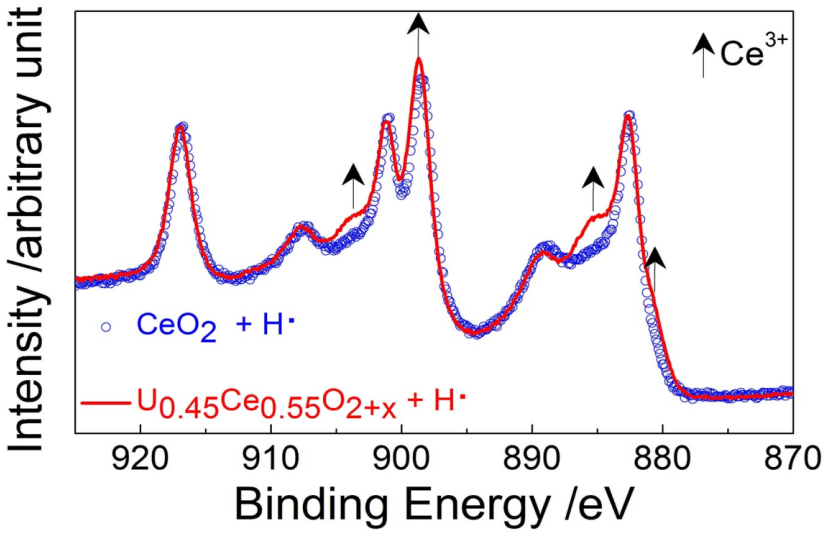


Figure 6.4: Ce-*3d* core level spectra of $CeO_2$ and $U_{0.45}Ce_{0.55}$ films after the exposure to atomic hydrogen at ambient temperature (Chapter 4 ).

In the first set of experiments atomic hydrogen were exposed onto $CeO_2$, $UO_3$ and (U-Ce) mixed oxide at ambient and high temperatures. While heating to high temperatures or exposure to atomic hydrogen at ambient temperatures did not show any prominent change on $CeO_2$, simultaneous heating and exposure showed a drastic change towards reduction as was shown by XPS analyses. However, $UO_3$ was reduced to $U_2O_5$ when exposed to atomic hydrogen at ambient temperature at the same time. This comparison alone indicates that uranium(VI) is more prone to reduction than cerium (IV), in line with thermodynamics. XPS data of (U-Ce) mixed oxide thin films indicate clear U(VI) and Ce(IV) states before any post treatment. In the case of exposure at ambi-

ent temperature, $UO_3$ was reduced to U(V) as in the single oxide, but cerium showed stronger reduction than its single oxide. Superposition of the data of single oxide and mixed oxide Ce-*3d* spectra after the same post treatment conditions is shown in Figure 6.4 for better comparison. The presence of uranium is clearly affecting the reduction of cerium.

In the second set of experiments, oxidation by exposure to oxygen of different partial pressures during and after deposition has been investigated. In the mixed thin films of uranium and cerium co-deposited with traces of oxygen, the oxidation states were identified as U(IV) and Ce(III). Increasing the partial pressure oxygen in the deposition chamber resulted in only slight oxidation to Ce(IV) and to U(V). Further oxidation with higher oxygen partial pressure led to complete transformation of uranium into U(V) and Ce(IV) with slight Ce(III) contribution. Next, $Ce_2O_3$, $U_2O_5$ and (U-Ce) mixed oxide thin films were exposed to atomic oxygen at high temperatures to observe the formation of higher oxides and their effect during the oxidation process. Both single cerium and uranium oxide reached their highest oxidation states as $CeO_2$ and $UO_3$ after the exposure. Normally, the formation of $U_2O_5$ is not observed during deposition but only after reduction of $UO_3$. However when uranium is mixed with cerium, it has the (V) oxidation state without the need of any post reduction. This phenomenon can be interpreted as a charge transfer between cerium and uranium helping the stabilization of U(V) state in the mixed oxide. When mixed oxide of (U-Ce) was exposed to atomic oxygen at high temperatures, both uranium and cerium formed their highest possible oxidation states.



Following the chapters above, the water coverage on thin films of the mixed actinide oxides of U-Th and U-Pu, and $NpO_2$ under ultra-high vacuum (UHV) conditions has been studied. The films were prepared by sputter deposition and measured by XPS and UPS without any contact with laboratory atmosphere. This has to be emphased here because it gives clear indication that the samples are contamination-free. The main goal was to investigate the influence of water on the surface and to follow the surface alteration under radiation enhanced conditions which leads to radiolysis of water.

A different approach had to be implemented in this study, because water cannot provide a full coverage under UHV conditions. Thus, ice the condensed form of water has been used to cover the surface. For enhanced radiation simulations, Ultra-violet (20-50 eV) light which is basically the one we used for UPS measurements was used. Previous studies indicated [4, 5] that $UO_{2+x}$ and $PuO_2$ surfaces were reduced to $UO_2$ and $Pu_2O_3$ by using ice under UV light. However, when the surfaces were exposed to most reductive agent, atomic hydrogen, only $UO_{2+x}$ was reduced but $PuO_2$ has shown no sign of change in oxidation state. In this study (Chapter 5), $NpO_2$, (U-Th) and (U-Pu) mixed oxides were examined. The results showed that $NpO_2$ was reduced to $Np_2O_3$, uranium was reduced from hyper-stoichiometric to stoichiometric in (U-Th) mixed oxide, and plutonium was reduced to $Pu_2O_3$ in (U-Pu) mixed oxide. It should be noted that uranium in the mixed oxides are already in their lowest oxidation states, and cannot be reduced to $U_2O_3$ as it does not exist. In $NpO_2$, it was quite interesting to observe $Np_2O_3$ on the surface because so far, the studies [6] have indicated that $Np_2O_3$ is an intermediate form observed during oxidation of Np metal.

The fact that reduction on the surfaces occurred only in the presence of ice and UV light together (Figure 6.5) can have two explanations: either it was a photocatalytic pro-

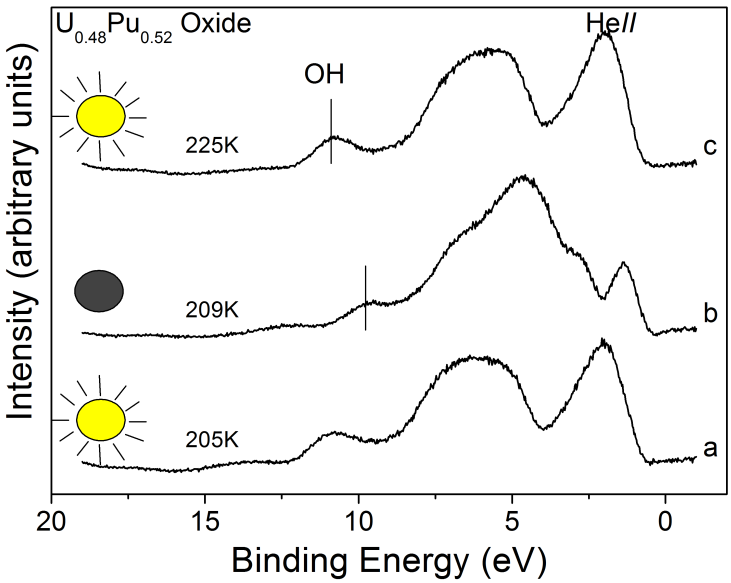


Figure 6.5: He*II* valence spectra of irradiated and dark areas of $U_{0.48}Pu_{0.52}$ oxide (Chapter 5).



cess driven by the photoexcited surface, or it was the reaction of the surface with photolysis products of ice. As mentioned above, atomic hydrogen (product of water photolysis) was not able to reduce $PuO_2$ to $Pu_2O_3$, and therefore reduction of neither $NpO_2$ nor $UO_2$ cannot be expected due to their unfavorable formation enthalpies for $An_2O_3$ (see Chapter 5, Table 5.1). This contradiction gives an indication about what might occur at the surface. The fact that reduction only took place when the surface was covered with ice and UV heated samples point toward photocatalytic processes. Photocatalytic processes require an energy equal or higher than the band gap to excite electrons from the valence band to the conduction band, creating $e^-$ and $h^+$ responsible for reduction and oxidation, respectively. Since the results show the reduction at the surface, water must be oxidized. It is therefore thought that the $h^+$ oxidize the water meanwhile $e^-$ reduces the surface. This process is also depending on the band gap energy. It was observed [7, 8] that reduction is more enhanced in wide band gap solids, which can explain the higher tendency of reduction of uranium when it is mixed with higher band gap actinides such as Th and Pu (Table 5.2).

The main outcomes of the studies are summarised below.

- Thin films of actinide and mixed actinide oxides showed good agreement with literature bulk results, promoting the films capability to be used as model surfaces for SNF studies.
- Using thin films instead of thick bulk materials has shown many advantageous throughout these studies. Mainly because of the semiconductor and insulator properties of actinide oxides, electrons could be tunneled without any disturbance.

Especially they have shown leverage over the photoelectron spectroscopy and electrochemical investigations.

- Due to the experimental conditions under UHV conditions, starting from preparations to measurements, contamination-free matrices have been obtained. This is important due to the fact that the complete understanding of the reaction mechanisms can only be obtained without any disturbance of foreign contribution.
- Successive mixed actinide oxide thin films were presented from simple to complex system, and their effect on uranium redox behaviors were successfully achieved.
- Cyclic voltammetry investigation of (U-Th) mixed oxide thin films were conducted and the results clearly indicated the positive effect of thorium on uranium oxidation behavior by following the anodic and cathodic reactions. After the cyclic voltammetry experiments, thorium has found to be enriched on the surface which indicates that it passivates the surface.
- Deposition of $CeO_2$, $Ce_2O_3$, $UO_2$ and $UO_{2+x}$ films by using reactive sputtering under UHV conditions could be made without any need of post treatment, however to reach $UO_3$ oxygen exposure is required, while $U_2O_5$ (U(V)) is made by the reduction of $UO_3$ (U(VI)). When uranium is mixed with cerium, the U(V) state was present without the need of any post treatment.
- Even though, presence of water and using UV light for short term individually are not thermodynamically favorable for reduction, using solid phase of water as ice at the same time applying UV assisted heating resulted in reduction on the surface.



## 6.2. DISCUSSION OF THE RESULTS

Understanding corrosion in a nuclear waste repository is a quite challenging task, as both the chemistry of uranium [3, 9] and the spent nuclear fuel matrix are complex [10] alongside different physical/chemical conditions of the host rock and the groundwater. The disposal conditions must be assured for up to $10^5$ years. Because only then the radioactivity emitted by the spent nuclear fuel decreases to naturally occurring levels. Therefore, the long-term safety assessments of spent fuel are essential. Beside its many different parameters, one main idea is to avoid contact between groundwater and the spent nuclear fuel. However, it is crucial to know what would happen in the case of groundwater contact.

Spent nuclear fuel mainly consists of uranium dioxide and the rest is formed by the fission products and activation products (transuranium elements) [10]. Although upon contact with water an instant release of radionuclides present at grain boundaries can occur, the release of most radionuclides from SNF is expected to proceed through the dissolution of uranium (via oxidation, corrosion) as they are incorporated and/or located in grains. Thus redox behavior of uranium dioxide is the first step for understanding the corrosion and the dissolution phenomenon [11]. There have been many works on oxidation mechanisms of uranium dioxide under different oxidative conditions [12–15] and how its redox behavior affects the dissolution rate[15]. It is well established that stoichiometric uranium dioxide, $UO_{2.00}$ (U(IV)), is highly insoluble [11]. However, in

contact with oxidative conditions (such as groundwater and the oxidants formed due to the radiation) the oxidation state of uranium is increasing from U(IV) to U(VI) thus increasing its solubility by many orders of magnitudes [3]. Knowing that uranium is not the sole element in the matrix, it is important to consider the elements formed during - irradiation in discussing the dissolution phenomenon. Therefore, simplified models are created from simple to more complex to understand the contribution of single elements in the corrosion scenarios of uranium dioxide.

One problem that electrochemical studies of actinide oxides suffer from is their semiconductor character. Thus, the assessment of the redox behavior and surface properties becomes more challenging when examining the changes in the electronic structure. As previous works stated [1, 2], the low sample thickness in binary oxide thin films enables the charge transfer despite the semiconductor character of actinide oxides and therefore allows electronic structure measurements.

Uranium dioxide forms solid solution with the dioxides of thorium and plutonium [16]. In solid solutions, the incorporated actinide is changing the redox stability of uranium as the lattice parameter and the electronic structure are related with each other. While uranium has three stable oxidation states, U(IV), U(V) and U(VI) in solid compounds, which may be mixed, thorium has only one stable oxidation state, Th(IV). Thorium dioxide, an insulator, has very limited solubility in water [17]. Sunder et al. [18] has stated that it was mixed not possible to examine uranium-thorium dioxides in electrochemical cells due to their high resistivity. However, our thin film samples released the measurements from the charging effect because the thickness is drastically reduced compared to the bulk material. In electrochemical analysis the parameters such as composition and pH of the groundwater of a relevant repository can be simulated, thus gives fingerprint-like information for corrosion and dissolution behavior. Electrochemistry of uranium dioxide has been studied under many different electrolyte compositions [12, 19–21], and uranium-thorium mixed oxides experiments with conventional dissolution experiments [18, 22–25], to the best to our knowledge this is the first attempt made for (U-Th) mixed oxide electrochemical analysis. The results show that thorium, when incorporated into uranium, is slowing the oxidation of uranium leading to lower dissolution rates compared to binary uranium dioxide. This is quite remarkable as using electrochemical methods on semiconductor mixed oxides thin films is possible and the redox behaviors can be evaluated.

Besides the direct contact of the surface with the water, there is also the radiation energy which poses as another important factor influencing the dissolution. The radioactivity from the spent nuclear fuel has enough energy to break the chemical composition of water, creating strong oxidants ($H_2O_2$, $H_2O^{\cdot}$, $O_2$) and reductants ($H_2$, $H^{\cdot}$, $e^-$)[26]. In such case, after the water reaches the surface of the SNF, oxidation and/or reduction should be expected. There have been many studies which have addressed this phenomenon [27–29]. Using highly reactive oxidants and reductants in experimental conditions gives information in short time as well as identifying the reactions occurring on the surface. This fundamental research approach is quite important as it identifies the interaction of the reactants with the surface and the role of each element´s in the oxidation and reduction. Despite the focus on the oxidation of SNF, there are also studies suggesting the inhibition of the corrosion due to the presence of hydrogen of radiolytic

or chemical origin[30, 31]. That is the reason, while water corrosion is an oxidative process, reduction due to such reductants must also be examined when investigating the corrosion scenarios. In uranium and cerium (as both substitute for plutonium and fission product) mixed oxides, cerium has two stable oxidation state, Ce(III) and Ce(IV). The examinations made after exposing the mixed oxide of uranium-cerium to atomic oxygen and hydrogen, revealed that U(V) state forms when cerium is incorporated. This is due to the charge transfer reaction occurring between Ce(IV)+U(IV)→ Ce(III)+U(V) as was proposed by Griffiths et al. [32]. The same phenomenon has been also observed for uranium-americium mixed oxide [33–35]. It has been also discussed that reduction of Am(IV) to Am(III) is more pronounced and leads to oxidation of U(IV) to U(V). Considering that cerium is also used in many studies [36, 37] for substituting plutonium, the charge transfer reactions was also discussed in (U-Pu) mixed oxides[38]. We obtained similar results for (U-Ce) mixed oxides thin films experiments compared to (U-Am) oxide, (U-Pu) oxide and (U-Ce) oxide bulk results [39–41]. This indicates that thin films can be used as model to investigate fundamental properties like oxidation and reduction for instance.

For studying the effects of water contact and of oxidants/reductants, contact with a high concentration of water under radiation conditions is used. This model examines all the joint effect of surface-water interactions and of radiolysis products forming near the surface. For a high water density, the surface was covered with ice. During the measurements, ice was warmed up by using UV light simulating the radiation to be able to form the oxidants and reactants. Considering the low temperature of ice nonthermal reactions are assured during the experiments. This is important as the only focus was given to light activated reactions. The previous studies on the binary oxides of $PuO_2$ and $UO_{2+x}$ [4, 5] thin films have shown that when the surface is covered by ice and heated under UV light reduction of the samples occurred. In contrast, reduction of those samples was not achieved when exposed to atomic hydrogen. It was then concluded that reduction is caused by photolysis. Further studies in the frame of this thesis confirmed the reduction of the mixed oxide of (U-Th) and (U-Pu) as well as $NpO_2$ by the joint effect of ice and UV showing the important role of trapping of the reductants created by UV light in the reduction of the surface[42, 43].

Looking at all the mechanisms involved in the redox studies and the complex nature of the spent nuclear fuel, models of both the samples and the surrounding conditions are bringing interpretations one step closer. In this thesis, high impact scenarios involving the corrosion phenomenon were investigated by using the thin film actinide mixed oxides surface approach. Beside the chemical interactions, physical changes are also playing a role when discussing the SNF properties. It is known that the thin films are quite close to the ideal surfaces therefore, physical appearances such as cracks and boundaries are not involved in the studies. For those, thicker and/or irradiated samples are needed.

The difference between thin films and conventional bulk samples, which are also produced to simulate the SNF, are that study and process of oxidation and reduction can be be done and followed in-situ. The films are not in contact with the atmosphere. This approach alone gives a clearer understanding of the possible reactions, and the role of the elements in the process. Consistency of the results throughout multiple experiments

following the electronic structure of the surfaces and their repeatability together with a high stability of the samples shows that films produced and studied *in-situ* are suitable methods.

Based on the current work it can be concluded that:

- Substitution of metal ions in the uranium dioxide matrix plays an important role for the dissolution behavior. Isovalent ions with one stable valence state such as Th(IV) stabilize the matrix, in line with thermodynamic considerations. Isovalent ions that can change their valence state such as Ce can cause charge transfer, leading to U(V) formation. In the latter case the dissolution of the matrix will be enhanced.
- Photoactivated reaction can lead to oxidation of water and surface reduction of the $UO_2$ matrix, restraining the dissolution.

In the real case of spent fuel corrosion these processes together with other features present in the SNF and not discussed in this thesis (i.e. fission product) act simultaneously, and competition between them will occur.

## 6.3. OUTLOOK

The research in this thesis on the actinide (-mixed) oxide thin films has provided interesting results, demonstrating their potential use as spent fuel model systems. Due to the complex aspect of SNF, there is plenty of room for future work by using thin films:

- The simultaneous study of the photoreduction and the charge-transfer mechanism in (U,Ce)$O_2$ is a logic next step, which could not be addressed in this work due to time limitations.
- Thin film studies of other important fission products present in the SNF matrix, for example by doping the films to simulate particle precipitate on the surface. Metal precipitates form another source for hydrogen production through reduction of water, due to the catalytic potential of some of the noble metals present as fission products.
- The morphology and grain structure of the films needs to be investigated and compared to the bulk. Electrochemical study using quartz crystal micro balance could be done using good and reproducible deposition of the films. A good adhesion of the films is necessary to avoid the flacking of the film during study of the interaction process in solution. Investigation of the stress occurring between the film and the substrate during and after deposition needs to be evaluated and limited.

## REFERENCES

[1] F. Miserque, T. Gouder, D. H. Wegen, and P. D W Bottomley. Use of UO2 films for electrochemical studies. *Journal of Nuclear Materials*, 298(3):280–290, 2001.

[2] A. Seibert, D.H. Wegen, T. Gouder, J. Römer, T. Wiss, and J.-P. Glatz. The use of the electrochemical quartz crystal microbalance (EQCM) in corrosion studies of UO2 thin film models. *Journal of Nuclear Materials*, 419(1-3):112–121, dec 2011.

[3] I. Grenthe, J. Fuger, R. J. M. Konings, R.J. Lemire, A. G. Muller, C. Nguyen-Trung Cregu, and H. Wanner. *Chemical thermodynamics of uranium*. North Holland, Amsterdam, 1992.

[4] T. Gouder, A. B. Shick, and F. Huber. Surface Interaction of PuO2, UO2+x and UO3 with Water Ice. *Topics in Catalysis*, 56(12):1112–1120, jul 2013.

[5] A. Seibert, T. Gouder, and F. Huber. Interaction of PuO 2 thin films with water. *Radiochimica Acta*, 98(9-11):647–657, nov 2010.

[6] J. R. Naegele, L. E. Cox, and J. W Ward. Photoelectron spectroscopy (UPS/XPS) study of Np203 formation on the surface of neptunium metal. *Inorganica Chemica Acta*, 139:327–329, 1987.

[7] J. A. Laverne and L. Tandon. H2 Production in the Radiolysis of Water on CeO2 and ZrO2. *Journal of Physical Chemistry B*, 106:380–386, 2002.

[8] J. T. Yates. Photochemistry on TiO2: Mechanisms behind the surface chemistry. *Surface Science*, 603(10-12):1605–1612, jun 2009.

[9] L. H. Johnson and D. W. Shoesmith. Spent Fuel. In W. B. Lutze and Rodney C. Ewing, editors, *Radioactive Waste Forms for the Future*, chapter 11, page 635. Amsterdam, The Netherlands, 1988.

[10] H. Kleykamp. The chemical state of the fission products in oxide fuels. *Journal of Nuclear Materials*, 131(2-3):221–246, apr 1985.

[11] D.W. Shoesmith. Fuel corrosion processes under waste disposal conditions. *Journal of Nuclear Materials*, 282(1):1–31, nov 2000.

[12] S. Sunder, D. W. Shoesmith, Robert J. Lemire, M. G. Bailey, and G. j. Wallace. The effect of pH on the corrosion of nuclear fuel (UO2) in oxygenated solutions. *Corrosion Science*, 32(4):373–386, 1991.

[13] M.E. Broczkowski, J.J. Noël, and D.W. Shoesmith. The influence of temperature on the anodic oxidation/dissolution of uranium dioxide. *Electrochimica Acta*, 52(25):7386–7395, sep 2007.

[14] B.G. Santos, J.J. Noël, and D.W. Shoesmith. The effect of pH on the anodic dissolution of SIMFUEL (UO2). *Journal of Electroanalytical Chemistry*, 586(1):1–11, jan 2006.

[15] D. W. Shoesmith, S. Sunder, and W. H. Hocking. Electrochemistry of UO2 Nuclear Fuel. In J. Lipkowski and N. P Ross, editors, *The Electrochemisty of Novel Materials*, pages 297–337. VCH, New York, 1994.

[16] C.A. Colmenares. The oxidation of thorium, uranium, and plutonium. *Progress in Solid State Chemistry*, 9:139–239, jan 1975.

[17] D. Langmuir and J. S. Herman. The Mobility of Thorium in Natural Waters at low Temperatures. *Geochimica et Cosmochimica Acta*, 44:1753–1766, 1980.

[18] S. Sunder and N.H. Miller. XPS and XRD studies of (Th,U)O2 fuel corrosion in water. *Journal of Nuclear Materials*, 279(1):118–126, mar 2000.

[19] J. C. Wren, D. W. Shoesmith, and S. Sunder. Corrosion Behavior of Uranium Dioxide in Alpha Radiolytically Decomposed Water. *Journal of The Electrochemical Society*, 152(11):B470, 2005.

[20] Linda Wu and David W. Shoesmith. An Electrochemical Study of H2O2 Oxidation and Decomposition on Simulated Nuclear Fuel (SIMFUEL). *Electrochimica Acta*, 137:83–90, aug 2014.

[21] D. W. Shoesmith and S. Sunder. An electrochemistry-based model for the dissolution of UO2. *Atomic Energy of Canada Limited, AECL (Report)*, (10488):1–97, 1991.

[22] G. Heisbourg, S. Hubert, N. Dacheux, and J. Ritt. The kinetics of dissolution of Th1-xUxO2 solid solutions in nitric media. *Journal of Nuclear Materials*, 321(2-3):141–151, sep 2003.

[23] G. Heisbourg, S. Hubert, N. Dacheux, and J. Purans. Kinetic and thermodynamic studies of the dissolution of thoria-urania solid solutions. *Journal of Nuclear Materials*, 335(1):5–13, oct 2004.

[24] S. Hubert, K. Barthelet, B. Fourest, G. Lagarde, N. Dacheux, and N. Baglan. Influence of the precursor and the calcination temperature on the dissolution of thorium dioxide. *Journal of Nuclear Materials*, 297(2):206–213, 2001.

[25] Erich Zimmer and Erich Merz. Dissolution of thorium-uranium mixed oxides in concentrated nitric acid. *Journal of Nuclear Materials*, 124:64–67, 1984.

[26] G. R. Choppin, J. O. Liljenzin, and J. Rydberg. *Radiochemistry and nuclear chemistry*. Butterworth-Heinemann, 2002.

[27] T. Gouder, A. Seibert, L. Havela, and J. Rebizant. Search for higher oxides of Pu: A photoemission study. *Surface Science*, 601(14):L77–L80, jul 2007.

[28] A. Seibert, T. Gouder, and F. Huber. Reaction of neptunium with molecular and atomic oxygen: Formation and stability of surface oxides. *Journal of Nuclear Materials*, 389(3):470–478, jun 2009.

[29] B. Chen, Y. Ma, L. Ding, L. Xu, Z. Wu, and Q. Yuan. Reactivity of Hydroxyls and Water on a CeO 2 ( 111 ) Thin Film Surface : The Role of Oxygen Vacancy. *The Journal of Physical Chemistry C*, 2(111):5800–5810, 2013.

[30] M.E. Broczkowski, J.J. Noël, and D.W. Shoesmith. The inhibiting effects of hydrogen on the corrosion of uranium dioxide under nuclear waste disposal conditions. *Journal of Nuclear Materials*, 346(1):16–23, nov 2005.

[31] P. Carbol, P. Fors, T. Gouder, and K. Spahiu. Hydrogen suppresses UO2 corrosion. *Geochimica et Cosmochimica Acta*, 73(15):4366–4375, aug 2009.

[32] T. R. Griffiths, H. V. St. A. Hubbard, and M. J. Davies. Electron transfer reactions in non-stoichiometric ceria and urania. *Inorganica Chimica Acta*, 225(1-2):305–317, oct 1994.

[33] Damien Prieur, Philippe M. Martin, Aurélien Jankowiak, Elisabeth Gavilan, Andreas C. Scheinost, Nathalie Herlet, Philippe Dehaudt, and Philippe Blanchart. Local structure and charge distribution in mixed uranium-Americium oxides: Effects of oxygen potential and am content. *Inorganic Chemistry*, 50(24):12437–12445, 2011.

[34] Florent Lebreton, Denis Horlait, Richard Caraballo, Philippe M. Martin, Andreas C. Scheinost, Andre Rossberg, Christophe J??gou, and Thibaud Delahaye. Peculiar Behavior of (U,Am)O2-x Compounds for High Americium Contents Evidenced by XRD, XAS, and Raman Spectroscopy. *Inorganic Chemistry*, 54(20):9749–9760, 2015.

[35] D. Prieur, F. Lebreton, P. M. Martin, M. Caisso, R. Butzbach, J. Somers, and T. Delahaye. Comparative XRPD and XAS study of the impact of the synthesis process on the electronic and structural environments of uranium-americium mixed oxides. *Journal of Solid State Chemistry*, 230:8–13, 2015.

[36] P. Martin, M. Ripert, T. Petit, T. Reich, C. Hennig, F. D'Acapito, J. L. Hazemann, and O. Proux. A XAS study of the local environments of cations in (U,Ce)O2. *Journal of Nuclear Materials*, 312(1):103–110, 2003.

[37] K. Suresh Kumar, T. Mathews, H. P. Nawada, and N. P. Bhat. Oxidation behaviour of uranium in the internally gelated urania–ceria solid solutions – XRD and XPS studies. *Journal of Nuclear Materials*, 324(2-3):177–182, jan 2004.

[38] Takeo Fujino, Toshiyuki Yamashita, Kinji Ohuchi, Keiji Naito, and Toshihide Tsuji. High temperature electrical conductivity and conduction mechanism of (U, Pu)O2 ± x at low oxygen partial pressures. *Journal of Nuclear Materials*, 202(1-2):154–162, jun 1993.

[39] S. Bera, V. K. Mittal, R. Venkata Krishnan, T. Saravanan, S. Velmurugan, K. Nagarajan, and S. V. Narasimhan. XPS analysis of UxCe1-xO2+y and determination of oxygen to metal ratio. *Journal of Nuclear Materials*, 393(1):120–125, 2009.

[40] I. Al-Shankiti, F. Al-Otaibi, Y. Al-Salik, and H. Idriss. Solar thermal hydrogen production from water over modified CeO2 materials. *Topics in Catalysis*, 56(12):1129–1138, 2013.

[41] Y. Al-Salik, I. Al-Shankiti, and H. Idriss. Core level spectroscopy of oxidized and reduced CexU1-xO2 materials. *Journal of Electron Spectroscopy and Related Phenomena*, 194:66–73, 2014.

[42] K. Kim, W. Choi, M. R. Hoffman, H. Yoon, and B.-K. Park. Photoreductive dissolution of iron oxides trapped in ice and its environmental implications. *Environmental Science Technology*, 44(11):4142–4148, 2010.

[43] D. Jeong, K. Kim, and W. Choi. Accelerated dissolution of iron oxides in ice. *Atmospheric Chemistry and Physics*, 12(22):11125–11133, nov 2012.

# CURRICULUM VITÆ

## Pelin ÇAKIR

12-01-1989 Born in Islahiye, Gazi Antep, Turkey.

## EDUCATION

2006–2011 Bachelor Degree in Chemistry
Ege University, Faculty of Sciences, Izmir, Turkey

2011–2013 Master Degree
Ege University, Institute of Nuclear Sciences, Izmir, Turkey

2017 Ph.D.
Delft University of Technology, The Netherlands
*Thesis:* Redox Behaviour of Model Systems for Spent Nuclear Fuel Surfaces
*Promotor:* Prof. dr. R. J. M. Konings

## PROFESSIONAL EXPERIENCES

2016 GENTLE Student Research Experiment Trainee
Reactive transport modelling in a spent nuclear fuel (SNF) repository
Karlsruhe Institute of Technology
Institute for Nuclear Waste Disposal, Karlsruhe Germany

2013–2016 Grant Holder, Research Fellow
Redox behaviour of model systems for spent nuclear fuel surfaces
European Commission, Joint Research Centre, Karlsruhe, Germany
Formerly known as Institute for Transuranium Elements, ITU

2012–2013 Trainee
High Temperature behavior of nuclear mixed oxide fuels
European Commission, Joint Research Centre, Karlsruhe, Germany
Formerly known as Institute for Transuranium Elements, ITU

# List of Publications

4. **P. Cakir**, **R. Eloirdi**, **F. Huber**, **R.J.M. Konings**, **T. Gouder** *An XPS and UPS study on the electronic structure of $ThO_x$ ( $x \leq 2$ ) Thin Films,* The Journal of Physical Chemistry C **118**, 24497 (2014).

3. **P. Cakir**, **R. Eloirdi**, **F. Huber**, **R.J.M. Konings**, **T. Gouder** *Surface reduction of neptunium dioxide and uranium mixed oxides with plutonium and thorium by photocatalytic reaction with ice,* The Journal of Physical Chemistry C **119**, 1330 (2015).

2. **P. Cakir**, **R. Eloirdi**, **F. Huber**, **R.J.M. Konings**, **T. Gouder**, *Thorium effect on the oxidation of uranium: Photoelectron spectroscopy (XPS/UPS) and cyclic voltammetry (CV) investigation on $(U_{1-x}Th_x)O_2$ (x = 0 to 1) thin films,* Applied Surface Science **393**, 204 (2017).

1. **R. Eloirdi**, **P. Cakir**, **F. Huber**, **A. Seibert**, **R.J.M. Konings**, **T. Gouder**, *X-ray photoemission spectroscopy study of the reduction and oxidation of uranium and cerium single oxide compared to (U-Ce) mixed oxide films,* Applied Surface Science **457**, 566 (2018).